

***In vitro* modeling of neuronal ceroid lipofuscinosis (NCL): Patient fibroblasts and their reprogrammed derivatives as human models of NCL**

**D I S S E R T A T I O N**

**zur Erlangung des akademischen Grades**

**Doctor rerum naturalium**

**(Dr. rer. nat.)**

**vorgelegt**

**der Fakultät Mathematik und Naturwissenschaften**

**der Technischen Universität Dresden**

**von**

**Diplomchemikerin Xenia Lojewski**

**geboren am 29.06.1985 in Strausberg**

**Eingereicht am 23.11.2012**

Die Dissertation wurde in der Zeit von November 2009 bis September 2012 im Institut für Neurologie, Universitätsklinikum Carl Gustav Carus, angefertigt.



**Gutachter:**

Prof. Dr. rer. nat. habil. Karl-Heinz van Pée

Prof. Dr. med. habil. Alexander Storch

**Tag der Verteidigung:**

09.07.2013

---

# Index

|  |           |
|--|-----------|
| <b>ABBREVIATIONS .....</b>   | <b>8</b>  |
| <b>1 INTRODUCTION.....</b>   | <b>10</b> |
| <b>1.1 Neuronal ceroid lipofuscinoses .....</b>  | <b>10</b> |
| 1.1.1 Late infantile neuronal ceroid lipofuscinosis.....                                 | 12        |
| 1.1.1.1 Tripeptidyl peptidase I .....  | 12        |
| 1.1.2 Juvenile neuronal ceroid lipofuscinosis.....                                       | 13        |
| 1.1.2.1 The ceroid-lipofuscinosis, neuronal 3 protein .....                              | 14        |
| 1.1.3 Model systems for late infantile and juvenile neuronal ceroid lipofuscinosis ..... | 15        |
| <b>1.2 Induced pluripotent stem cells.....</b>   | <b>16</b> |
| 1.2.1 Characterization of induced pluripotent stem cells .....                           | 17        |
| 1.2.2 Neuronal differentiation of induced pluripotent stem cells .....                   | 18        |
| 1.2.3 Human induced pluripotent stem cells for modeling neurodegenerative diseases ..... | 21        |
| <b>1.3 Objective.....</b>  | <b>24</b> |
| <b>2 MATERIALS AND METHODS.....</b>  | <b>25</b> |
| <b>2.1 Materials.....</b>  | <b>25</b> |
| 2.1.1 Instruments.....   | 25        |
| 2.1.2 Chemicals and reagents.....  | 26        |
| 2.1.3 Enzymes.....   | 27        |
| 2.1.4 Commercial available kits.....   | 28        |
| 2.1.5 Cell culture media and supplements.....  | 28        |
| 2.1.6 Growth factors, cytokines and small molecules.....                                 | 29        |
| 2.1.7 Antibodies .....   | 29        |
| 2.1.8 Primers .....  | 31        |
| 2.1.9 Cell lines and bacterial strains.....  | 33        |
| <b>2.2 Tissue and cell culture .....</b>   | <b>33</b> |
| 2.2.1 Cell culture media .....   | 34        |
| 2.2.2 Coatings .....   | 36        |
| 2.2.2.1 Gelatin coating .....  | 36        |
| 2.2.2.2 Matrigel™ coating .....  | 36        |
| 2.2.2.3 Poly-L-Ornithine/Laminin coating.....  | 36        |

---

|            |   |           |
|------------|---|-----------|
| 2.2.3      | Fibroblast preparation and propagation.....                       | 37        |
| 2.2.4      | Preparation of CF-1 feeder cells .....                            | 38        |
| 2.2.5      | Preparation of conditioned media .....                            | 39        |
| 2.2.6      | Generation and maintenance of induced pluripotent stem cells..... | 40        |
| 2.2.6.1    | Reprogramming.....  | 40        |
| 2.2.6.2    | Single colony picking and establishment of stable clones.....     | 43        |
| 2.2.6.3    | Expansion of induced pluripotent stem cell clones .....           | 44        |
| 2.2.6.4    | Freezing and thawing of induced pluripotent stem cells .....      | 45        |
| 2.2.7      | Characterization of induced pluripotent stem cells .....          | 45        |
| 2.2.7.1    | Transgene silencing.....  | 45        |
| 2.2.7.2    | Confirmation of pluripotency.....                                 | 46        |
| 2.2.7.3    | Embryoid body formation and differentiation.....                  | 46        |
| 2.2.8      | 5-bromo-2'-deoxyuridine incorporation assay .....                 | 46        |
| 2.2.9      | Derivation and propagation of neural progenitor cells.....        | 47        |
| 2.2.9.1    | Monolayer culture .....   | 47        |
| 2.2.9.2    | Neurosphere culture .....   | 49        |
| 2.2.10     | Neuronal differentiation .....                                    | 49        |
| <b>2.3</b> | <b>Molecular biology .....</b>                                    | <b>50</b> |
| 2.3.1      | Plasmid preparation.....  | 50        |
| 2.3.1.1    | Bacterial culture .....   | 50        |
| 2.3.1.2    | Plasmid DNA purification.....                                     | 50        |
| 2.3.2      | RNA isolation .....   | 51        |
| 2.3.3      | Reverse transcription.....  | 52        |
| 2.3.4      | Polymerase chain reaction.....                                    | 53        |
| 2.3.5      | Quantitative real-time polymerase chain reaction.....             | 53        |
| 2.3.6      | Agarose gel electrophoresis .....                                 | 55        |
| <b>2.4</b> | <b>Protein biochemistry.....</b>                                  | <b>56</b> |
| 2.4.1      | Western blot analysis .....                                       | 56        |
| 2.4.1.1    | Protein extraction and quantification.....                        | 56        |
| 2.4.1.2    | Protein separation.....   | 57        |
| 2.4.1.3    | Protein transfer .....  | 58        |
| 2.4.1.4    | Protein detection.....  | 58        |
| 2.4.2      | Alkaline phosphatase assay.....                                   | 59        |
| 2.4.3      | Terminal deoxynucleotidyl transferase assay.....                  | 60        |
| 2.4.4      | Tripeptidyl peptidase I enzyme activity assay .....               | 61        |
| <b>2.5</b> | <b>Microscopy .....</b>   | <b>62</b> |
| 2.5.1      | Immunofluorescence .....  | 62        |

---

|            |   |           |
|------------|---|-----------|
| 2.5.1.1    | General staining procedure.....   | 62        |
| 2.5.1.2    | 5-bromo-2'-deoxyuridine staining.....   | 63        |
| 2.5.1.3    | Imaging .....   | 63        |
| 2.5.2      | Electron microscopy .....   | 64        |
| 2.5.3      | Statistics .....  | 65        |
| <b>3</b>   | <b>RESULTS.....</b>   | <b>66</b> |
| <b>3.1</b> | <b>Induced pluripotent stem cells.....</b>  | <b>67</b> |
| 3.1.1      | Patient tissue-derived cell lines.....  | 67        |
| 3.1.2      | Characterization of induced pluripotent stem cell clones.....                         | 68        |
| 3.1.2.1    | Transgene silencing and endogenous gene expression.....                               | 68        |
| 3.1.2.2    | Confirmation of pluripotency.....   | 72        |
| 3.1.2.3    | Genotyping of generated induced pluripotent stem cell clones.....                     | 73        |
| 3.1.3      | Assessment of growth rate.....  | 74        |
| 3.1.4      | Phenotypic studies of cell organelles and compartments.....                           | 75        |
| 3.1.4.1    | Immunofluorescence .....  | 75        |
| 3.1.4.2    | Western blot analysis .....   | 77        |
| 3.1.4.3    | Electron microscopy.....  | 80        |
| 3.1.5      | Tripeptidyl peptidase I enzyme activity in human induced pluripotent stem cells ..... | 81        |
| <b>3.2</b> | <b>Neural progenitor cells.....</b>   | <b>82</b> |
| 3.2.1      | Derivation of neural progenitor cells from induced pluripotent stem cells.....        | 82        |
| 3.2.2      | Confirmation of neural progenitor identity.....                                       | 83        |
| 3.2.3      | Phenotypic studies of cell organelles in neural progenitor cells .....                | 88        |
| 3.2.3.1    | Immunofluorescence .....  | 88        |
| 3.2.3.2    | Western blot analysis .....   | 91        |
| 3.2.3.3    | Electron microscopy.....  | 95        |
| 3.2.4      | Tripeptidyl peptidase I enzyme activity in neural progenitor cells .....              | 97        |
| 3.2.5      | Assessment of cell death in neural progenitor cells .....                             | 98        |
| <b>3.3</b> | <b>Mature neurons.....</b>  | <b>98</b> |
| 3.3.1      | Differentiation of neural progenitor cells into mature neurons .....                  | 98        |
| 3.3.2      | Assessment of cell death in neuronal cultures.....                                    | 101       |
| 3.3.3      | Phenotypic studies of cell organelles and compartments in neuronal cultures .....     | 102       |
| 3.3.3.1    | Immunofluorescence .....  | 102       |
| 3.3.3.2    | Western blot analysis .....   | 106       |
| 3.3.3.3    | Electron microscopy.....  | 108       |
| 3.3.4      | Astrocytes in neuronal cultures.....  | 111       |

---

|            |  |            |
|------------|--|------------|
| <b>4</b>   | <b>DISCUSSION .....</b>  | <b>113</b> |
| <b>4.1</b> | <b>Modeling neuronal ceroid lipofuscinosis.....</b>                    | <b>113</b> |
| 4.1.1      | Juvenile neuronal ceroid lipofuscinosis disease model .....            | 116        |
| 4.1.2      | Late infantile neuronal ceroid lipofuscinosis disease model .....      | 120        |
| <b>4.2</b> | <b>The established disease models represent early phenotypes .....</b> | <b>122</b> |
| <b>5</b>   | <b>SUMMARY.....</b>  | <b>124</b> |
| <b>6</b>   | <b>REFERENCES.....</b>   | <b>125</b> |
| <b>7</b>   | <b>ACKNOWLEDGMENTS .....</b>   | <b>137</b> |
| <b>8</b>   | <b>VERSICHERUNG UND ERKLÄRUNG.....</b>                                 | <b>138</b> |

---

## Abbreviations

|        |  |
|--------|--|
| ANOVA  | Analysis of variance                     |
| AP     | Alkaline phosphatase                     |
| ATP    | Adenosine triphosphate                   |
| BDNF   | Brain-derived neurotrophic factor        |
| BrdU   | 5-bromo-2'-deoxyuridine                  |
| BSA    | Bovine serum albumin                     |
| cAMP   | Cyclic adenosine monophosphate           |
| CLN    | Ceroid-lipofuscinosis, neuronal          |
| CM     | Conditioned media                        |
| COX IV | Cytochrome c oxidase subunit IV          |
| DAPI   | 4',6-Diamidino-2-phenylindol             |
| DMEM   | Dulbecco's modified eagle medium         |
| DMSO   | Dimethyl sulfoxide                       |
| DPBS   | Dulbecco's phosphate buffered saline     |
| EB     | Embryoid body                            |
| EDTA   | Ethylenediaminetetraacetic acid          |
| EEA-1  | Early endosome antigen 1                 |
| EGF    | Epidermal growth factor                  |
| EM     | Electron microscopy                      |
| ER     | Endoplasmic reticulum                    |
| ESC    | Embryonic stem cell                      |
| FGF2   | Fibroblast growth factor 2               |
| GAG    | Group-specific antigen                   |
| GAPDH  | Glyceraldehyde-3-phosphate dehydrogenase |
| GFAP   | Glial fibrillary acidic protein          |
| GM130  | Golgin A2                                |
| GRP75  | Mortalin                                 |
| HEK    | Human embryonic kidney                   |
| iPSC   | Induced pluripotent stem cell            |
| JNCL   | Juvenile neuronal ceroid lipofuscinosis  |



---

|        |  |
|--------|--|
| KLF4   | Kruppel-like factor 4  |
| KRT18  | Keratin 18   |
| LAMP-1 | Lysosomal-associated membrane protein 1                      |
| LINCL  | Late infantile neuronal ceroid lipofuscinosis                |
| MAP2ab | Microtubule-associated protein 2                             |
| MEF    | Mouse embryonic fibroblast                                   |
| MYC    | Myelocytomatosis viral oncogene homolog                      |
| NPC    | Neural progenitor cell                                       |
| OCT4   | Octamer transcription factor 4                               |
| PAX6   | Paired box 6   |
| PBS    | Phosphate buffered saline                                    |
| PDI    | Protein disulfide isomerase                                  |
| PFA    | Paraformaldehyde   |
| PLO/L  | Poly-L-ornithine/laminin                                     |
| POL    | Polymerase   |
| PVDF   | Polyvinylidene fluoride                                      |
| qPCR   | Quantitative real-time polymerase chain reaction             |
| RT     | Room temperature   |
| SDS    | Sodium dodecyl sulfate                                       |
| SEM    | Standard error of the mean                                   |
| SHH    | Sonic hedgehog   |
| SMA    | Smooth muscle actin  |
| SOX    | Sex determining region Y-box                                 |
| SSEA   | Stage-specific embryonic antigen                             |
| T      | Brachyury homolog  |
| TAE    | Tris-acetate- ethylenediaminetetraacetic acid                |
| TBS    | Tris-buffered saline   |
| TPP1   | Tripeptidyl peptidase I                                      |
| TRA    | Tumor-related antigen  |
| TUJ1   | Neuron-specific class III beta-tubulin                       |
| TUNEL  | Terminal deoxynucleotidyl transferase dUTP nick end labeling |
| VSV-G  | Vesicular stomatitis virus G protein                         |

# 1 Introduction

## 1.1 Neuronal ceroid lipofuscinoses

The neuronal ceroid lipofuscinoses (NCLs) comprise a group of genetically distinct lysosomal storage disorders with onset mostly during childhood. NCLs are autosomal recessive, with the exception of rare, adult-onset dominant forms, and represent the most common inherited neurodegenerative diseases of childhood. Their prevalence strongly varies ethnically and geographically and ranges from 0.1 to 7 in 100,000 live births (Santavuori, 1988; Uvebrant *et al.*, 1997). The clinical spectrum of symptoms includes mental and motor deterioration, epilepsy, visual loss, in most cases, ataxia and premature death (Haltia, 2003). The hallmark of all forms of NCLs is the accumulation of autofluorescent storage material in multiple tissues, including neurons. However, the ultrastructure of storage material found in various tissues, differs in the different subtypes of NCLs, making it a valuable tool in clinical diagnostics (Rapola, 1993). Distinctions are made between granular osmiophilic deposits (GROD) and organized storage material such as fingerprint, curvilinear, and rectilinear deposits (Kousi *et al.*, 2012). Since the storage material consists of unmodified, natural compounds normally found in cells, it clearly delimits the NCLs from neurodegenerative disorders occurring during old age such as Alzheimer's, Parkinson's and Huntington's disease in which the accumulated proteins are structurally and/or chemically modified, although the storage is not believed to be of lysosomal origin in these disorders.

In addition to the broad clinical spectrum, NCLs are as well characterized by a genetic heterogeneity. Until recently, nine NCL-associated genes were known. The resulting subtypes of NCLs were historically classified based on age of onset, clinical symptoms and neuropathology. More recent nomenclatures comprise the mutated gene which denotes the specific subtype (Kousi *et al.*, 2012). The following table (Table 1.1) shows an assembly of the current state of knowledge about the different subtypes of NCLs including four very recent described forms of NCL (table adapted and modified from Kousi *et al.*, 2012 and Wisniewski *et al.*, 2001).

**Table 1.1: Overview of the spectrum of neuronal ceroid lipofuscinoses**

| Gene                       | Age of onset        | Eponym  | Diseases   | Former abbreviation   |
|----------------------------|---------------------|---|--|-----------------------|
| CLN1/PPT1                  | Birth – 37 years    | Haltia-Santavuori   | CLN1 disease, classic infantile<br>CLN1 disease, late infantile<br>CLN1 disease, juvenile<br>CLN1 disease, adult | INCL<br>JNCL/GROD     |
| CLN2/TPP1                  | 2 – 8 years         | Janský-Bielschowsky   | CLN2 disease, classic late infantile<br>CLN2 disease, juvenile<br>CLN2 disease, infantile                        | LINCL                 |
| CLN3                       | 4 – 10 years        | Spielmeier-Sjögren  | CLN3 disease, classic juvenile<br>CLN3 disease, protracted<br>CLN3 disease, infantile                            | JNCL                  |
| CLN4/DNAJC5                | ~30 years           | Kufs (type A or type B) or Parry                                      | Adult (autosomal recessive) NCL disease or Kufs<br>Adult (autosomal dominant) NCL disease or Parry               | ANCL<br>ANCL          |
| CLN5                       | 4 – 7 years         | Finnish variant late infantile  | CLN5 disease, late infantile variant<br>CLN5 disease, juvenile<br>CLN5 disease, adult<br>CLN5 disease, infantile | vLINCL                |
| CLN6                       | 18 months – 8 years | Lake-Cavanagh early juvenile variant or Indian variant late infantile | CLN6 disease, late infantile variant<br>CLN6 disease, adult or Kufs type A                                       | vLINCL<br>Kufs type A |
| CLN7/MFSD8                 | 1 – 6 years         | Turkish variant late infantile  | CLN7 disease, late infantile variant<br>CLN7 disease, juvenile   | vLINCL                |
| CLN8                       | 5 – 10 years        | Variant late infantile and Northern epilepsy/EPMR                     | CLN8 disease, late infantile variant,<br>CLN8 disease, EPMR  | vLINCL<br>EPMR        |
| CLN9 <sup>1</sup>          |                     |   |  |                       |
| CLN10/CTSD                 | congenital          | Congenital  | CLN10 disease, congenital<br>CLN10 disease, juvenile   | CNCL                  |
| CLN11/GRN <sup>2</sup>     | 22-23 years         |   |  |                       |
| CLN12/ATP13A2 <sup>3</sup> | 13-16 years         |   |  |                       |
| CLN13/CTSF <sup>4</sup>    | 20-30 years         | Kufs type B   |  |                       |
| CLN14/KCTD7 <sup>5</sup>   | 8 months            |   |  |                       |

ANCL, adult onset neuronal ceroid lipofuscinosis; ATP13A2, ATPase type 13A2; CLN, ceroid-lipofuscinosis, neuronal; CNCL, congenital neuronal ceroid lipofuscinosis; CTSD, cathepsin D; CTSF, cathepsin F; DNAJC5, DnaJ homolog, subfamily C, member 5; EPMR, progressive epilepsy with mental retardation; GRN, granulin; GROD, granular osmiophilic deposits; INCL, infantile neuronal ceroid lipofuscinosis; JNCL, juvenile neuronal ceroid lipofuscinosis; KCTD7, potassium channel tetramerisation domain containing 7; LINCL, late infantile neuronal ceroid lipofuscinosis; vLINCL, variant late infantile neuronal ceroid lipofuscinosis; MFSD8, major facilitator superfamily domain containing 8; PPT1, palmitoyl-protein thioesterase 1; TPP1, tripeptidyl peptidase I

<sup>1</sup> provisionally assigned to a variant juvenile onset of NCL described by Schulz *et al.*, 2004 but now reclassified to as CLN5 disease (Haddad *et al.*, 2012, unpublished data)

<sup>2</sup> very recent mutation described by Smith *et al.*, 2012b

<sup>3</sup> very recent mutation described by Bras *et al.*, 2012

<sup>4</sup> very recent mutation described by Smith *et al.*, 2012a (unpublished data)

<sup>5</sup> very recent mutation described by Staropoli *et al.*, 2012

Although mutations in different genes can cause NCL, the encoded proteins affected can be classified into two main groups. The first group encodes soluble lysosomal proteins (*PPT1*, *TPP1*, *CTSD* and *CLN5*) and the second group encodes transmembrane proteins that reside either within the lysosomes (*CLN3* and *MFSD8*) or within the endoplasmic reticulum (*CLN6*

---

and *CLN8*) (Jalanko *et al.*, 2009). In addition, there is a correlation between the ultrastructure and the main component of storage material. For example, granular osmiophilic deposits are mainly composed of saposins (primarily variants A and D), which are sphingolipid activator proteins, whereas the predominant protein found in fingerprint, curvilinear and rectilinear profiles is the subunit c of the mitochondrial ATP synthase  $F_0$  (Cotman *et al.*, 2012, Jalanko *et al.*, 2009).

Despite the fact that NCL proteins are expressed ubiquitously, neurons are mostly affected by mutations in NCL causing genes. To date, there are no existing therapies that could cure any of the different NCLs. So far, treatment of the NCLs is limited to symptomatic management, although several clinical trials are in progress, including enzyme replacement therapy for TPP1 deficiency (Sibigroth *et al.*, 2012; Tecedor *et al.*, 2012; unpublished data).

### 1.1.1 Late infantile neuronal ceroid lipofuscinosis

Mutations in the *TPP1* gene cause classic late infantile CLN2 (LINCL) or Jansky-Bielschowsky disease. To date, 89 mutations and 22 polymorphisms, that are associated with LINCL, are known (Kousi *et al.*, 2012). The two most common mutations are the intron change c.509-1 G>C which leads to an aberrant splicing and the nonsense mutation c.622 C>T, p.Arg208X (Jalanko *et al.*, 2009). The age of onset varies between 2 and 8 years and clinical features include seizures, ataxia and myoclonus. In contrast to patients suffering from JNCL, vision loss occurs late during the course of disease (Steinfeld *et al.*, 2002). The hallmark of LINCL are curvilinear profiles which are found in lysosomal residual bodies. The storage material mainly consists of subunit c of the mitochondrial ATP synthase  $F_0$ , although saposins A and D are found as well to a lesser extent (Jalanko *et al.*, 2009).

*TPP1* encodes the protein tripeptidyl peptidase I (TPP1). All mutations result in a complete loss or marked deficiency in enzyme activity. Thus, a definitive diagnosis is made based on an enzymatic test for TPP1 activity, followed by the detection of mutations within the *TPP1* gene (Golabek *et al.*, 2006).

#### 1.1.1.1 Tripeptidyl peptidase I

The human gene encoding TPP1 consists of 13 exons spanning 6.65 kb (Liu *et al.*, 1998) and was mapped to chromosome 11p15 (Sharp *et al.*, 1997). TPP1, a lysosomal pepstatin-insensitive carboxypeptidase, is synthesized as an inactive 67 kDa precursor which is then

---

autocatalytically converted to an active 46 kDa mature enzyme (Lin *et al.*, 2001). TPP1 is expressed ubiquitously in human tissue with the highest levels found in heart and placenta. Interestingly, TPP1 enzyme activity does not always reflect its expression levels which suggests tissue-specific factors that regulate enzyme activity *in vivo* (Golabek *et al.*, 2006). The enzyme has a broad substrate specificity and it was shown, at least *in vitro*, to participate in bone resorption (Page *et al.*, 1993). TPP1 cleaves tripeptides from the amino terminus of small, unstructured oligopeptides of <5 kDa at an optimal pH of 4.0-4.5 (Vines *et al.*, 1998; Bernardini *et al.*, 2001). Further studies suggested an endopeptidase activity at pH 3.0 (Ezaki *et al.*, 2000). Nonetheless, the nature of storage material found in LINCL patient tissues does not provide immediate clues to the natural substrate of TPP1. However, one study demonstrated that subunit c serves as a substrate for TPP1 (Ezaki *et al.*, 1999). As with most of the NCLs, the lysosomal storage material mainly consists of the subunit c of the mitochondrial ATP synthase, which was shown to be indistinguishable from subunit c isolated from mitochondria (Chen *et al.*, 2004). So far, the exact mechanism of action and the specific role of TPP1 in LINCL are unknown, but storage of the intact molecule of subunit c in lysosomes of LINCL patients suggests that TPP1 might initiate its degradation (Golabek *et al.*, 2006).

### 1.1.2 Juvenile neuronal ceroid lipofuscinosis

The juvenile neuronal ceroid lipofuscinosis (JNCL) also known as Batten disease, usually occurs at an age of onset of 4 – 10 years. First symptoms include progressive visual loss from pigmentary retinopathy, followed by loss of motor coordination, mental decline and seizures. Later on, behavioral abnormalities might occur accompanied by hallucinations and/or neuropsychiatric symptoms (Kousi *et al.*, 2012). As is characteristic for all NCLs, the hallmark for JNCL is intracellular autofluorescent storage material. In the case of JNCL, the ultrastructure of storage material appears as fingerprint profiles or as a combination of fingerprint and curvilinear profiles (Santavuori, 1988). The subunit c of the mitochondrial ATP synthase was found to be the major component of the storage material (Palmer *et al.*, 1992).

To date, 59 mutations and nine polymorphisms are associated with JNCL. The most common mutation which causes approximately 81% of JNCL cases reported is a homozygous 1.02 kb deletion spanning exons seven and eight of the ceroid-lipofuscinosis, neuronal 3 (CLN3) gene, namely c.461-280\_677+382del966 (Kousi *et al.*, 2012).

### 1.1.2.1 The ceroid-lipofuscinosis, neuronal 3 protein

*CLN3* was mapped to chromosome 16p12.1 (Eiberg *et al.*, 1989). The *CLN3* protein, which is also referred to as Battenin, consists of 438 amino acids. The very hydrophobic nature of the *CLN3* protein renders functional and structural studies complicated. However, computational tools predict six transmembrane domains with both, amino and carboxyl, termini facing the cytoplasm (Mao *et al.*, 2003, Nugent *et al.*, 2008). Due to the transmembrane topology of the protein, it is furthermore predicted to have three large luminal loops, one which may contain an amphipathic helix, and one large cytoplasmic loop (Nugent *et al.*, 2008). The following figure represents a very simple illustration of the predicted *CLN3* protein structure (Figure 1.1).

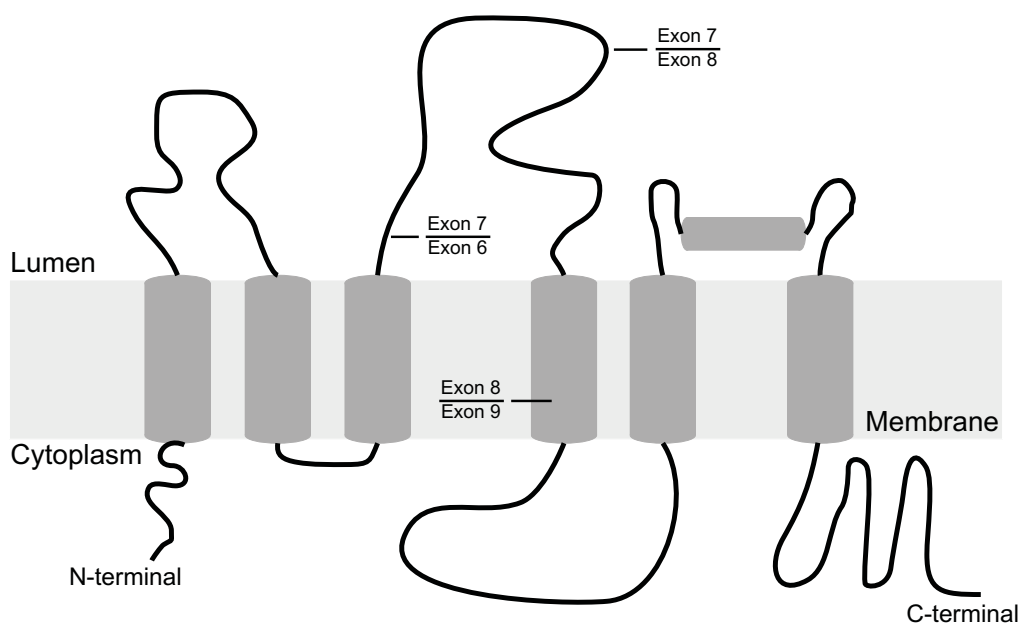


**Figure 1.1: Schematic model of the human *CLN3* protein structure**

Human *CLN3* is a transmembrane protein predicted to have six transmembrane domains, three luminal and one large cytoplasmic loop. The amino- and carboxyl-termini face the cytoplasm. The common 1.02 kb deletion removes exons seven and eight and leads to a frameshift and premature stop codon. (Figure adapted from Nugent *et al.*, 2008 and Cotman *et al.*, 2012)

The most common mutation within the *CLN3* gene associated with JNCL is a 1.02 kb deletion which leads to the deletion of the adjacent exons 7 and 8 (Figure 1.1). Studies suggested that this mutation causes a truncated protein or a spliced variant lacking exons 7 and 8 which bears residual function rather than a complete loss of the protein function (Kitzmuller *et al.*, 2008).

Although studies on *CLN3* protein localization are complicated because of the hydrophobic nature of the protein, it is widely believed that *CLN3* protein primarily localizes to late

---

endosomal and lysosomal membranes (Cotman *et al.*, 2012). As with TPP1, the function of CLN3 in the context of JNCL is unknown, so far. But the highly conserved sequence among eukaryotes suggests that the cellular function might be conserved as well (Taschner *et al.*, 1997). More recent studies suggest a possible role of CLN3 protein within the endosomal-lysosomal pathway as well as a possible regulatory role in post-Golgi anterograde and retrograde trafficking (reviewed by Cotman *et al.*, 2012).

### 1.1.3 Model systems for late infantile and juvenile neuronal ceroid lipofuscinosis

To date, only a handful of model systems are established for LINCL. There are reports on a Dachshund model with a frame-shift mutation within the *Tpp1* gene that exhibits neurological decline similar to that seen in LINCL patients (Awano *et al.*, 2006; Sanders *et al.*, 2010). Furthermore, a mouse model has been established by Sleat *et al.* (2004) which faithfully reproduces the neuropathology observed in LINCL patients. *Tpp1* mutant mice, generated by targeted disruption of the *Tpp1* gene, develop progressive locomotor dysfunction, followed by seizures at later age, and analysis of accumulated autofluorescent material revealed curvilinear profiles (Sleat *et al.*, 2004). Based on the *Tpp1*-targeted mouse model, *Tpp1* mouse hypomorphs were created (Sleat *et al.*, 2008). This mouse model, expressing various amounts of *Tpp1* protein, could show that even residual amounts of enzyme activity ameliorate the course of disease in the LINCL mouse model. However, despite the fact that neuropathology is well established in these model systems it still remains unknown which function of *Tpp1* deficiency mediates neurodegeneration.

In contrast to LINCL, many more model systems are established for JNCL. These include yeast and four distinct mouse models as well as very recent studies in *Drosophila* (Tuxworth *et al.*, 2011). The mouse models comprise two *Cln3* knockout variants (Greene *et al.*, 1999; Katz *et al.*, 2008) as well as two different *Cln3* knock-in models (Cotman *et al.*, 2002; Ding *et al.*, 2011); of these only the *Cln3*<sup>Δex7/8</sup> knock-in model established by Cotman *et al.*, 2002, truly recapitulates the genotype underlying most of the JNCL cases reported. As reported for LINCL mouse models, *Cln3* mutant mice recapitulate the course of disease seen in JNCL patients. However, this varies between the different mouse models and it is yet unknown if this fact is attributed to the different genotypes or the background of the mice used. However, these models could provide insight into the localization and possible function of CLN3 protein. Although it is believed to be mainly localized to lysosomes and endosomes, CLN3 was also proposed to be localized to the plasma membrane, Golgi, mitochondria, the cell

---

nucleus and synapses (reviewed by Getty *et al.*, 2011). Studies on cerebellar cells from *Cln3* <sup>$\Delta$ ex7/8</sup> knock-in mice suggested a function for the CLN3 protein within the autophagy pathway (Cao *et al.*, 2006). In yeast, the CLN3 orthologue Btn1 was shown to regulate lysosomal pH (Pearce *et al.*, 1999) and very recently the endosome-Golgi retrograde transport (Pearce *et al.*, 1999; Kama *et al.*, 2011).

Taken together, the existing model systems for LINCL and JNCL do recapitulate major aspects of the course of disease seen in patients and are a powerful tool to get first insights into the possible function of the proteins underlying these diseases. However, there is no human model for the disease available to date. Furthermore, none of the systems listed above could provide a suitable platform for drug screenings which could directly be used for clinical trials since none of these model systems is based on patient-derived cells.

## 1.2 Induced pluripotent stem cells

The term induced pluripotent stem cells (iPSCs), describes a finally differentiated somatic cell that has been reset to an embryonic stem cell (ESC) like state by introduction of defined transcription factors. Thus, iPSCs are just like ESCs able to give rise to any kind of cell type. These cells were first generated and described by Takahashi and Yamanaka in 2006 (Takahashi *et al.*, 2006). They narrowed down a set of 24 candidate genes to four transcription factors that were then introduced, using retroviral vectors, into mouse embryonic and adult fibroblasts. The transcription factors that were able to reset cells to an ESC-like state were *Pou5f1*, *Sox2*, *c-Myc* and *Klf4*. To date, this process is called reprogramming and the four factors are also referred to as Yamanaka factors. Only one year later, the generation of iPSCs from adult human fibroblasts, using the same set of four transcription factors, was reported (Takahashi *et al.*, 2007). Since that breakthrough, an entire scientific field has been established which was dedicated to the modification and improvement of the reprogramming process. Indeed, it appears that the method of factor delivery is not critical. Several groups successfully generated iPSCs using non-retroviral vector systems such as excisable polycistronic vectors (Sommer *et al.*, 2010), piggyBac transposons (Woltjen *et al.*, 2009), transient episomal delivery (Okita *et al.*, 2008) as well as RNA (Warren *et al.*, 2010) and even protein delivery (Kim, D. *et al.*, 2009; Zhou *et al.*, 2009).

Similar to the advances made in the reprogramming process itself, researchers have broadened the spectrum of tissue that can be used for the purpose of reprogramming somatic cells into iPSCs. In addition to human fibroblasts, iPSCs can nowadays also be generated from



keratinocytes (Aasen *et al.*, 2008), dental tissue (Yan *et al.*, 2010) and peripheral blood T lymphocytes (Brown *et al.*, 2010). That leads to the assumption that any cell from the human body might be converted into an ESC-like state which would then in return give rise to any cell type of the human body. The only restriction herein is the tissue accessibility.

Figure 1.2 summarizes the sources for derivation of human iPSCs, the various methods available for their generation, and shows options for further differentiation.

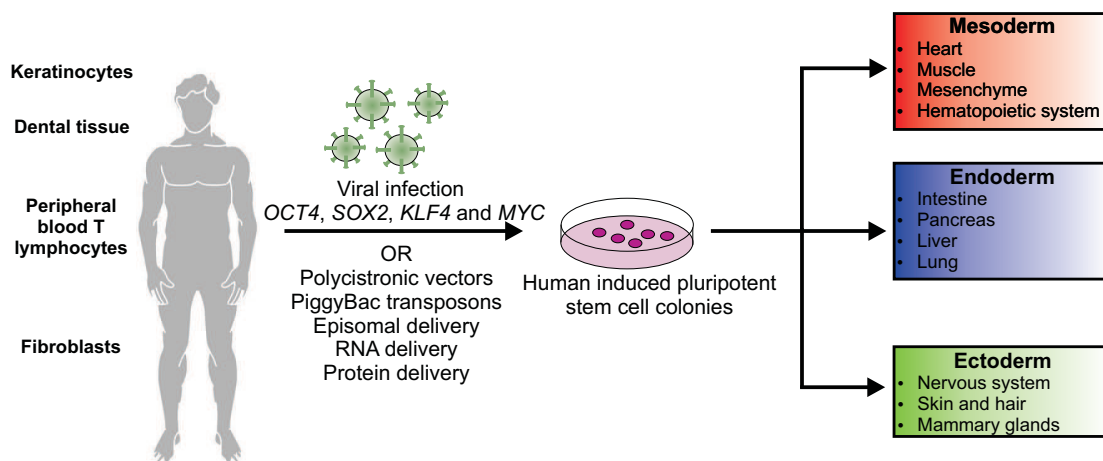


**Figure 1.2: Derivation of human induced pluripotent stem cells**

Human induced pluripotent stem cells (iPSCs) can be derived from various tissues. Nowadays, multiple methods are available for their generation. Since iPSCs are pluripotent, they can give rise to any cell type of the human body, which makes them a valuable tool for research and clinical applications.

### 1.2.1 Characterization of induced pluripotent stem cells

In order to confirm the resemblance of induced pluripotent stem cells to embryonic stem cells in terms of global gene expression, epigenetic profile, long-term self-renewal capacity, and developmental potential, a number of tests proving their pluripotency have been performed. In their original publication, Takahashi *et al.* (2007) performed a couple of tests that were, at that time, established to prove pluripotency in ESCs. iPSCs were chosen according to their morphology, which resembled ESC morphology. Colonies were then tested for expression of human ESC-specific proteins. These include stage-specific embryonic antigen (SSEA) 3 and 4 as well as expression of NANOG and the tumor-related antigen (TRA)-1-60, 1-80 and 2-49/6E. Furthermore, they analyzed gene expression of ESC marker genes such as *POU5F1* (also known as *OCT4*), *SOX2*, *NANOG*, *MYC* and *LIN28A*. In addition to these individual gene expression results, the authors also included a global gene expression pattern analysis

with oligonucleotide DNA microarrays, which showed strong similarity, at the level of gene expression, between human iPSCs and human ESCs. Epigenetic analysis, using bisulfite sequencing of the promoter regions showed that the promoters for *POU5F1*, *REX1* and *NANOG* were highly unmethylated demonstrating that they were open for transcription. Another important aspect of pluripotency is the differentiation into cell types derived from the three germ layers. This was shown, *in vitro*, through formation of so-called embryoid bodies which could then be differentiated into cells derived from meso-, endo- and ectoderm. In order to demonstrate pluripotency *in vivo*, iPSCs were injected subcutaneously into the dorsal flanks of immunodeficient mice. Teratoma formation, a tumor that consists of cells from all three germ layers, demonstrated the pluripotency of generated iPSCs *in vivo*. Later on, showing that the retroviral vectors have been silenced and that the ESC-specific enzyme alkaline phosphatase (AP) was reactivated became very meaningful (Maherali *et al.*, 2007; Hotta *et al.*, 2008). Due to the fact that since their first generation, iPSCs have been generated in various laboratories using different methods and tissues leading to a standardized procedure for generation of iPSCs, the experiments that are needed to prove their pluripotent state have been narrowed down to a minimum. Currently, the experiments which still need to be performed include proof of pluripotency by AP enzyme activity assay, and demonstration of core iPSC marker expression at the DNA and protein level. Furthermore, retroviral silencing of the reprogramming factors should be assessed. In order to demonstrate their capability to differentiate into cells derived from the three germ layers, embryoid body (EB) formation and subsequent differentiation are widely accepted to be sufficient.

### **1.2.2 Neuronal differentiation of induced pluripotent stem cells**

Human induced pluripotent stem cells harbor the exceptional feature that they can give rise to any cell type of the human body. This includes neural cell types, which can not be studied under non-pathological circumstances. This fact makes iPSCs a valuable tool for studying neural development or human neurodegenerative disorders. However, a central challenge in using these iPSCs as source for neurons is the directed differentiation into the desired cell type. Numerous developmental decisions have to be made before a pluripotent stem cell differentiates into a post-mitotic neuron. Similar to ESCs, directed neuronal differentiation of iPSCs follows three major developmental steps: neural induction, differentiation, and fate specification. In practice, these steps are realized through formation of embryoid bodies, neural rosettes and neural precursor cells (NPCs) which will, upon treatment with specific

factors, give rise to mature neurons. Figure 1.3 describes the differentiation of human iPSCs into various neuronal cell types.

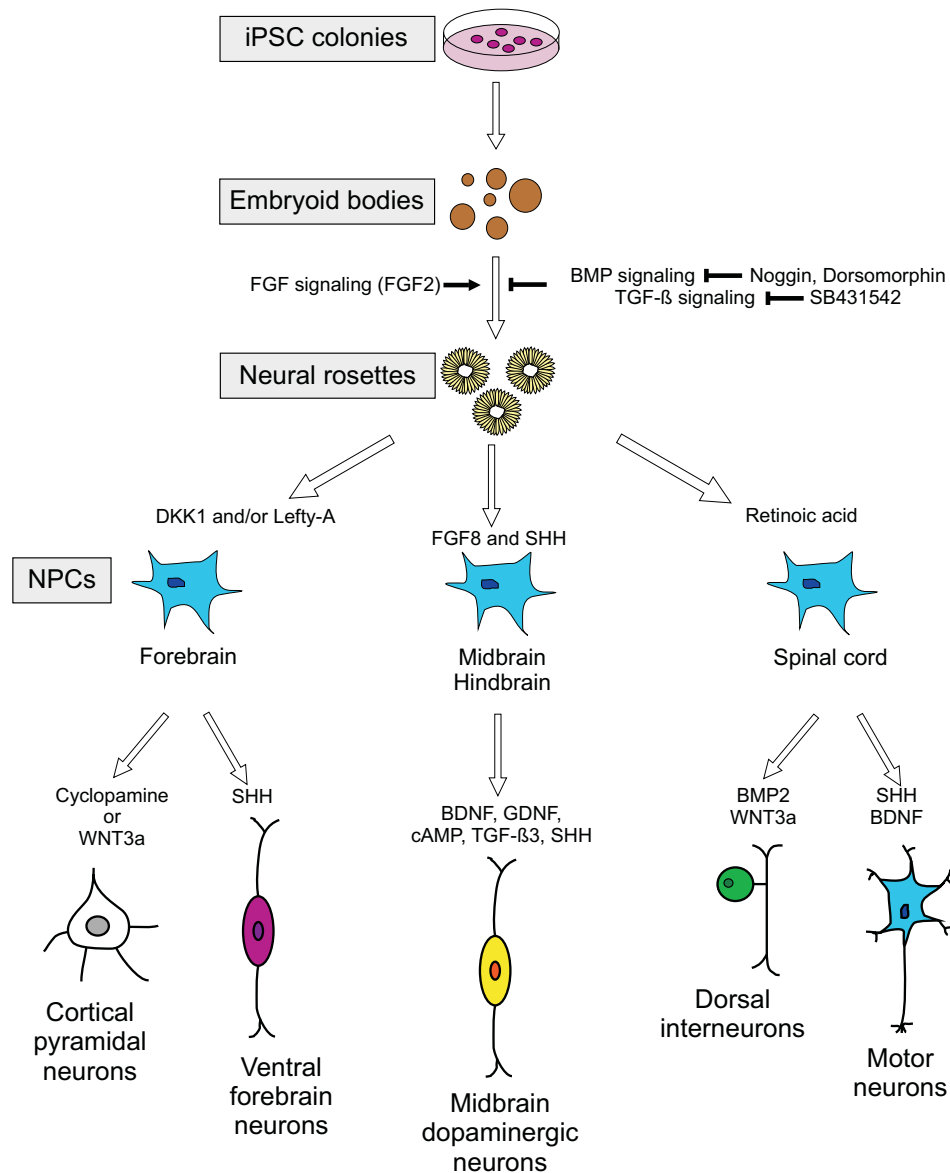


**Figure 1.3: Schematic representation of neuronal differentiation of induced pluripotent stem cells**

Human iPSCs can give rise to numerous neuronal cell types. Generation of post-mitotic neurons from human iPSCs is achieved by neural induction, differentiation, and fate specification. Inhibition and activation of specific developmental pathways drives neural rosettes towards a neuroectodermal fate. Further patterning of NPCs will determine their neuronal fate. Only the main inducers of fate specification are shown. Detailed information is given in the main text. (Figure adapted from Gaspard *et al.*, 2010). BDNF, brain-derived neurotrophic factor; BMP, bone morphogenetic protein; cAMP, cyclic adenosine monophosphate; DKK1, Dickkopf1; FGF, fibroblast growth factor; GDNF, glial cell derived neurotrophic factor; iPSC, induced pluripotent stem cell; NPC, neural progenitor cell; SHH, sonic hedgehog; TGF, transforming growth factor; WNT, wingless-type mouse mammary tumor virus integration site family.

Before a pluripotent stem cell can be directed towards a neuroectodermal fate, a transition from the pluripotent to the primitive ectodermal state needs to take place. This transition and subsequent adoption of the neuroectodermal fate can be achieved by inhibition of bone morphogenic protein (BMP) and transforming growth factor- $\beta$  (TGF- $\beta$ ) signaling (Chambers *et al.*, 2009) and activation of the fibroblast growth factor (FGF) pathway. Small molecules known to act on these pathways are Noggin and Dorsomorphin, inhibitors of BMP signaling, and SB431542, which is an inhibitor of TGF- $\beta$  signaling. An early intermediate between neuroectodermal tissue and neurons is the neural rosette. This structure is composed of radially organized columnar epithelial cells that express a broad range of neural stem cell specific marker proteins such as PAX6, SOX1, NCAM and Nestin (Elkabetz *et al.*, 2008b). Neural rosettes are rapidly proliferating and they are capable of being patterned into neural tissue that is specific to different regions of the central nervous system namely forebrain, midbrain/hindbrain and spinal cord. After initial patterning of neural rosettes, neural precursor cells can be isolated and propagated for further fate specification. Using this approach, it was shown that iPSCs can be differentiated into motor neurons by treatment with brain-derived neurotrophic factor (BDNF), retinoic acid, and sonic hedgehog (SHH) (Dimos *et al.*, 2008; Karumbayaram *et al.*, 2009). In order to differentiate iPSC-derived neural rosettes into dopaminergic neurons which reside in the midbrain/hindbrain region a multistep differentiation protocol is required involving patterning with BDNF, ascorbic acid, SHH and fibroblast growth factor 8 (FGF8) followed by treatment of neural precursor cells with BDNF, glial cell derived neurotrophic factor (GDNF), ascorbic acid, TGF- $\beta$ 3 and cyclic adenosine monophosphate (cAMP) (Cooper *et al.*, 2010; Chambers *et al.*, 2011). Differentiation of neural rosettes towards a forebrain fate usually involves patterning with Lefty-A and Dickkopf1 (DKK1) (Jin *et al.*, 2011; Tucker *et al.*, 2011). Further differentiation into cortical pyramidal neurons or ventral forebrain neurons involves treatment with cyclopamine and SHH according to studies performed on ESC- and iPSC-derived neural rosettes (Watanabe *et al.*, 2005; Zeng *et al.*, 2010). In order to generally differentiate iPSCs towards a neuroectodermal fate, selective inhibition of TGF- $\beta$  signaling with SB431542 followed by treatment of neural precursor cells with BDNF and ascorbic acid or cAMP gives rise to a broad spectrum of post-mitotic neurons (Chambers *et al.*, 2011; Falk *et al.*, 2012).

### 1.2.3 Human induced pluripotent stem cells for modeling neurodegenerative diseases

Clinical research that aims to elucidate the pathogenesis of human neurodegenerative diseases traditionally uses post-mortem tissue and/or transgenic animal model systems. However, post-mortem tissue is not always available and in addition, it represents the end stage of the disease. Transgenic mouse models have an important impact on the understanding of some pathological mechanisms. However, some of the models do not always fully recapitulate the diseased phenotype, leading to a need for a more accurate disease model. The discovery of human induced pluripotent stem cells and their potential for clinical applications has been of great interest to the medical and scientific communities. Although harboring the same pluripotent and therefore differentiation capacities as human ESCs, iPSCs possess a couple of advantages. First of all, they overcome the political and ethical issues related to the use of human ESCs. Since patient-derived, there will be no risk of immune rejection if iPSCs are therapeutically used. In addition, the fact that they are patient-derived offers a singular opportunity to physicians and scientists to model the disease *in vitro* on a patient-specific basis, enabling screenings for individual genomic differences. Indeed, their use could contribute to personalized medicine. The opportunity to study the course of disease *in vitro*, by means of phenotypic analyses, could lead to the determination of better therapeutic approaches. Thus, one of the main advantages in using iPSCs as disease model system is the fact that they mimic neurodegenerative disorders from the early stage of development. This might thus lead to an understanding how mutated genes alter cellular processes and therefore could provide new insights into the disease mechanism and the development of selective therapeutics.

Drug development is a very cost intensive and time consuming process, considering that a candidate drug needs to show efficacy in an animal model and clear three phases of clinical trials. In the worst case scenario, a drug that showed efficacy in an animal model may have little or no effect in patients. The use of patient-specific iPSCs may resolve a couple of difficulties connected to drug development. First of all, iPSCs can be generated for most of the common diseases. This is of special interest for neurodegenerative diseases since neurons are not easily available under normal conditions. Thus, the reprogramming technique allows researchers to generate iPSCs from diagnosed living patients which overcomes the restriction of accessibility of post-mortem tissue. Second, the chances for a candidate drug to work in patients are much higher when it was proven to be efficient in a human cell model. Drug screenings can be performed on iPSC-derived NPCs or mature neurons. Small scale drug

screenings using only a few components have already been performed on neurons derived from patients suffering from Rett syndrome (Marchetto *et al.*, 2010), Alzheimer's disease (Yagi *et al.*, 2011; Yahata *et al.*, 2011) and spinal muscular atrophy (Ebert *et al.*, 2009). These findings are very promising since they confirm the utility of iPSCs in drug screenings, which should soon include hundreds of components from different drug libraries.

Another important aspect of patient-derived iPSCs is their use in animal models. This provides a unique opportunity to test the functionality of iPSC-derived neurons *in vivo*. For example, it was shown that dopaminergic neurons derived from human iPSCs can improve symptoms in a rat model for Parkinson's disease (Wernig *et al.*, 2008; Hargus *et al.*, 2010). Furthermore, it was shown that iPSC-derived NPCs can functionally integrate into mouse models for spinal cord injury (Fujimoto *et al.*, 2012) and brain ischemia (Gomi *et al.*, 2012). These findings prove the functional integrity of human iPSC-derived NPCs and mature neurons.

Some neurodegenerative diseases are caused by a known genetic defect and are thus inherited. It might therefore be obvious that a correction of the genetic defect could improve the course of disease. Patient-derived iPSCs or derived progenitor cells are therefore a valuable tool to test this hypothesis. An and colleagues recently demonstrated that the disease phenotype of iPSCs derived from patients suffering from Huntington's disease was reversed through genetic correction, by replacement of the expanded CAG repeat with a normal repeat using homologous recombination (An *et al.*, 2012). This approach was also undertaken for various other diseases such as gyrate atrophy (Howden *et al.*, 2011), Duchenne muscular atrophy (Kazuki *et al.*, 2010) and  $\beta$ -thalassemia (Wang *et al.*, 2012). Although these groups corrected the genetic defect in the patient-derived iPSCs, it should also be considered that genetic correction might as well be possible in iPSC derivatives. However, the disease process in progenitor cells might be too advanced to be rescued by genetic manipulation. So far, no studies have been undertaken to investigate the best stage of differentiation for genetic correction.

Figure 1.4 represents an overview of potential applications of patient-specific iPSCs and their derivatives in modeling neurodegenerative diseases.

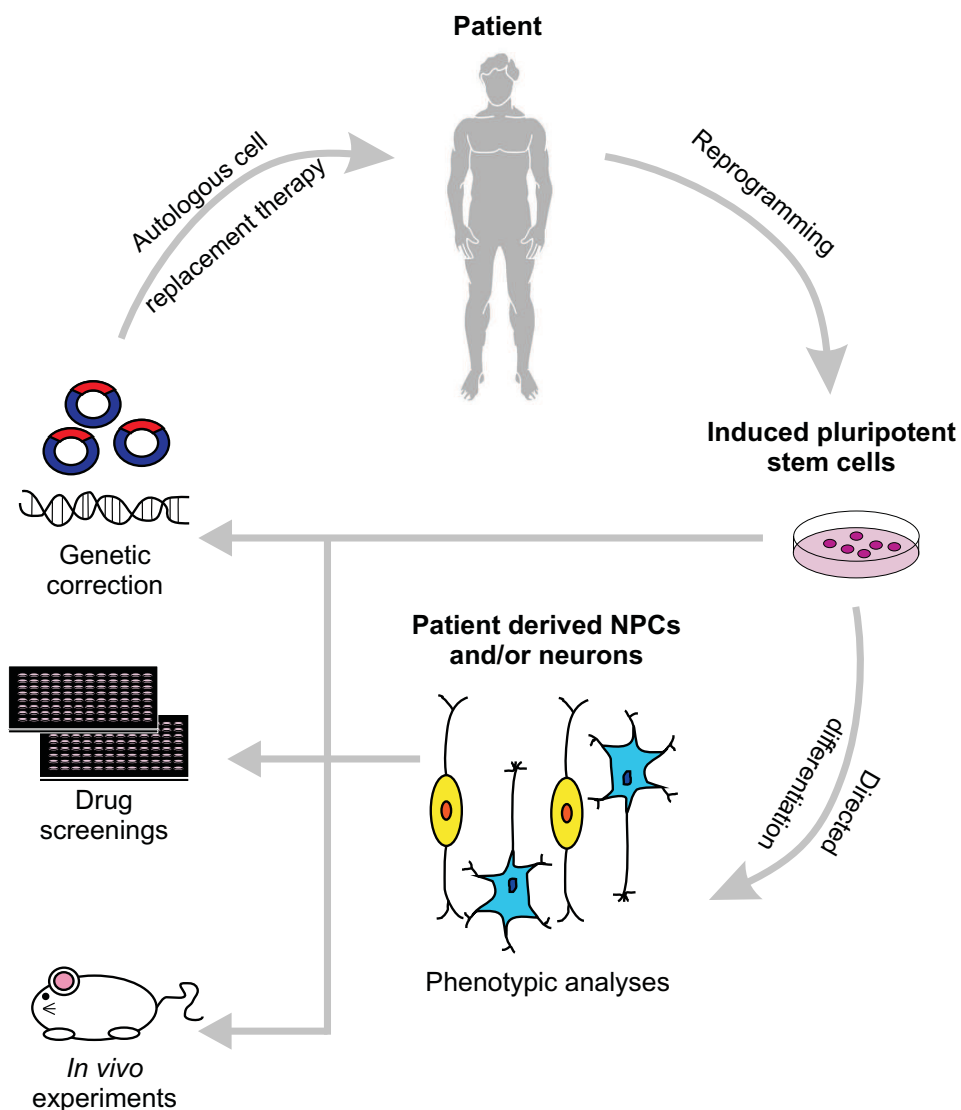


**Figure 1.4: Modeling neurodegenerative diseases using patient-specific induced pluripotent stem cells**

Patient-specific iPSCs offer multiple possibilities for disease modeling. Derived neural progenitor cells (NPCs) and neurons can be used in drug screenings, *in vivo* experiments, and might be suitable for genetic correction. The ultimate goal would be an autologous cell replacement therapy, which would avoid immune rejection and overcomes obstacles linked to the use of embryonic stem cells.

### 1.3 Objective

The overall aim of this thesis was to establish disease models for two forms of neuronal ceroid lipofuscinosis, namely late infantile (LINCL) and juvenile neuronal ceroid lipofuscinosis (JNCL), using patient-derived induced pluripotent stem cells. This thesis can thus be subdivided into three subprojects:

- 1) The first goal is to establish stable induced pluripotent stem cell lines derived from skin fibroblasts taken from patients suffering from LINCL or JNCL by means of retroviral introduction of *POU5F1*, *SOX2*, *KLF4* and *MYC*. This includes proof of pluripotency using established methods.
- 2) The second goal will be to derive neural progenitor cells from established induced pluripotent stem cell lines in order to obtain a self-renewing and proliferative population of neural stem cells for phenotypic analyses. Characterization of derived neural progenitor cells will be performed to ensure pure populations of neural progenitor cells.
- 3) Finally, neural progenitor cells will be differentiated into mature neurons with the hope of reproducing some of the NCL-related features *in vitro* in patient-specific neurons.

Since this will be the first report on NCL-derived induced pluripotent stem, neural progenitor cells, and mature neurons, this thesis will emphasize phenotypic studies based on the established animal models of NCL. The aim herein is to establish robust disease-related phenotypes that could be applied to future therapeutic screenings.



## 2 Materials and Methods

### 2.1 Materials

#### 2.1.1 Instruments

**Table 2.1: Instruments**

| <b>Instruments</b>   | <b>Company</b>                               |
|--|--|
| Analytical balance <i>SBA52</i>  | Scaltec Instruments GmbH, Göttingen, D       |
| Biosafety cabinet <i>Cleanwizard 100 V</i>                               | Kojair, Vilppula, FIN                        |
| Biosafety cabinet <i>Laminair<sup>®</sup> HB24448</i>                    | Heraeus Holding GmbH, Hanau, D               |
| Biosafety cabinet <i>Thermo Forma classII A/B3</i>                       | Thermo Fisher Scientific Inc., Waltham, USA  |
| Blotting equipment <i>Novex<sup>®</sup> Mini-Cell</i>                    | Life Technologies Corporation, Carlsbad, USA |
| Centrifuge <i>Mini Spin Plus</i>   | Eppendorf AG, Hamburg, D                     |
| Centrifuge <i>5810R</i>  | Eppendorf AG, Hamburg, D                     |
| Centrifuge <i>Heraeus Multifuge X 3R</i>                                 | Thermo Fisher Scientific Inc., Waltham, USA  |
| Confocal microscope <i>Leica TCS SP5</i>                                 | Leica Microsystems GmbH, Wetzlar, D          |
| Electrophoresis equipment <i>Peqlab 400708/401214</i>                    | Peqlab Biotechnologie GmbH, Erlangen, D      |
| Film processor <i>KODAK X-OMAT 2000A</i>                                 | KODAK Canada Inc., Toronto, CA               |
| Incubator <i>Hera Cell 150</i>   | Thermo Fisher Scientific Inc., Waltham, USA  |
| Incubator <i>Forma Series II HEPA class 100</i>                          | Thermo Scientific, Wilmington, USA           |
| Incubation shaker <i>Multitron 2</i>                                     | Infors AG, Bottmingen, CH                    |
| Microscope <i>Axioskop2 mot plus</i>                                     | Carl Zeiss AG, Oberkochen, D                 |
| Microscope <i>Leica DM IRE2</i>  | Leica Microsystems GmbH, Wetzlar, D          |
| Microscope <i>Nikon Eclipse TE2000-U</i>                                 | Nikon Inc., Melville, USA                    |
| Microscope <i>Nikon Eclipse TS100</i>                                    | Nikon Inc., Melville, USA                    |
| Power supply <i>Power Pac 300</i>  | Bio-Rad Laboratories, Hercules, USA          |
| Real-time PCR machine <i>LightCycler<sup>®</sup> MX300P<sup>TM</sup></i> | Stratagene <sup>®</sup> , La Jolla, CA, USA  |
| Real-time PCR machine <i>LightCycler<sup>®</sup> 480II</i>               | Roche Pharma AG, Grenzach-Wyhlen, D          |
| Shaking table <i>MAXI Rotor</i>  | Labline Scientific Instrument, Mumbai, India |
| Spectrophotometer <i>NanoDrop<sup>®</sup>, ND-1000</i>                   | Thermo Scientific, Wilmington, USA           |
| Spectrophotometer <i>SPECTRAmax M2</i>                                   | Molecular Devices Corp., Sunnyvale, USA      |
| Spectrophotometer <i>SPECTRAmax PLUS</i>                                 | Molecular Devices Corp., Sunnyvale, USA      |
| Thermocycler <i>Mastercycler<sup>®</sup> personal</i>                    | Eppendorf AG, Hamburg, D                     |
| Thermomixer <i>Thermomixer Comfort</i>                                   | Eppendorf AG, Hamburg, D                     |

---

|   |  |
|---|--|
| Tissue processor <i>Leica Lynx</i>                                | Leica Microsystems GmbH, Wetzlar, D    |
| Transmission electron microscope <i>FEI Morgagni<sup>TM</sup></i> | FEI, Hillsboro, USA                    |
| Ultramicrotome <i>LKB 8801</i>                                    | LKB Bromma, Bromma, SE                 |
| UV Transilluminator <i>Bioview</i>                                | Biostep GmbH, Jahnsdorf, D             |
| Water bath <i>Julambo SW22</i>                                    | JULAMBO Labortechnik GmbH, Seelbach, D |

---

### 2.1.2 Chemicals and reagents

**Table 2.2: Chemicals and reagents**

| <b>Name</b>   | <b>Company</b>   |
|---|--|
| Agarose   | Biozym Biotech Trading GmbH, Oldendorf, D                    |
| Ala-Ala-Phe-7-Amido-4-methylcoumarin                  | Sigma-Aldrich, St. Louis, USA                                |
| Ampicillin  | Carl Roth GmbH & Co. KG, Karlsruhe, D                        |
| Calcium Chloride                                      | Sigma-Aldrich, St. Louis, USA                                |
| cOmplete, Mini Protease Inhibitor Cocktail<br>Tablets | Roche Pharma AG, Grenzach-Wyhlen, D                          |
| DMSO  | Sigma-Aldrich, St. Louis, USA                                |
| Donkey Serum  | Jackson ImmunoResearch Laboratories Inc., West<br>Grove, USA |
| Dry Milk Powder                                       | LabScientific, Inc., Livingston, USA                         |
| EmbryoMax <sup>®</sup> 0.1% Gelatin Solution          | EMD Millipore, Billerica, USA                                |
| Ethanol   | Sigma-Aldrich, St. Louis, USA                                |
| Fugene <sup>®</sup> 6                                 | Roche Pharma AG, Grenzach-Wyhlen, D                          |
| Glacial Acetic Acid                                   | Sigma-Aldrich, St. Louis, USA                                |
| Glutaraldehyde  | Sigma-Aldrich, St. Louis, USA                                |
| Hoechst   | Life Technologies Corporation, Carlsbad, USA                 |
| Hydrochloric acid                                     | Sigma-Aldrich, St. Louis, USA                                |
| Kanamycin   | Carl Roth GmbH & Co. KG, Karlsruhe, D                        |
| Laemmli's SDS Sample Buffer (4X)                      | Boston BioProducts, Ashand, USA                              |
| Laminin from Engelbreth-Holm-Swarm                    | Sigma-Aldrich, St. Louis, USA                                |
| Murine Sarcoma Basement Membrane                      |  |
| Loading Buffer (6X)                                   | peqLab Biotechnologie GmbH, Erlangen, D                      |
| Magnesium Sulfate                                     | Sigma-Aldrich, St. Louis, USA                                |
| Matrigel <sup>TM</sup> Basement Membrane              | BD Biosciences, Bedford, USA                                 |
| Methanol  | Sigma-Aldrich, St. Louis, USA                                |
| Mitomycin C   | Tocris Bioscience, Bristol, UK                               |

---

|  |  |
|--|--|
| Novex <sup>®</sup> Tris-Glycine Transfer Buffer              | Life Technologies Corporation, Carlsbad, USA |
| Nupage Reducing Agent (10X)                                  | Life Technologies Corporation, Carlsbad, USA |
| Paraformaldehyde, 32% Solution                               | Electron Microscopy Sciences, Hatfield, USA  |
| Pepstatin A  | Sigma-Aldrich, St. Louis, USA                |
| peqGOLD O'range 50 bp DNA Ladder                             | peqLab Biotechnologie GmbH, Erlangen, D      |
| Phosphate Buffered Saline                                    | Boston BioProducts, Ashand, USA              |
| Protamine Sulfate  | Sigma-Aldrich, St. Louis, USA                |
| Poly-L-Ornithine   | Sigma-Aldrich, St. Louis, USA                |
| Ponceau S Stain  | Boston BioProducts, Ashand, USA              |
| Prolong <sup>®</sup> Gold Antifade Reagent with DAPI         | Life Technologies Corporation, Carlsbad, USA |
| Rainbow Molecular Weight Standard Marker                     | GE Healthcare, Glattbrugg, CH                |
| RedSafe <sup>™</sup> Nucleic Acid Staining Solution          | Chembio Ltd, Lye Lane, UK                    |
| Sodium Acetate   | Sigma-Aldrich, St. Louis, USA                |
| Sodium Cacodylate Buffer                                     | Sigma-Aldrich, St. Louis, USA                |
| Sodium Chloride  | Sigma-Aldrich, St. Louis, USA                |
| Sodium Citrate   | Sigma-Aldrich, St. Louis, USA                |
| Sodium-EDTA  | Merck KGaA, Darmstadt, D                     |
| Trans-Epoxy succinyl-L-leucylamido-(4-guanidino)butane (E64) | Sigma-Aldrich, St. Louis, USA                |
| Tris   | Carl Roth GmbH & Co. KG, Karlsruhe, D        |
| Tris Buffered Saline (10X)                                   | Boston BioProducts, Ashand, USA              |
| Tris Buffered Saline Tablets                                 | Sigma-Aldrich, St. Louis, USA                |
| Tris/EDTA Buffer   | Qiagen GmbH, Hilden, D                       |
| Tris-Glycine SDS (10X)                                       | Boston BioProducts, Ashand, USA              |
| Triton-X100  | Fisher Scientific, Pittsburgh, USA           |
| Trypsin Inhibitor from Chicken Egg White                     | Sigma-Aldrich, St. Louis, USA                |
| Trypsin Inhibitor from <i>Glycine max</i> (Soybean)          | Sigma-Aldrich, St. Louis, USA                |
| Tween-20   | Fisher Scientific, Pittsburgh, USA           |
| Western Lightening <sup>™</sup> Plus-ECL                     | PerkinElmer Inc., Waltham, USA               |

---

### 2.1.3 Enzymes

**Table 2.3: Enzymes**

---

| Name                | Company                                      |
|---------------------|--|
| Collagenase Type II | PAA Laboratories GmbH, Pasching, A           |
| Collagenase Type IV | Life Technologies Corporation, Carlsbad, USA |

---

---

|  |  |
|--|--|
| DNase I RNase-free Solution from Bovine Pancreas | Sigma-Aldrich, St. Louis, USA                |
| 0.05% Trypsin/EDTA (1X), Phenol Red              | Life Technologies Corporation, Carlsbad, USA |
| 0.25% Trypsin/EDTA (1X), Phenol Red              | Life Technologies Corporation, Carlsbad, USA |
| Trypsin from Bovine Pancreas                     | Sigma-Aldrich, St. Louis, USA                |
| Maxima™ Hot Start Taq DNA Polymerase             | Fermentas GmbH, St. Leon-Rot, D              |

---

## 2.1.4 Commercial available kits

**Table 2.4: Commercial available kits**

| Name                                 | Company                             |
|--------------------------------------|-------------------------------------|
| Alkaline Phosphatase Detection Kit   | EMD Millipore, Billerica, USA       |
| NucleoBond® Xtra Maxi Kit            | MACHEREY-NAGEL GmbH, Düren, D       |
| Pierce® BCA Protein Assay Kit        | Pierce Biotechnology, Rockford, USA |
| QuantiTect Reverse Transcription Kit | Qiagen GmbH, Hilden, D              |
| QuantiTect SYBR Green PCR Kit        | Qiagen GmbH, Hilden, D              |
| RNeasy® Mini Kit                     | Qiagen GmbH, Hilden, D              |

---

## 2.1.5 Cell culture media and supplements

**Table 2.5: Cell culture media and supplements**

| Name  | Company                                      |
|---|--|
| β-Mercaptoethanol                               | Life Technologies Corporation, Carlsbad, USA |
| B-27 Supplement (50x)                           | Life Technologies Corporation, Carlsbad, USA |
| B-27 Supplement minus Vitamin A (50X)           | Life Technologies Corporation, Carlsbad, USA |
| BSA Fraction V                                  | Life Technologies Corporation, Carlsbad, USA |
| DMEM/F-12                                       | Life Technologies Corporation, Carlsbad, USA |
| DMEM High Glucose                               | Life Technologies Corporation, Carlsbad, USA |
| DPBS with Ca <sup>2+</sup> /Mg <sup>2+</sup>    | Life Technologies Corporation, Carlsbad, USA |
| DPBS without Ca <sup>2+</sup> /Mg <sup>2+</sup> | Life Technologies Corporation, Carlsbad, USA |
| Fetal Bovine Serum                              | Sigma-Aldrich, St. Louis, USA                |
| Fetal Calf Serum                                | PAA Laboratories GmbH, Pasching, A           |
| Hank's Balanced Salt Solution                   | Life Technologies Corporation, Carlsbad, USA |
| Knockout™DMEM                                   | Life Technologies Corporation, Carlsbad, USA |
| Knockout™ Serum Replacement                     | Life Technologies Corporation, Carlsbad, USA |
| N2-Supplement (100X)                            | Life Technologies Corporation, Carlsbad, USA |

|  |  |
|--|--|
| Sodium Pyruvate (100X)                   | Life Technologies Corporation, Carlsbad, USA |
| Neurobasal™                              | Life Technologies Corporation, Carlsbad, USA |
| MEM Non Essential Amino Acids (100X)     | Life Technologies Corporation, Carlsbad, USA |
| Penicillin-Streptomycin (100X)           | Life Technologies Corporation, Carlsbad, USA |
| Penicillin-Streptomycin-Glutamine (100X) | Life Technologies Corporation, Carlsbad, USA |
| Uridine                                  | Sigma-Aldrich, St. Louis, USA                |

### 2.1.6 Growth factors, cytokines and small molecules

Growth factors and inhibitors which were used to maintain the pluripotent state as well as cytokines and small molecules which were used to promote differentiation are listed below (Table 2.6).

**Table 2.6: Growth factors, cytokines and small molecules**

| Name                    | Company                            |
|-------------------------|------------------------------------|
| cAMP                    | Sigma-Aldrich, St. Louis, USA      |
| Dorsomorphin            | Tocris Bioscience, Bristol, UK     |
| EGF                     | Sigma-Aldrich, St. Louis, USA      |
| FGF2                    | Sigma-Aldrich, St. Louis, USA      |
| SB431542                | Tocris Bioscience, Bristol, UK     |
| Valproic Acid           | Sigma-Aldrich, St. Louis, USA      |
| Y27632 (ROCK inhibitor) | AbcamBiochemicals®, Cambridge, USA |

### 2.1.7 Antibodies

The following antibodies (Table 2.7 and Table 2.8) were used for immunofluorescence.

**Table 2.7: Primary antibodies used for immunofluorescence**

| Primary Antibody                      | Host   | Dilution | Company and Reference Number                       |
|---------------------------------------|--------|----------|--|
| Actin, N-Terminal<br>( $\alpha$ -SMA) | rabbit | 1:500    | Sigma-Aldrich, St. Louis, USA (A2103)              |
| $\alpha$ -Fetoprotein                 | mouse  | 1:500    | Abcam®, Cambridge, USA (ab3980)                    |
| BrdU                                  | rat    | 1:250    | Abcam®, Cambridge, USA (ab6326)                    |
| GFAP                                  | rabbit | 1:1000   | Dako North America, Inc., Carpinteria, USA (Z0334) |
| GM130                                 | mouse  | 1:200    | BD Biosciences, Bedford, USA (610822)              |

|           |        |        |   |
|-----------|--------|--------|---|
| GRP75     | mouse  | 1:200  | Abcam <sup>®</sup> , Cambridge, USA (ab82591)                 |
| LAMP-1    | mouse  | 1:100  | Santa Cruz Biotechnology, Santa Cruz, USA (sc-18821)          |
| MAP2ab    | rabbit | 1:500  | EMD Millipore, Billerica, USA (ab5622)                        |
| Musashi1  | rabbit | 1:500  | Abcam <sup>®</sup> , Cambridge, USA (ab52865)                 |
| Nestin    | mouse  | 1:500  | EMD Millipore, Billerica, USA (MAB5326)                       |
| OCT4      | rabbit | 1:1000 | Abcam <sup>®</sup> , Cambridge, USA (ab19857)                 |
| PDI       | mouse  | 1:100  | Enzo <sup>®</sup> Life Sciences, Farmingdale, USA (SPA-891)   |
| SSEA4     | mouse  | 1:500  | Abcam <sup>®</sup> , Cambridge, USA (ab16287)                 |
| SOX1      | rabbit | 1:500  | EMD Millipore, Billerica, USA (AB15766)                       |
| SOX2      | mouse  | 1:500  | R&D Systems, Minneapolis, USA (MAB2018)                       |
| Subunit c | rabbit | 1:200  | Generated in the Cotman laboratory (Cao <i>et al.</i> , 2011) |
| TRA-1-60  | mouse  | 1:500  | Abcam <sup>®</sup> , Cambridge, USA (ab16288)                 |
| TUJ1      | mouse  | 1:1000 | Covance, Princeton, USA (MMS-435P)                            |

**Table 2.8: Secondary antibodies used for immunofluorescence**

| Secondary Antibody  | Host   | Dilution | Company                                      |
|---------------------|--------|----------|--|
| Anti-goat IgG 568   | donkey | 1:500    | Life Technologies Corporation, Carlsbad, USA |
| Anti-mouse IgG 488  | donkey | 1:500    | Life Technologies Corporation, Carlsbad, USA |
| Anti-mouse IgM 595  | goat   | 1:500    | Life Technologies Corporation, Carlsbad, USA |
| Anti-rabbit IgG 488 | donkey | 1:500    | Life Technologies Corporation, Carlsbad, USA |
| Anti-rabbit IgG 568 | goat   | 1:500    | Life Technologies Corporation, Carlsbad, USA |
| Anti-rat IgG 568    | goat   | 1:500    | Life Technologies Corporation, Carlsbad, USA |

The antibodies listed below (Table 2.9) were used for Western blotting.

**Table 2.9: Primary antibodies used for Western blotting**

| Primary Antibody | Host   | Dilution | Company and Reference Number                                  |
|------------------|--------|----------|---|
| $\beta$ -Actin   | mouse  | 1:2000   | Santa Cruz Biotechnology, Santa Cruz, USA (sc-81178)          |
| COX IV           | rabbit | 1:1000   | Cell Signaling, Danvers, USA (4844)                           |
| EEA-1            | goat   | 1:250    | Santa Cruz Biotechnology, Santa Cruz, USA (sc-6415)           |
| GRP75            | mouse  | 1:1000   | Abcam <sup>®</sup> , Cambridge, USA (ab82591)                 |
| LAMP-1           | mouse  | 1:100    | Santa Cruz Biotechnology, Santa Cruz, USA (sc-18821)          |
| Subunit c        | rabbit | 1:500    | Generated in the Cotman laboratory (Cao <i>et al.</i> , 2011) |

**Table 2.10: Secondary antibodies used for Western blotting**

| Secondary Antibody  | Host   | Dilution | Company                                   |
|---------------------|--------|----------|---|
| Anti-goat IgG-HRP   | rabbit | 1:5000   | Santa Cruz Biotechnology, Santa Cruz, USA |
| Anti-mouse IgG-HRP  | donkey | 1:5000   | Santa Cruz Biotechnology, Santa Cruz, USA |
| Anti-rabbit IgG-HRP | donkey | 1:5000   | Santa Cruz Biotechnology, Santa Cruz, USA |

### 2.1.8 Primers

Primers were designed using the open-access program Primer3 (<http://frodo.wi.mit.edu/primer3/>). Where possible, primers that were intron spanning were chosen. Retroviral silencing was confirmed using primer sequences published by Kim, J.B. *et al.*, 2009. Primers were purchased from Metabion and IDT®.

All primers were designed for quantitative real-time polymerase chain reaction (qPCR) except for primers confirming the 1.02 kb deletion within the CLN3 gene.

**Table 2.11: Primer sequences**

| Gene   | Sequence (forward, reverse)   | Product Length |
|--|---|----------------|
| <i>CLN3</i><br>(Ceroid-Lipofuscinosis, Neuronal 3)         | 5'-GTCCTGGTTGCCTTTTCTCA-3'<br>5'-CGGGGCCTCGGTTCTTAT-3'                | 360 bp         |
| <i>GAPDH</i><br>(Glyceraldehyde-3-Phosphate Dehydrogenase) | 5'-CTGGTAAAGTGGATATTGTTGCCAT-3'<br>5'-TGGAATCATATTGGAACATGTAAACC-3'   | 80 bp          |
| <i>GATA4</i><br>(GATA Binding Protein 4)                   | 5'CTAGACCGTGGGTTTTGCAT-3'<br>5'TGGGTAAAGTGCCCCTGTAG-3'                | 247 bp         |
| <i>KLF4</i> endogenous<br>(Kruppel-Like Factor 4)          | 5'-ACAGTCTGTTATGCACTGTGGTTTCA-3'<br>5'-CATTTGTTCTGCTTAAGGCATACTTGG-3' | 83 bp          |
| <i>KLF4</i> viral<br>(Kruppel-Like Factor 4)               | 5'-CCTCGCCTTACACATGAAGAGACA-3'<br>5'-CACCAGACCAACTGGTAATGGTAGC-3'     | 120 bp         |
| <i>KRT18</i><br>(Keratin 18)                               | 5'-TGATGACACCAATATCACACGA-3'<br>5'-GGCTTGTAGGCCTTTTACTTCC-3'          | 112 bp         |

---

|  |   |        |
|--|---|--------|
| <i>LIN28A</i><br>(Lin-28 Homolog A)                                | 5'-GGAGGCCAAGAAAGGGAATATGA-3'<br>5'-AACAATCTTGTGGCCACTTTGACA-3' | 97 bp  |
| <i>MYC</i> endogenous<br>(Myelocytomatosis Viral Oncogene Homolog) | 5'-CCAGCAGCGACTCTGAGG-3'<br>5'-GAGCCTGCCTCTTTTCCACAG-3'         | 74 bp  |
| <i>MYC</i> viral<br>(Myelocytomatosis Viral Oncogene Homolog)      | 5'-GCTACGGA ACTCTTGTGCGTG-3'<br>5'-CACCAGACCAACTGGTAATGG-3'     | 108 bp |
| <i>NANOG</i>   | 5'-GCTTGCCTTGCTTTGAAGCA-3'<br>5'-TTCTTGACCGGGACCTTGTC-3'        | 256 bp |
| <i>PAX6</i><br>(Paired Box 6)                                      | 5'AACAGACACAGCCCTCACAAACA-3'<br>5'CGGGA ACTTGA ACTGGA ACTGAC-3' | 252 bp |
| <i>POU5F1</i> endogenous<br>(POU Class 5 Homeobox 1)               | 5'-GGAAGGAATTGGGAACACAAAGG-3'<br>5'-AACTTCACCTTCCCTCCAACCA-3'   | 70 bp  |
| <i>POU5F1</i> viral<br>(POU Class 5 Homeobox 1)                    | 5'-GGCTCTCCCATGCATTCAAAC-3'<br>5'-CATGGCCTGCCCCGTTATTA-3'       | 105 bp |
| <i>SOX1</i><br>(Sex Determining Region Y-Box 1)                    | 5'-ACCAGGACCGGGTCAAAC-3'<br>5'-TGATCTCCGAGTTGTGCATC-3'          | 105 bp |
| <i>SOX2</i> endogenous<br>(Sex Determining Region Y-Box 2)         | 5'-TGGCGAACCATCTCTGTGGT-3'<br>5'-CCAACGGTGTCAACCTGCCAT-3'       | 110 bp |
| <i>SOX2</i> viral<br>(Sex Determining Region Y-Box 2)              | 5'-GCACACTGCCCTCTCACAC-3'<br>5'-CACCAGACCAACTGGTAATGG-3'        | 110 bp |
| <i>T</i><br>(Brachyury Homolog)                                    | 5'ACCCAGTTCATAGCGGTGAC-3'<br>5'CAATTGTCATGGGATTGCAG-3'          | 392 bp |

---



### 2.1.9 Cell lines and bacterial strains

The following cell lines were either purchased or obtained from collaborators in order to expand them for further experiments (Table 2.12).

**Table 2.12: Cell lines obtained from other sources**

| Name            | Origin   | Company                       |
|-----------------|--|-------------------------------|
| CLN3 iPSC 1A    | Skin fibroblasts   | Donation by Dr. Cotman        |
| CLN3 iPSC 1B    | Skin fibroblasts   | Donation by Dr. Cotman        |
| CLN3 iPSC 2A    | Skin fibroblasts   | Donation by Dr. Cotman        |
| CLN3 iPSC 2B    | Skin fibroblasts   | Donation by Dr. Cotman        |
| Control BJ iPSC | Skin fibroblasts   | Donation by Prof. Haggarty    |
| Control FS iPSC | Skin fibroblasts   | Donation by Prof. Schöler     |
| Control GM iPSC | Skin fibroblasts   | Donation by Prof. Haggarty    |
| EnStemA         | H9-ESC-derived NPCs  | EMD Millipore, Billerica, USA |
| HEK 293T        | Human embryonic kidney   | Donation by Prof. Schöler     |
| hNP-1           | H9-ESC-derived NPCs  | Aruna GmbH, Berlin, D         |
| hNSC 21         | Human iPSC-derived NPCs  | GlobalStem, Rockville, USA    |
| MEF CF-1        | Mouse embryonic fibroblasts  | GlobalStem, Rockville, USA    |
| RenCell VM      | Immortalized cell line derived from 10-week human ventral mesencephalon brain tissue | EMD Millipore, Billerica, USA |
| TPP1-1DD        | Skin fibroblasts   | Donation by Prof. Steinfeld   |
| TPP1 iPSC 1A    | Skin fibroblasts   | Donation by Dr. Cotman        |
| TPP1 iPSC 1B    | Skin fibroblasts   | Donation by Dr. Cotman        |
| TPP1 iPSC 1C    | Skin fibroblasts   | Donation by Dr. Cotman        |

The bacterial strain *Escherichia coli* TOP 10 was purchased from Life Technologies Corporation, Carlsbad, USA.

## 2.2 Tissue and cell culture

All cells used during this thesis were grown at 37°C in a tissue culture incubator maintaining a stable content of 21% O<sub>2</sub> and 5% CO<sub>2</sub>.

DPBS without Ca<sup>2+</sup>/Mg<sup>2+</sup> was used for preparation of dilutions and washing purposes if not indicated otherwise.

### 2.2.1 Cell culture media

Media supplements were stored as aliquots at -20°C in order to avoid multiple freeze thaw cycles. Aliquots of freshly prepared media were kept at 4°C and used within two weeks. Growth factors were always added prior to use of the pre-warmed media.

#### EB medium for ectodermal differentiation

|  |             |
|--|-------------|
| DMEM/F-12                                | 48.6% (v/v) |
| Neurobasal™                              | 48.6% (v/v) |
| B-27 Supplement minus Vitamin A (50X)    | 1% (v/v)    |
| Penicillin-Streptomycin-Glutamine (100X) | 1% (v/v)    |
| N2-Supplement (100X)                     | 0.5% (v/v)  |
| BSA Fraction V                           | 0.2% (v/v)  |
| β-Mercaptoethanol (50 mM)                | 0.1% (v/v)  |

#### EB medium for meso- and endodermal differentiation

|  |              |
|--|--------------|
| DMEM High Glucose                        | 48.95% (v/v) |
| Fetal Bovine Serum                       | 48.95% (v/v) |
| MEM Non Essential Amino Acids (100X)     | 1% (v/v)     |
| Penicillin-Streptomycin-Glutamine (100X) | 1% (v/v)     |
| β-Mercaptoethanol (50 mM)                | 0.1% (v/v)   |

#### ES medium

|  |             |
|--|-------------|
| Knockout™DMEM                            | 77.8% (v/v) |
| Knockout™ Serum Replacement              | 20% (v/v)   |
| MEM Non Essential Amino Acids (100X)     | 1% (v/v)    |
| Penicillin-Streptomycin-Glutamine (100X) | 1% (v/v)    |
| β-Mercaptoethanol (50 mM)                | 0.2% (v/v)  |

#### ES freezing medium

|                             |           |
|-----------------------------|-----------|
| Knockout™ Serum Replacement | 50% (v/v) |
| Knockout™DMEM               | 40% (v/v) |
| DMSO                        | 10% (v/v) |
| Y27632                      | 10 μM     |

**Fibroblast medium**

|  |             |
|--|-------------|
| DMEM High Glucose                        | 87.9% (v/v) |
| Fetal Calf Serum                         | 10% (v/v)   |
| Sodium Pyruvate (100X)                   | 1.1% (v/v)  |
| Penicillin-Streptomycin-Glutamine (100X) | 1% (v/v)    |
| Uridine                                  | 0.2 µg/ml   |

**Final differentiation medium**

|  |              |
|--|--------------|
| DMEM/F-12                                | 48.75% (v/v) |
| Neurobasal™                              | 48.75% (v/v) |
| B-27 Supplement minus Vitamin A (50X)    | 1% (v/v)     |
| Penicillin-Streptomycin-Glutamine (100X) | 1% (v/v)     |
| N2-Supplement (100X)                     | 0.5% (v/v)   |

**MEF medium**

|  |             |
|--|-------------|
| Knockout™DMEM                            | 87.9% (v/v) |
| Fetal Bovine Serum                       | 10% (v/v)   |
| MEM Non Essential Amino Acids (100X)     | 1% (v/v)    |
| Penicillin-Streptomycin-Glutamine (100X) | 1% (v/v)    |
| β-Mercaptoethanol (50 mM)                | 0.1% (v/v)  |

**MEF freezing medium**

|                    |           |
|--------------------|-----------|
| Fetal Bovine Serum | 50% (v/v) |
| Knockout™DMEM      | 40% (v/v) |
| DMSO               | 10% (v/v) |

**NPC medium**

|  |           |
|--|-----------|
| DMEM/F-12                                | 97% (v/v) |
| B-27 Supplement (50X)                    | 2% (v/v)  |
| Penicillin-Streptomycin-Glutamine (100X) | 1% (v/v)  |

**N2 medium**

|                                |             |
|--------------------------------|-------------|
| DMEM/F-12                      | 97.7% (v/v) |
| Penicillin-Streptomycin (100X) | 1% (v/v)    |
| N2-Supplement (100X)           | 1.3% (v/v)  |

---

**Rosette medium**

|  |           |
|--|-----------|
| DMEM/F-12                                | 98% (v/v) |
| N2-Supplement (100X)                     | 1% (v/v)  |
| Penicillin-Streptomycin-Glutamine (100X) | 1% (v/v)  |
| Heparin                                  | 2 µg/ml   |

**2.2.2 Coatings**

The volume used for the following coating procedures was 250 µl per well of a 4-well plate. For coating of 12-well and 6-well plates the amount used was doubled and tripled respectively. 15 cm cell culture dishes were coated with 5 ml of gelatin solution.

*2.2.2.1 Gelatin coating*

In order to improve attachment of CF-1 feeder cells and to promote meso- and endodermal differentiation of EBs, plastic surfaces were coated with 0.1% gelatin solution.

Surfaces were incubated for about 5 min at RT. Gelatin solution was removed prior to use without any further washing steps.

*2.2.2.2 Matrigel™ coating*

In order to eliminate the background contribution of feeder cells during analysis of iPSCs, they were grown on Matrigel™. It was further used to induce ectodermal differentiation of EBs.

Matrigel™ was thawed overnight at 4°C on ice. Thawed Matrigel™ was diluted 1:5 in cold Knockout™DMEM using pre-cooled pipettes and stored at -20°C. For coatings pre-diluted Matrigel™ was further diluted 1:15 in cold Knockout™DMEM. Coated plates were kept at 4°C overnight prior to use and were stored up to two weeks. Plates were allowed to warm to RT prior to use. Matrigel™ solution was then removed and plates were used without any further washing steps.

*2.2.2.3 Poly-L-Ornithine/Laminin coating*

Neural precursor cells (NPCs) were propagated and differentiated on Poly-L-Ornithine/Laminin (PLO/L) coated plates.

PLO solution was diluted in DPBS to a final concentration of 15 µg/ml and coated wells were incubated overnight at 37°C. Plates were then washed three times with DPBS. Laminin was diluted in DPBS to a final concentration of 5 µg/ml and PLO pre-coated plates were incubated with laminin solution overnight at 37°C. Prior to use, plates were washed three times with DPBS. Coated plates were stored at -20°C until use for up to four weeks.

### **2.2.3 Fibroblast preparation and propagation**

Skin biopsies from the upper leg were taken from male patients with the common mutation within the CLN3 gene as well as from one heterozygous male donor. All procedures were in accordance with the Helsinki Convention and approved by the Ethical Committee of the University of Dresden (EK 45022009).

Tissue samples were stored at 4°C in fibroblast media until further processed. Samples were placed onto a petri dish and minced using a scalpel. Sample pieces were collected in fibroblast media and centrifuged for 4 min at 200xg. Supernatant was removed and sample pieces were incubated for 20 min at RT in trypsin solution (2.5 mg/ml). Following digestion, the sample was centrifuged for 4 min at 200xg. Supernatant was carefully removed and the pellet was incubated for 10 min at 37°C in 2 ml DNase I solution (0.04 mg/ml). The suspension was centrifuged at 200xg for 4 min, supernatant was removed and the sample was incubated in 4 ml collagenase type II solution (20 mg/ml) for 30 min at 37°C. Following centrifugation for 4 min at 200xg, the cell pellet was resuspended in 3 ml fibroblast media and plated onto four wells of a 4-well plate. At about six days after initial plating, first fibroblasts appeared. Half of the media was then replaced by fresh fibroblast media and supernatant was plated onto a new 4-well plate. After two weeks in culture, fibroblasts were confluent and could be passaged. For this, media was aspirated and cells were incubated in 250 µl of 0.05% Trypsin/EDTA for 5 min at 37°C. Detached cells were transferred with warm fibroblast media into a 15 ml falcon tube and collected through centrifugation for 4 min at 200xg. Supernatant was removed, cells were resuspended in warm fibroblast media and plated onto one well of a 6-well plate. Fibroblasts were in general split in a 1:2 ratio.

For freezing fibroblasts down, they were detached and collected as described above. The cell pellet was then resuspended in fibroblast media containing 10% DMSO and cells were frozen down at -80°C using a Nalgene™ Cryo freezing container. For long term storage, cells were kept in a liquid nitrogen tank. As a rule, one confluent well of a 6-well plate was frozen down into one cryovial using 1 ml of freezing media.

For thawing fibroblasts, one cryovial was placed into the 37°C warm water bath for about 1 min. The content was then collected in 5 ml of pre-warmed fibroblast media and centrifuged for 4 min at 200xg. The supernatant was removed and the cell pellet was resuspended in 3 ml fibroblast media and plated onto one well of a 6-well plate.

### Trypsin solution

|                               |        |
|-------------------------------|--------|
| Trypsin from bovine pancreas  | 250 mg |
| Hank's Balanced Salt Solution | 100 ml |

Trypsin was dissolved in Hank's Balanced Salt Solution, filter-sterilized (0.45 µm) and aliquots were stored at -20°C.

### DNase I solution

|   |          |
|---|----------|
| DNase I RNase-free solution from bovine pancreas    | 4 mg     |
| Trypsin inhibitor from <i>Glycine max</i> (Soybean) | 15 mg    |
| Magnesium sulfate                                   | 181,2 mg |
| Hank's Balanced Salt Solution                       | 100 ml   |

Reagents were dissolved in Hank's Balanced Salt Solution, filter-sterilized (0.45 µm) and aliquots were stored at -20°C.

### Collagenase type II stock solution

|                     |      |
|---------------------|------|
| Collagenase type II | 1 g  |
| Water               | 5 ml |

Collagenase was dissolved in water, filter-sterilized (0.45 µm) and aliquots were stored at -20°C. For use, stock solution was further diluted 1:10 in PBS.

#### 2.2.4 Preparation of CF-1 feeder cells

CF-1 mouse embryonic fibroblasts (MEFs) are known to support growth and survival of pluripotent stem cells such as embryonic stem cells from mouse and humans (Brook *et al.*, 1997, Eiselleova *et al.*, 2008). They are therefore used as feeder cells for induced pluripotent stem cells (iPSCs). In order to prevent them from overgrowing iPSC cultures, they have to be mitotically inactivated.

One cryovial containing four million untreated MEFs was quickly thawed at 37°C. Cells were immediately resuspended in 10 ml cold MEF media and centrifuged for 4 min at 200xg. The

cell pellet was then resuspended in 30 ml of warm MEF media and plated onto one 15 cm cell culture dish pre-coated with 0.1% gelatin. When cells reached confluency, they were split in a 1:3 ratio. For this purpose, media was removed, the plate was washed once with DPBS, and 4 ml of 0.05% Trypsin/EDTA were added to the dish. After an incubation of 5 min at 37°C, cells were detached, collected with 10 ml MEF media in a 50 ml falcon tube and centrifuged for 4 min at 200xg. Meanwhile 25 ml MEF media were added to each gelatin pre-coated 15 cm dish. The cell pellet was then resuspended in 15 ml MEF media and 5 ml cell suspension were evenly distributed per dish. This entire procedure was repeated once when cells reached confluency again.

Mitomycin C treatment was started when MEFs became confluent after the second passage. For that, mitomycin C was diluted in fresh MEF medium to a final concentration of 10 µg/ml. Media was removed from the dishes and replaced by 10 ml of MEF media containing mitomycin C. Cells were then incubated for 2 h at 37°C. Media was removed, dishes were washed three times with DPBS and cells were trypsinized as described above and collected by centrifugation for 4 min at 200xg. Supernatant was removed and the cell pellet was resuspended in 1 ml cold MEF medium. Cells were counted with a hemocytometer and diluted in cold MEF freezing media to a final concentration of 1 million cells/ml. Cryovials containing 1 million cells/ml were kept at -80°C until use. Mitomycin C-treated MEFs were then referred to as feeder cells.

#### **Mitomycin C stock solution**

|             |       |
|-------------|-------|
| Mitomycin C | 10 mg |
| Water       | 10 ml |

Mitomycin C was resuspended in water and solution was sonicated until the crystals were completely dissolved. Aliquoted stock solution was stored at -80°C for up to 6 months.

#### **2.2.5 Preparation of conditioned media**

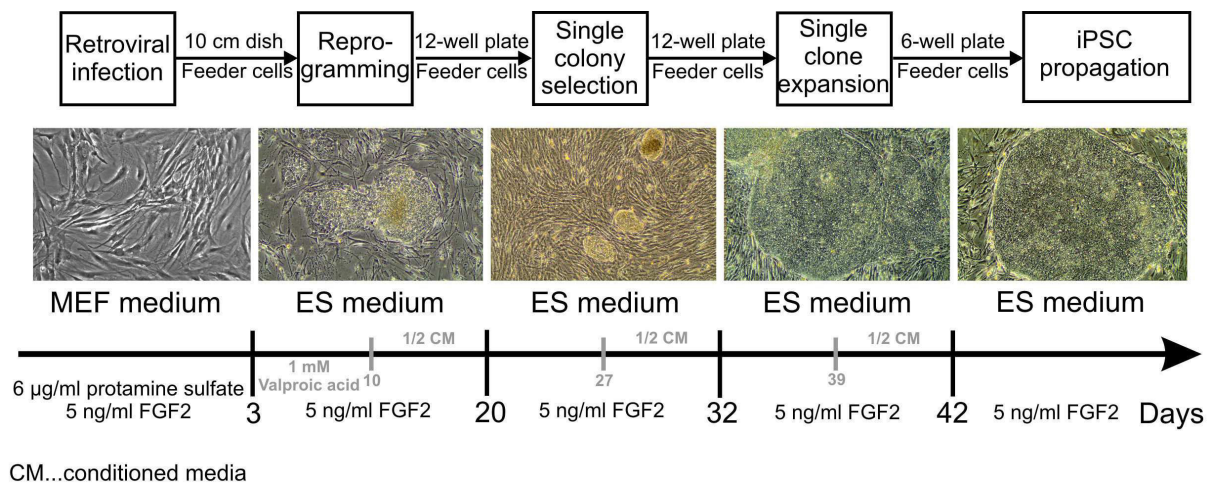
Since feeder cells provide sufficient nutrients to the iPSCs for only about 6 days, supplementation of nutrients to the regular ES media was necessary. For this, feeder cells were incubated in ES media in order to pre-condition it.

Feeder cells were plated in MEF media at a density of 50.000 cells/cm<sup>2</sup> on gelatin coated 150 cm<sup>2</sup> cell culture flasks. The next day medium was removed and replaced by 75 ml ES media supplemented with 5 ng/ml FGF2. Media change was performed every day for five

consecutive days, collected and stored at  $-20^{\circ}\text{C}$ . At day five, collected conditioned media (CM) was thawed, filter-sterilized using a bottle-top filter and aliquots were stored at  $-20^{\circ}\text{C}$ .

### 2.2.6 Generation and maintenance of induced pluripotent stem cells

Generation of induced pluripotent stem cells (iPSCs) is a tedious process which can be divided into three main stages: reprogramming, single colony picking and expansion of promising iPSC clones. The following scheme (Scheme 2.1) provides an overview of all steps involved in iPSC generation.

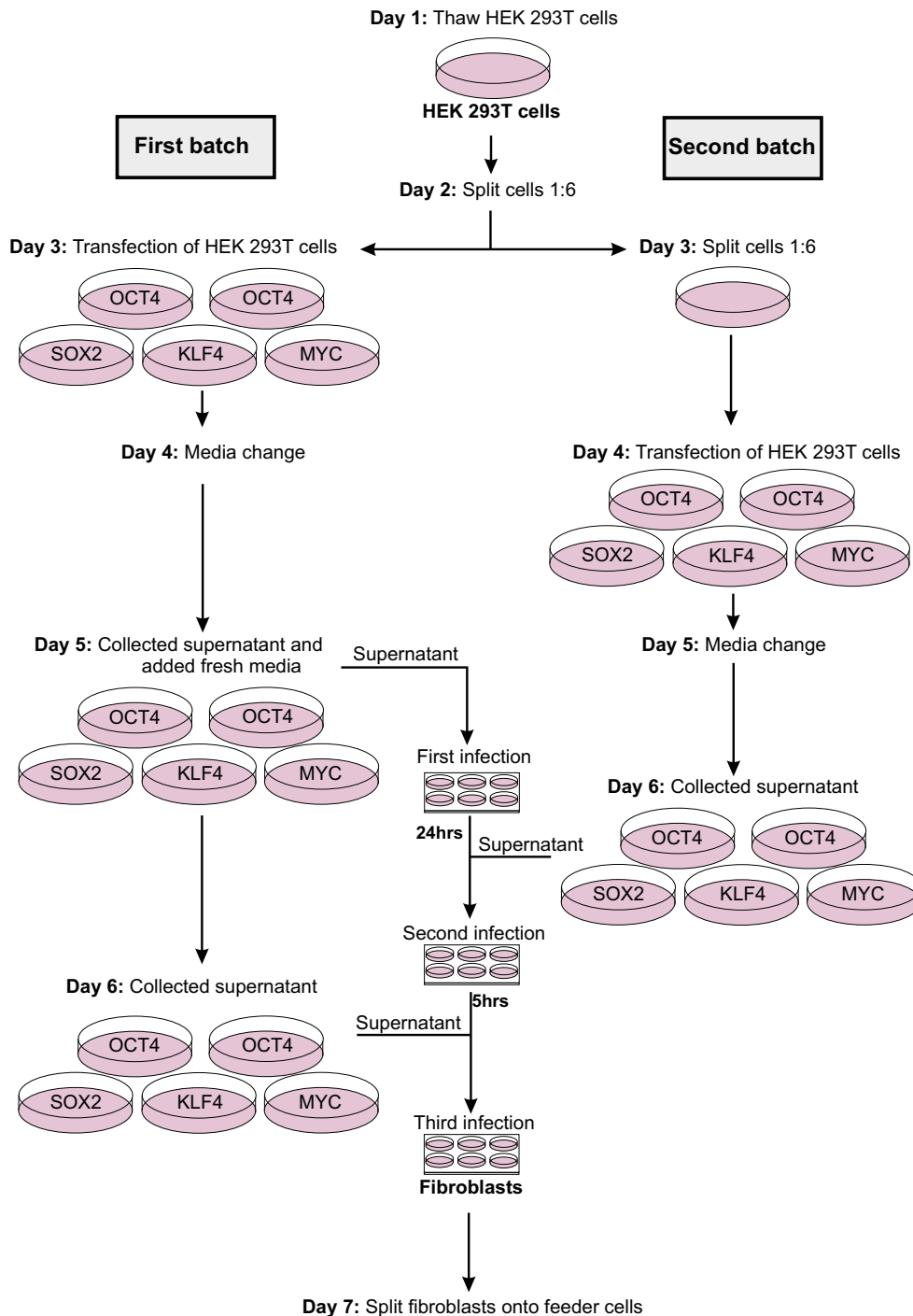


**Scheme 2.1: Schematic representation of induced pluripotent stem cell generation**

#### 2.2.6.1 Reprogramming

Reprogramming of human fibroblasts in order to generate iPSCs is a process that takes several days. Therefore, three to four fibroblast lines were in parallel subjected to reprogramming. The following scheme (Scheme 2.2) illustrates the reprogramming procedure. Detailed information are given in the text below.





**Scheme 2.2: Schematic representation of the reprogramming procedure**

### 1<sup>st</sup> day

Human embryonic kidney (HEK) 293T cells were thawed as described for MEFs in 2.2.4. Cells were resuspended in 8 ml MEF media and plated onto one 10 cm tissue culture dish.

### 2<sup>nd</sup> day

Within 24 hours, HEK 293T cells usually reached confluency and could be split, as described for MEFs in 2.2.4, in a 1:6 ratio.

**3<sup>rd</sup> day**

One 10 cm dish of HEK 293T cells was again split in a 1:6 ratio for the second transfection which will be referred in the following to as second batch of HEK 293T cells.

The remaining five 10 cm dishes were kept for the first transfection which will be referred to as first batch of HEK 293T cells. Since fibroblasts were always reprogrammed using all four factors, in a ratio of OCT4:SOX2:KLF4:MYC 2:1:1:1, the following steps were performed for five individual viral transfections. For this purpose, in five independent Eppendorf tubes 4.5 µg of pMX vector, containing the gene of interest, were mixed with 4.05 µg gag-pol and 450 ng VSV-G. In another set of five Eppendorf tubes, 500 µl Knockout<sup>TM</sup>DMEM were mixed with 27 µl Fugene<sup>®</sup>. This mixture was incubated for 5 min at RT. Then, the individual plasmid mixtures were added and after vortexing, the entire mixture was incubated at RT for 30 min. After incubation time, media from the first batch of HEK 293T cells was replaced by fresh MEF media, followed by drop wise addition of one plasmid mixture per dish. Cells were then incubated overnight at 37°C.

**4<sup>th</sup> day**

Media from the first batch of transfected HEK 293T cells was replaced by 12 ml of fresh MEF media. Transfection of the second batch took place as described for the first batch on day 3.

Fibroblasts were plated onto five wells of a gelatin pre-coated 6-well plate, as described in 2.2.3, at a density of 50.000 cells/well.

**5<sup>th</sup> day**

Media change of the second batch of HEK 293T cells was performed as described on day 4.

Media from the first batch of HEK 293T cells was now collected for further viral infection. For this, the media from one dish was passed through a 0.45 µm PVDF filter, collected in a 15 ml falcon tube and placed on ice. Fresh MEF media was added to the dish for the third infection. This procedure was repeated for the remaining four HEK 293T cell dishes of the first batch. Equal amounts of media, containing the viral supernatants, were then combined and fresh MEF media was added in a 1:6 ratio together with 5 ng/ml FGF2 and 6 µg/ml protamine sulfate. Media from the fibroblasts was then replaced by 2 ml of virus containing media per well. This first viral infection of fibroblasts was carried out overnight.

**6<sup>th</sup> day**

Virus containing media from the second batch of HEK 293T cells was collected as described on day 5 without any further use of HEK 293T cells. The second viral infection of fibroblasts was performed as described for the first infection on day 5.

---

5 h post-infection the third infection took place. For this, media from the first batch of HEK 293T cells was collected in a 15 ml falcon tube and centrifuged at 200xg for 5 min. The supernatant was passed through a 0.45  $\mu\text{m}$  PVDF filter. Equal amounts of filtered media were mixed and fresh MEF media was added in a 1:6 ratio. After addition of FGF2 (5 ng/ml) and protamine sulfate (6  $\mu\text{g}/\text{ml}$ ) the media was used to infect fibroblasts a third time. In general, only two wells per fibroblast plate were subjected to a third infection.

Feeder cells were thawed and 1 million cells were plated onto one gelatin pre-coated 10 cm dish. At least two feeder dishes per fibroblast line were prepared for the next day.

#### **7<sup>th</sup> day**

Media from the fibroblasts was removed, cells were washed three times with DPBS (with  $\text{Ca}^{2+}/\text{Mg}^{2+}$ ) and fresh MEF media was added. Fibroblasts were trypsinized and cells from two as well as from three infections were combined and collected by centrifugation for 4 min at 200xg. Supernatant was removed, cells were resuspended in 1 ml MEF media and counted with a hemocytometer. Fibroblasts were then plated at a density of 25.000 cells as well as 50.000 cells/10 cm feeder dish in 7 ml of MEF media supplemented with 1 mM valproic acid and 5 ng/ml FGF2. In addition, 50.000 cells were plated onto one well of a 6-well plate. These cells were later used as infection control for qPCR.

#### **8<sup>th</sup> day**

Media change of plated fibroblasts was performed. Three third of MEF media were replaced by ES media supplemented with 1 mM valproic acid and 5 ng/ml FGF2.

RNA was isolated from the infection control plated onto the 6-well plate (2.3.2).

#### **9<sup>th</sup> day**

Media was entirely replaced by ES media containing valproic acid (1 mM) and FGF2 (5 ng/ml). From now on, media was changed to the same conditions every day and amount of media was increased as necessary. After seven days media was changed to  $\frac{1}{2}$  ES media and  $\frac{1}{2}$  CM supplemented with 5 ng/ml FGF2.

#### *2.2.6.2 Single colony picking and establishment of stable clones*

At about 20 days after the first infection, single colonies were suitable for picking.

24 h prior to picking colonies, 1 million feeder cells were plated onto one gelatin pre-coated 12-well plate. At least two plates were needed per fibroblast line.

4 h prior to picking, MEF media from the feeder plates was replaced by ES media containing 5 ng/ml FGF2 and 10  $\mu\text{M}$  Y27632.

---

Media from one 10 cm dish was removed and 3 ml of 1X collagenase type IV were added. Cells were incubated at 37°C for about 5 min. Collagenase was then aspirated and 5 ml fresh ES media were added. The following procedure was carried out under an inverted brightfield microscope. With the help of a pipette tip, surrounding feeder cells and differentiation around the edges of a promising colony were entirely removed by carefully scratching them away. The cleaned colony was then carefully detached using a 10 µl pipette tip. The free floating colony was collected and transferred into one well of the prepared 12-well plate. Overall 24 to 36 single colonies were picked per cell line. Depending on their size, some colonies were carefully triturated three times.

The next day, media was replaced by ES media containing 5 ng/ml FGF2 and 10 µM Y27632. From the second day on after picking, media was changed every day to the same conditions without Y27632. From day 7 post-picking, media was changed to ½ ES and ½ CM supplemented with 5 ng/ml FGF2. At about 12 days post-picking, colonies were picked once more. For this, steps for single colony picking, as described above, were repeated but this time multiple colonies from one well were transferred together into one well of a new 12-well feeder plate. In general, 6 to 10 clones could be picked a second time. Media changes were performed as described above.

#### *2.2.6.3 Expansion of induced pluripotent stem cell clones*

24 h prior to passaging iPSCs, feeder cells were plated onto gelatin pre-coated 6-well plates at a density of 250.000 cells/well. 4 h prior to passaging iPSCs, MEF media from the feeder cells was replaced by ES media containing 5 ng/ml FGF2 and 10 µM Y27632.

When iPSC clones from 12-well plates reached confluency, iPSCs were passaged for the first time. Prior to passaging, iPSCs were cleaned under an inverted brightfield microscope using a pipette tip. During the cleaning procedure, completely differentiated colonies were entirely removed and differentiation within or at the edges of a colony were carefully scratched away using a pipette tip. Media, containing cell debris, was removed and colonies were incubated with 1X collagenase type IV for 5 min at 37°C. Collagenase was replaced by 500 µl ES media and colonies were detached by passing a cell lifter throughout the well. Colonies were carefully triturated, collected in a 15 ml falcon tube and centrifuged at 200xg for 15 s. Supernatant was removed and the colonies were resuspended using media from the prepared feeder plate. Colonies from one well of a 12-well plate were then plated onto one well of a 6-well plate. Media change was performed as described above and when iPSCs became

confluent, they were passaged again at a 1:4 ratio. iPSC colonies were in general grown on 6-well plates.

#### *2.2.6.4 Freezing and thawing of induced pluripotent stem cells*

In order to freeze iPSCs down, colonies were cleaned and collected as described in 2.2.6.3. Colonies were then resuspended in ES freezing media and immediately placed at -80°C using a Nalgene™ Cryo freezing container which ensures a cooling rate of 1°C/min. For long term storage, iPSCs were kept in a liquid nitrogen tank. As a rule, one confluent well of a 6-well plate was frozen down into one cryovial using 1 ml of freezing media.

For thawing, the cryovial was placed for about 1 min at 37°C. Colonies were resuspended in cold ES media, collected in a 15 ml falcon tube and centrifuged at 200xg for 1 min. Supernatant was removed, cells were resuspended in warm ES media from a prepared feeder plate and evenly distributed throughout this plate. After thawing iPSCs, Y27632 was added to the media for the next two days.

#### **Collagenase (10X)**

|                     |        |
|---------------------|--------|
| Collagenase Type IV | 1 g    |
| Knockout™DMEM       | 100 ml |

Collagenase was dissolved in Knockout™DMEM and filter-sterilized (0.45 µm). Aliquots were snap frozen and stored at -20°C. In order to obtain 1X and 2X solutions, 10X collagenase was further diluted in ES media and stored at -20°C.

### **2.2.7 Characterization of induced pluripotent stem cells**

#### *2.2.7.1 Transgene silencing*

For analysis of transgene silencing, colonies from one confluent well of a 6-well plate were used. Colonies were cleaned (2.2.6.3) and detached using a cell lifter. Floating cells were transferred into an Eppendorf tube and centrifuged at 200xg for 4 min. Supernatant was removed and the cell pellet was stored at -80°C for later RNA extraction (2.3.2).

### 2.2.7.2 Confirmation of pluripotency

To avoid background staining from feeder cells, iPSC colonies were grown on Matrigel™ for staining purposes (2.2.2.2).

After cleaning (2.2.6.3), media was aspirated and cells were incubated with 1 ml 2X collagenase at 37°C until colonies were completely detached. They were collected in a 15 ml falcon tube and centrifuged at 200xg for 1 min. Supernatant was carefully removed and colonies were plated in media consisting of ½ ES media and ½ CM supplemented with 5 ng/ml FGF2 and 10 µM Y27632. The next days media was changed to the same conditions without Y27632. iPSCs were grown until they had formed well-sized colonies and could be analyzed by immunofluorescence (2.5.1).

### 2.2.7.3 Embryoid body formation and differentiation

In order to generate sufficient embryoid bodies (EBs) for confirmation of pluripotency, one well of a 6-well plate was used per germ layer. iPSCs were grown under standard conditions until confluent. After cleaning (2.2.6.3), colonies were detached using 2X collagenase and collected as described in 2.2.7.2. Colonies were resuspended in 8 ml ES media supplemented with either 5 µM Y27632, 10 µM SB431542 and 1 µM dorsomorphin for ectodermal or 5 µM Y27632 for meso-/endodermal differentiation. Colonies were then plated into 6 cm petri dishes for EB formation. Media was changed two days later to the same conditions but without Y27632. Another two days later, EBs were collected through gravity flow in 15 ml falcon tubes. EBs for ectodermal differentiation were plated onto Matrigel™ pre-coated 4-well plates (2.2.2.2) using EB media for ectodermal differentiation. EBs for meso-/endodermal differentiation were plated onto gelatin pre-coated plates (2.2.2.1) using EB media for meso-/endodermal differentiation. Media change was performed twice a week and EBs were allowed to differentiate for 14 d.

## 2.2.8 5-bromo-2'-deoxyuridine incorporation assay

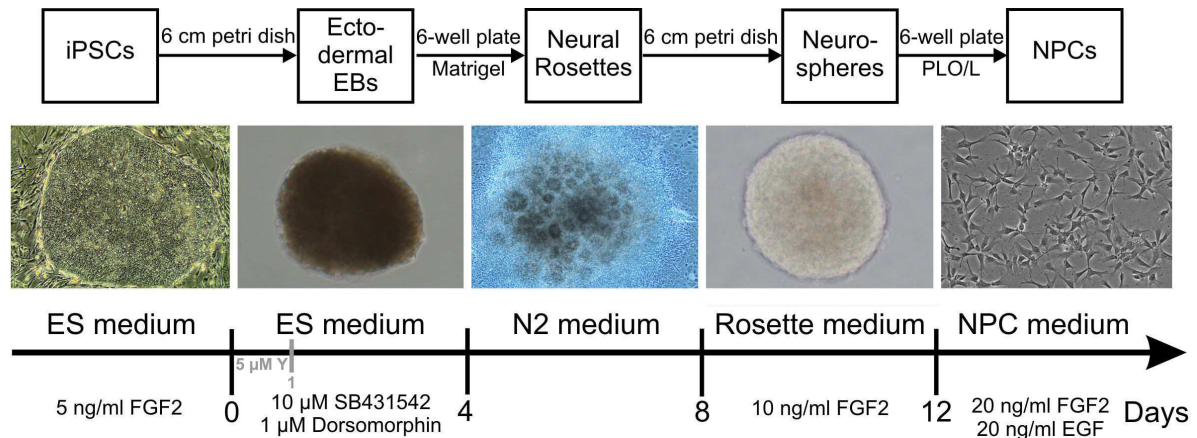
In order to determine the growth rate of iPSCs, cells were treated with 10 µM 5-bromo-2'-deoxyuridine (BrdU).

Prior to treatment, iPSCs were grown for 48 h on Matrigel™ as described in 2.2.7.2. Media was then supplemented with BrdU. 6, 12 and 24 h post-treatment, cells were washed once with DPBS and fixed in 4% PFA for 10 min at RT.

## 2.2.9 Derivation and propagation of neural progenitor cells

### 2.2.9.1 Monolayer culture

Derivation of neural progenitor cells (NPCs) from iPSCs is a process that includes multiple steps. The following scheme (Scheme 2.3) represents the major events involved in NPC derivation.



Y...Y27632

**Scheme 2.3: Schematic representation of neural progenitor cell derivation**

For derivation of NPCs from iPSCs, colonies from three confluent wells of a 6-well plate were needed. iPSCs were grown under standard conditions until they became confluent. At that day, all cleaned colonies were subjected to the ectodermal EB formation protocol as described in 2.2.7.3. The next day, EBs were collected in a 15 ml falcon tube by gravity flow. Media was aspirated and collected EBs were resuspended in 8 ml fresh ES media containing 10  $\mu$ M SB431542 and 1  $\mu$ M dorsomorphin. Media was changed by this manner the next two days. On day four of EB formation, collected EBs were resuspended in 4 ml N2 media and plated onto two wells of a 6-well plate pre-coated with Matrigel<sup>TM</sup> (2.2.2.2). Daily media change was performed the following four days. During that time EBs attached to the coated surface and neural rosettes were formed. When rosettes started to emerge from the majority of the plated EBs, usually at day four after plating, rosettes were manually picked. Picking of rosettes took place under an inverted brightfield microscope. Using a needle, rosette islands were cut out from the plated EBs. Media, containing floating rosettes, was collected in a 15 ml falcon tube and centrifuged for 1 min at 200xg. Supernatant was aspirated, rosettes were resuspended in 6 ml rosette media containing 10 ng/ml FGF2 and plated into one 6 cm petri dish. The next day, loosely attached rosettes were collected, transferred into a new 6 cm

---

petri dish and fresh FGF2 (10 ng/ml) was added. Two days after rosette picking, neurospheres, which had formed meanwhile, were collected in a 15 ml falcon tube, centrifuged for 1 min at 200xg, resuspended in fresh rosette media containing FGF2 and plated into a 6 cm petri dish. On day three after picking, fresh FGF2 was added and on day four, NPCs were either kept in suspension for neurosphere cultures (2.2.9.2) or plated as single cells in order to obtain monolayer cultures. For this, neurospheres were collected in a 15 ml falcon tube as described. Cells were then resuspended in 250  $\mu$ l of 0.25% Trypsin/EDTA, transferred into one well of a 24-well plate and incubated for 10 min at 37°C. After 5 min cells were gently triturated with a 1000  $\mu$ l pipette. After 10 min cells were again triturated and complete disaggregation of neurospheres was confirmed under the microscope. Cells were collected in a 15 ml falcon tube containing 250  $\mu$ l trypsin inhibitor and 2 ml NPC media. Cells were centrifuged at 200xg for 4 min. Supernatant was removed, cells were carefully resuspended in 2 ml NPC media containing 20 ng/ml FGF2 and EGF and were plated onto one well of a 6-well plate pre-coated with PLO/L (2.2.2.3). The first media change was performed 48 h after plating.

Three days after initial plating, NPCs were in general confluent and could be passaged. For this, media was aspirated and 350  $\mu$ l of 0.05% Trypsin/EDTA was evenly added to the cells and allowed to incubate for 2 min at 37°C. Cells were collected into a 15 ml falcon tube using 3 ml NPC media containing 350  $\mu$ l trypsin inhibitor. NPCs were centrifuged for 4 min at 200xg. Media was removed, cells were resuspended in 4 ml NPC media containing EGF and FGF2 (20 ng/ml each) and NPCs were plated onto two wells of a 6-well plate pre-coated with PLO/L. NPCs were always passaged in a 1:2 ratio. Media change was in general performed every third day.

For freezing, NPCs were detached and collected as described. The cell pellet was then resuspended in NPC media containing 10% DMSO and cells were frozen down at -80°C using a Nalgene<sup>TM</sup> Cryo freezing container. For long term storage, cells were kept in a liquid nitrogen tank. As a rule, one confluent well of a 6-well plate was frozen down into one cryovial using 1 ml of freezing media.

For thawing NPCs, the cryovial was placed into the 37°C warm water bath until most of its content was thawed. Cells were resuspended in 5 ml of cold NPC media, collected in a 15 ml falcon tube and centrifuged for 4 min at 200xg. Supernatant was removed, cells were resuspended in 2 ml warm NPC media containing growth factors and plated onto one well of a PLO/L pre-coated 6-well plate.



---

**Trypsin inhibitor**

|  |        |
|--|--------|
| Trypsin inhibitor from chicken egg white | 250 mg |
| DPBS                                     | 250 ml |

Trypsin inhibitor was dissolved in DPBS and after filter sterilization (0.45  $\mu$ m) stored in aliquots at -20°C. Once thawed, trypsin inhibitor was stored at 4°C for up to two weeks.

**2.2.9.2 Neurosphere culture**

Four days after rosette picking (Scheme 2.3), neurospheres that had formed were collected in a 15 ml falcon tube and centrifuged for 4 min at 200xg. The supernatant was aspirated and the remaining spheres were resuspended in 7 ml NPC media, supplemented with EGF and FGF2 (20 ng/ml each), and transferred into a new 6 cm petri dish. Media change was performed twice a week. For this, neurospheres were collected and centrifuged for 4 min at 200xg, supernatant was removed and spheres were gently triturated with a 200  $\mu$ l pipette tip in order to disrupt the spheres in smaller pieces. Cells were then collected in 7 ml NPC media supplemented with growth factors and plated into a new 6 cm petri dish.

**2.2.10 Neuronal differentiation**

In order to differentiate NPCs into mature neurons, cells were detached and collected as described in 2.2.9. NPCs were resuspended in 1 ml NPC media and counted using a hemocytometer. They were plated in NPC media containing EGF and FGF2 (20 ng/ml each) at a density of 40.000 cells/cm<sup>2</sup> onto PLO/L pre-coated 4-well plates. The next day, media was changed to final differentiation media (2.2.1) supplemented with 0.5 mM cAMP. Media change was performed every third day and cells were allowed to differentiate for 14 days.

In order to differentiate neurospheres, spheres were collected as described in 2.2.9.2. Supernatant was removed, spheres were resuspended in 2 ml NPC media containing EGF and FGF2 (20 ng/ml each) and plated onto four wells of a PLO/L pre-coated 4-well plate. The next day media was changed to differentiation media. Media change was performed every third day and cells were allowed to differentiate for 14 days.

---

## 2.3 Molecular biology

### 2.3.1 Plasmid preparation

All plasmids needed for reprogramming were kindly provided by the Schöler group (Max-Planck-Institute, Münster). LB-media as well as agar plates were provided by the Max-Planck-Institute CORE facility.

#### 2.3.1.1 Bacterial culture

Chemical competent *Escherichia coli* TOP10 were thawed on ice. In a 1.5 ml Eppendorf tube, 20 µl of bacterial culture were mixed with 0.5 µl of plasmid preparation. The mixture was first incubated for 10 min on ice, then incubated for 90 s at 42°C and placed immediately on ice again. Following addition of 250 µl LB-media, the Eppendorf tube was placed into a thermomixer and incubated for 1 h at 37°C. Bacteria which were transformed with plasmids containing sequences for *POU5F1*, *SOX2*, *MYC*, *KLF4* or *VSV-G* were plated onto agar plates containing ampicillin. Bacteria transformed with the plasmid containing the *gag-pol* sequence were plated onto agar plates containing kanamycin. Agar plates were incubated overnight at 37°C.

The next day, 13 ml bacterial tubes were prepared with 5 ml LB-media containing either 50 µg/ml ampicillin or 25 ng/ml kanamycin. From each agar plate, prepared the day before, only one colony was picked and transferred into the appropriate tube. The tube was incubated at 37°C for 8 h in an incubation shaker at 200 rpm. After 8 h, 500 µl of the bacterial starter culture were added to a 1 L flask containing 300 ml LB-media and the appropriate antibiotic. Flasks were shaken at 200 rpm overnight at 37°C.

The next day, bacteria cultures were centrifuged at 4°C and 4700xg for 20 min. The supernatant was decanted and plasmid DNA was isolated from the remaining bacterial cell pellet.

#### 2.3.1.2 Plasmid DNA purification

Plasmid DNA purification was performed using the *NucleoBond<sup>®</sup> Xtra Maxi Kit* from MACHEREY-NAGEL. The purification was performed according to the manufacturer's instructions for high-copy plasmids.

---

The bacterial pellet was resuspended in 12 ml RES buffer containing RNase A (60 µg/ml) and transferred into a 50 ml falcon tube. Following addition of 12 ml LYS buffer, the tube was inverted 5 times and incubated for 5 min at RT. Meanwhile the *NucleoBond<sup>®</sup> Xtra* column, containing the inserted column filter, was equilibrated with 25 ml EQU buffer by applying the buffer carefully along the rim of the column filter. 12 ml of NEU buffer were added to the mixture and the tube was inverted 10 times. The homogeneous suspension containing white precipitate was then applied onto the rim of the column. The column was washed once with 15 ml EQU buffer and the *NucleoBond<sup>®</sup> Xtra* column filter was discarded. The column was washed once more with 25 ml WASH buffer and plasmid DNA was eluted while applying 15 ml of ELU buffer onto the column. Eluate was collected in a 50 ml falcon tube. DNA was precipitated while adding 10.5 ml isopropanol to the eluate. The tube was vortexed and the mixture was allowed to settle for 2 min at RT. Meanwhile the *NucleoBond<sup>®</sup> finalizer* was applied to a 30 ml syringe. The precipitation mixture was filled into the syringe and pressed slowly through the *finalizer*. The flow through was discarded and DNA retained within the *finalizer* was washed once with 5 ml of 70% ethanol. The *finalizer* was blow dried by removing and reattaching the syringe plunger several times. The *finalizer* was attached onto a 1 ml syringe and plasmid DNA was eluted by applying 800 µl TE buffer onto the *finalizer*. Plasmid DNA concentration was measured using *NanoDrop<sup>®</sup>* and further stored at -20°C.

### 2.3.2 RNA isolation

RNA was in general extracted from one confluent well of a 6-well plate. This was also true for EBs since they were generated out of one well of a 6-well plate. The following specifications are given per sample.

RNA isolation was performed using the *RNeasy Mini Kit* from Qiagen. The cell pellet was resuspended in 350 µl RLT lysis buffer containing 1% β-mercaptoethanol. The lysate was loaded onto the QIAshredder column and centrifuged for 2 min at full speed. 350 µl ethanol (70%) were added to the homogenized lysate. The 700 µl of sample were then transferred onto a new column and centrifuged at 8000xg for 15 s. The column was loaded with 350 µl RW1 buffer and centrifuged again for 15 s at 8000xg. DNase digestion was performed by mixing 10 µl DNase I stock solution (1000 U/ml) with 70 µl RDD buffer. DNase solution was added onto the column and allowed to incubate for 15 min at RT. Following incubation, the column was loaded with 350 µl RW1-buffer and centrifuged for 15 s at 8000xg. The filtrate was removed, the column was loaded with 500 µl RPE buffer and centrifuged for 15 s at

8000xg. Again, the filtrate was removed, the column was loaded with 500  $\mu$ l RPE buffer and centrifuged this time for 2 min at 8000xg. The column was placed onto a new collecting tube and centrifuged for 1 min at full speed. The column was then placed onto a 1.5 ml Eppendorf tube, loaded with 30  $\mu$ l RNase free water and RNA was eluted through centrifugation at 8000xg for 1 min. RNA concentration was determined using *NanoDrop*<sup>®</sup> and further stored at -80°C.

### 2.3.3 Reverse transcription

Reverse transcription was carried out using the *QuantiTect Reverse Transcription Kit* from Qiagen. The reverse transcription reaction mix was prepared in two steps:

**Table 2.13: Reaction mix for reverse transcription**

| Step one            |                            | Step two                           |                             |
|---------------------|----------------------------|------------------------------------|-----------------------------|
| gDNA Wipeout Buffer | 2 $\mu$ l                  | Quantiscript Reverse Transcriptase | 1 $\mu$ l                   |
| 1 $\mu$ g RNA       | x $\mu$ l                  | Quantiscript RT Buffer 5X          | 4 $\mu$ l                   |
| RNase free water    | <u>x <math>\mu</math>l</u> | RT Primer Mix                      | 1 $\mu$ l                   |
|                     | $\Sigma$ 14 $\mu$ l        | RNA mix from step one              | <u>14 <math>\mu</math>l</u> |
|                     |                            |                                    | $\Sigma$ 20 $\mu$ l         |

The RNA mix from step one was prepared in a 0.5 ml Eppendorf tube, incubated in a thermocycler for 2 min at 42°C and immediately placed on ice. The reverse transcription mix (step two) was prepared and 6  $\mu$ l were added to the RNA mix from step one. The reaction mix was mixed and cDNA synthesis was carried out in a thermocycler running the following temperature program:

**Table 2.14: Temperature program for reverse transcription**

| Program            |             |
|--------------------|-------------|
| <u>Temperature</u> | <u>Time</u> |
| 42°C               | 30 min      |
| 95°C               | 3 min       |

cDNA was placed on ice and stored at -20°C.

### 2.3.4 Polymerase chain reaction

In order to confirm the common 1.02 kb deletion within the CLN3 gene in patient-derived fibroblasts and iPSCs, a genotyping PCR was performed. The following tables (Table 2.15 and Table 2.16) list the components of the 25  $\mu$ l reaction as well as the temperature program. All items were purchased from Fermentas.

**Table 2.15: Reaction mix for genotyping PCR**

| Component   | Concentration | Volume                     |
|---|---------------|----------------------------|
| PCR grade water   |               | 12,4 $\mu$ l               |
| Taq Reaction buffer 5X                                  |               | 5 $\mu$ l                  |
| MgCl <sub>2</sub>                                       | 2 mM          | 2 $\mu$ l                  |
| dNTP  | 10 $\mu$ M    | 2 $\mu$ l                  |
| Primer forward  | 10 $\mu$ M    | 1.25 $\mu$ l               |
| Primer reverse  | 10 $\mu$ M    | 1.25 $\mu$ l               |
| <i>Maxima<sup>TM</sup> Hot Start Taq DNA Polymerase</i> | 5 U/ $\mu$ l  | 0.1 $\mu$ l                |
| cDNA  |               | <u>1 <math>\mu</math>l</u> |
|   |               | $\Sigma$ 25 $\mu$ l        |

**Table 2.16: Program for genotyping PCR**

| Step                  | Temperature | Duration |
|-----------------------|-------------|----------|
| Polymerase activation | 94°C        | 3min     |
| Denaturation          | 94°C        | 30 s     |
| Annealing             | 56°C        | 45 s     |
| Elongation            | 72°C        | 1 min    |
|                       | 72°C        | 5 min    |
| Cooling               | 4°C         | hold     |

} 35 Cycles

### 2.3.5 Quantitative real-time polymerase chain reaction

In order to compare relative gene expression levels, quantitative real-time polymerase chain reaction (qPCR) was performed. This specific kind of PCR is based on the SYBR<sup>®</sup> green dye, which fluoresces when bound to double-stranded DNA. The fluorescence emitted during the course of PCR reaction can be measured and allows quantitative analysis of gene expression levels.

qPCR was performed using the *QuantiTect SYBR Green PCR Kit* from Qiagen. Amplification was carried out in 25  $\mu$ l reactions. Table 2.17 lists the components of one 25  $\mu$ l reaction.

**Table 2.17: Reaction mix for qPCR**

| Component                                 | Concentration | Volume                     |
|---|---------------|----------------------------|
| Quantitect SYBR Green PCR-Master Mix      |               | 12,5 $\mu$ l               |
| PCR grade water                           |               | 8,5 $\mu$ l                |
| Primer forward                            | 10 $\mu$ M    | 1 $\mu$ l                  |
| Primer reverse                            | 10 $\mu$ M    | 1 $\mu$ l                  |
| cDNA (1:10 prediluted in PCR grade water) |               | <u>2 <math>\mu</math>l</u> |
|   |               | $\Sigma$ 25 $\mu$ l        |

Since primer sequences for transgene silencing were taken from Kim, J.B. *et al.*, 2009, two different qPCR conditions were chosen for analysis of silencing and for gene expression levels of neural progenitor cells (Table 2.18 and Table 2.19 respectively). In addition, experiments were performed in two different laboratories. Therefore, transgene silencing was analyzed using the *LightCycler<sup>®</sup> MX300P<sup>TM</sup>* from the company Stratagene and the software *MXpro* for data analysis whereas NPC gene expression levels were analyzed using the *LightCycler<sup>®</sup> 480II* from the company Roche and the *LightCycler 480* software

**Table 2.18: qPCR program for retroviral silencing**

| Step                                     | Temperature | Duration |
|--|-------------|----------|
| Polymerase activation                    | 95°C        | 15 min   |
| Denaturation                             | 94°C        | 15 s     |
| Annealing                                | 57°C        | 30 s     |
| Elongation and single signal measurement | 72°C        | 30 s     |
| Melting curve analysis                   | 95°C        | 1 min    |
|  | 55°C        | 30 s     |
|  | 95°C        | 30 s     |
| Cooling                                  | 37°C        | hold     |

} 40 Cycles

**Table 2.19: qPCR program for NPC gene expression levels**

| Step                                     | Temperature | Duration |             |
|--|-------------|----------|-------------|
| Polymerase activation                    | 95°C        | 15 min   |             |
| Denaturation                             | 95°C        | 10 s     | } 50 Cycles |
| Annealing                                | 60°C        | 20 s     |             |
| Elongation and single signal measurement | 72°C        | 30 s     |             |
| Melting curve analysis                   | 95°C        | 10 s     |             |
|  | 55°C        | 20 s     |             |
|  | 98°C        | 30 s     |             |
| Cooling                                  | 37°C        | hold     |             |

Gene expression analysis was performed in duplicates and quantification of gene expression was analyzed using the  $\Delta\Delta C_t$  method, where  $C_t$  signifies the cycle threshold:

$$\Delta C_{t_{\text{sample}}} = C_{t_{\text{gene of interest}}} - C_{t_{\text{reference gene}}}$$

$$\Delta C_{t_{\text{control}}} = C_{t_{\text{gene of interest}}} - C_{t_{\text{reference gene}}}$$

$$\text{Ratio} = 2^{-(\Delta C_{t_{\text{sample}}} - \Delta C_{t_{\text{control}}})}$$

Viral silencing was calculated using the following formula which has been established in the Schöler laboratory:

$$\text{Percentage of } GAPDH \text{ expression} = 2^{-(\Delta C_{t_{\text{sample}}})} \times 100$$

Gene expression levels of *GAPDH* were used as reference for all experiments. Appropriate controls were used according to the samples analyzed and are given in detail in the results part of this thesis.

In order to confirm the specificity of the qPCR signal, each amplification product was analyzed by agarose gel electrophoresis for correct product length. This analysis was done for each primer pair once using one control and sample amplification products.

### 2.3.6 Agarose gel electrophoresis

Analysis of PCR and qPCR products was performed using agarose gel electrophoresis. The following instructions are given for a small gel; for larger ones three times the amount of reagents were used. Electrophoresis was performed using a chamber system of the Peqlab company.

---

For the preparation of a 2% gel (w/v), 1 g agarose and 50 ml 1X TAE buffer were mixed in an Erlenmeyer flask and microwaved until the agarose was completely dissolved. The agarose solution was allowed to cool down and 5  $\mu$ l of RedSafe™ were added and evenly dispensed within the solution. Agarose solution was filled into the chamber and the air bubble-free gel was allowed to completely polymerize. The gel was placed into the electrophoresis chamber and covered with 1X TAE buffer. 2  $\mu$ l of sample were mixed with 1  $\mu$ l of 6X loading buffer and filled into the well of the gel. The *peqGOLD O'range 50 bp DNA ladder* was used as a reference. Electrophoresis was performed using 100 V direct current voltage. Bands were then detected and imaged with a UV transilluminator.

### 10X TAE buffer

|   |        |
|---|--------|
| TRIS                                    | 400 mM |
| Na <sub>2</sub> EDTA·2 H <sub>2</sub> O | 20 mM  |

Adjusted with glacial acetic acid to pH 8 and filled up to 1 L with deionized water.

## 2.4 Protein biochemistry

### 2.4.1 Western blot analysis

#### 2.4.1.1 Protein extraction and quantification

Cell pellets which were stored at -80°C for further protein extraction, were placed on ice and allowed to thaw. According to the size, cell pellets were in general resuspended in 80-100  $\mu$ l of lysis buffer containing protease and phosphatase inhibitors. Samples were shaken at 4°C for 45 min, followed by centrifugation at 14700xg for 30 min at 4°C. The supernatant was transferred into a new Eppendorf tube and protein concentration was determined using the *Pierce® BCA Protein Assay Kit* from Thermo Fisher. For this, a working solution was prepared according to the following equation:

$$(9 \text{ standards} + n \text{ samples}) \times (3 \text{ replicates}) \times (0.2 \text{ ml}) = \text{working solution required (50:1 reagent A:B)}$$

Prior to analysis, samples were diluted 1:10 in lysis buffer and 10  $\mu$ l of each, samples and standards, were placed into a microwell plate. Following addition of 190  $\mu$ l working solution, the plate was incubated at 37°C for 30 min in the dark. Protein determination was carried out



at a wave length of 562 nm using the spectrophotometer *SPECTRAmax Plus*. Protein extracts were stored in aliquots at -80°C.

### Lysis buffer

|  |            |
|--|------------|
| Tris buffered saline                               | 2 tablets  |
| Triton-X100  | 0.2% (v/v) |
| cOmplete, mini protease inhibitor cocktail tablets | 3 tablets  |
| Phosphatase inhibitor                              | 3 tablets  |
| Deionized water                                    | 30 ml      |

Tablets were dissolved in 30 ml deionized water. The final concentration of NaCl was 150 mM and of Tris 50 mM. The pH was 7.5.

#### 2.4.1.2 Protein separation

In a 1.5 ml Eppendorf tube 10 µg of total protein extract were mixed with 4X loading buffer, 10X reducing agent (β-mercaptoethanol) and adjusted with lysis buffer to a final volume of 20 µl. Samples were heated for 10 min at 70°C or at 50°C for LAMP-1 and EEA-1. Meanwhile the ready-to-use gel was placed into the *Novex*<sup>®</sup> *Mini-Cell* electrophoresis chamber and the middle compartment was filled up with running buffer. Denatured samples as well as 8 µl of *Rainbow* molecular weight standard were loaded into the wells. The outer compartments were filled up with running buffer and electrophoresis was started. The following table indicates the different conditions used for protein separation according to their molecular weight.

**Table 2.20: Conditions for protein separation**

|                         | Low molecular weight proteins | High molecular weight proteins |
|-------------------------|-------------------------------|--------------------------------|
| Molecular weight range: | 4 kDa – 75 kDa                | 60 kDa – 130 kDa               |
| Loading buffer:         | 1X Laemmli buffer             | 1X Laemmli buffer              |
| Running buffer:         | 1X Tris-Glycine SDS           | 1X Tris-Glycine SDS            |
| Polyacrylamide gel:     | Tris-glycine 4-20%            | Tris-glycine 4-12%             |
| Voltage:                | 125 V                         | 125 V                          |
| Duration:               | 90 min                        | 120 min                        |

Buffers were purchased as stock solutions from Boston Bioproducts and prepared with deionized water to 1X running buffers. Gels were purchased from Life Technologies Corporation.

#### 2.4.1.3 Protein transfer

In preparation for the protein transfer, four blotting pads, two pieces of filter paper, and the nitrocellulose membrane (0.2  $\mu\text{m}$ , BioRad) were soaked with transfer buffer. The blotting pads were placed into the transfer chamber followed by a filter paper, the polyacrylamide gel, the nitrocellulose membrane and the second filter paper. After removal of air bubbles, the remaining two blotting pads were placed on top and the transfer chamber was placed into the *Novex<sup>®</sup> Mini-Cell* equipment. The blotting chamber was filled with transfer buffer whereas the outer compartments were filled with deionized water. The entire apparatus was placed into a bucket filled with ice and the transfer was started. The following table indicates the transfer conditions for the proteins according to their molecular weight.

**Table 2.21: Transfer conditions**

|                         | <b>Low molecular weight proteins</b>               | <b>High molecular weight proteins</b>              |
|-------------------------|--|--|
| Molecular weight range: | 4 kDa – 75 kDa                                     | 60 kDa – 130 kDa                                   |
| Transfer buffer:        | 1X Novex <sup>®</sup> tris-glycine transfer buffer | 1X Novex <sup>®</sup> tris-glycine transfer buffer |
|                         | 10% MeOH   | 10% MeOH   |
| Voltage:                | 25 V   | 30 V   |
| Duration:               | 90 min   | 120 min  |

Transfer buffers were purchased as stock solutions from Life Technologies and adjusted to 1X working solutions with deionized water.

#### 2.4.1.4 Protein detection

After completion of transfer, the membrane was washed twice in TBS/Tween and proper protein transfer was verified. For this, the membrane was incubated at a shaking table for 15 min at RT in *Ponceau S Stain* solution. Membrane was then quickly rinsed three times with deionized water. Distinct bands were now visible by eye which gave information about the quality of protein transfer. This staining procedure was reversible and *Ponceau S Stain* was removed by washing the membrane three times with TBS/Tween.

For protein detection, membrane was incubated at RT on a shaking table for 1 h in blocking solution. Primary antibodies (Table 2.9) were diluted in blocking solution and membrane was incubated overnight at 4°C on a shaking table with antibody solution.

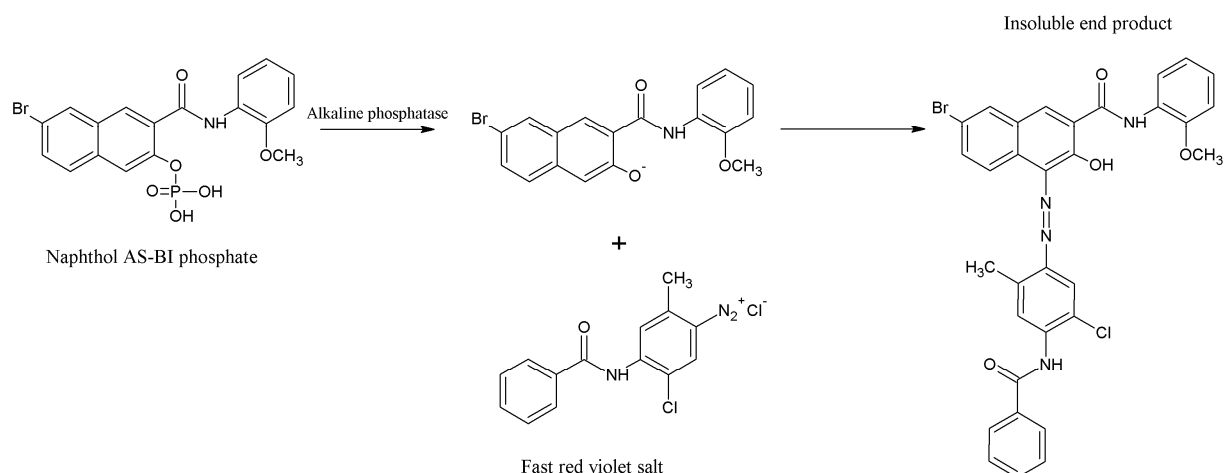
The next day, membrane was washed with TBS/Tween while shaking three times for 10 min at RT. Horseradish peroxidase conjugated secondary antibodies (Table 2.10) were diluted in blocking solution and membrane was incubated for 1 h at RT on a shaking table. After removal of secondary antibody solution through washing of membrane for several times with TBS/Tween, membrane was incubated for 2 min at RT with 600 µl of *Western Lightening™ PLUS-ECL*. Excess ECL reagent was drained, and membrane was wrapped into a piece of saran wrap. Developing took place in a dark room using a high performance chemiluminescence film (Amersham Hyperfilm™ ECL, GE Healthcare). In general, three different exposure times were taken (30 s, 2 min and 2 h). The developed film was scanned and bands were quantified using the program *Quantity One 4.6.9* from Bio-rad.

#### **Blocking buffer**

|                  |          |
|------------------|----------|
| TBS (1X)         | 99,9%    |
| Tween 20         | 0.1%     |
| Non-fat dry milk | 5% (w/v) |

#### **2.4.2 Alkaline phosphatase assay**

Alkaline phosphatase (AP) is an enzyme which is highly active in pluripotent embryonic stem cells. Hence, detection of alkaline phosphatase in iPSCs demonstrates their pluripotent state (O'Connor *et al.*, 2008). AP assay was performed by using the *Alkaline Phosphatase Detection Kit* from Millipore. The enzymatic reaction mediated by AP is shown below (Scheme 2.4).



**Scheme 2.4: Enzymatic reaction mediated by alkaline phosphatase**

IPSCs were grown on 4-well Matrigel™ pre-coated plates (2.2.7.2) for five days. Media was removed and cells were fixed with 4% PFA for 2 min. PFA was aspirated and cells were washed once with 1X rinse buffer. Fast Red Violet was mixed with Naphthol AS-BI phosphate solution and water (2:1:1 ratio). Rinse buffer was removed and 500  $\mu$ l Fast Red mix were added per well of a 4-well plate. Cells were incubated in the dark at RT for 15 min. The Fast Red mix was aspirated and cells were washed once with 1X rinse buffer. Cells were covered with PBS and stained iPSC colonies were imaged.

### Rinse buffer (1X)

|                  |             |
|------------------|-------------|
| Tris-HCl, pH 7.4 | 20 mM       |
| NaCl             | 0.15 M      |
| Tween-20         | 0.05% (v/v) |

### 2.4.3 Terminal deoxynucleotidyl transferase assay

During apoptosis, genomic DNA is cleaved, which yields in double-stranded, low molecular weight DNA fragments as well as in single strand breaks of high molecular weight DNA. DNA strand breaks, presenting free 3'-OH termini, can then be identified by labeling with modified nucleotides in an enzymatic reaction. This reaction is mediated by terminal deoxynucleotidyl transferase in a template-independent manner (TUNEL reaction; Gavrieli *et al.*, 1992; Gorczyca *et al.*, 1993).

TUNEL assay was performed using the *In Situ Cell Death Kit* from Roche. NPCs were grown under standard conditions (2.2.9) for 24 h post-plating onto 4-well plates. Media was

removed, cells were washed once with PBS, allowed to dry for 2 min at RT and then fixed for 1 h at RT with freshly prepared PFA solution (4%). Cells were washed once with PBS and incubated for 2 min on ice with permeabilization solution. Cells were washed twice with PBS. Cells incubated with 250  $\mu$ l DNase I solution (0.01 U/ $\mu$ l) for 10 min at RT were used as a positive control. Positive control was washed once with PBS. Enzyme mix was diluted 1:10 in TUNEL solution and 100  $\mu$ l of the mixture were added per well. The plate was wrapped with Parafilm<sup>®</sup> to prevent it from drying out, covered in aluminium foil and incubated for 1 h at 37°C. Cells were washed twice with PBS and cell nuclei were stained using Hoechst (2.5.1.1). TUNEL assay was immediately analyzed.

For analysis of TUNEL-positive cells in neuronal cultures, cells were differentiated as described in 2.2.10. After 7 days of differentiation, TUNEL reaction was performed as described above but without performing the nuclear staining with Hoechst. Instead, cells were subjected to staining with primary and secondary antibodies as described in 2.5.1.1.

#### **Permeabilization solution**

|                |             |
|----------------|-------------|
| PBS (1X)       | 99.8% (v/v) |
| Triton-X100    | 0.1% (v/v)  |
| Sodium Citrate | 0.1% (w/v)  |

#### **2.4.4 Tripeptidyl peptidase I enzyme activity assay**

Since deficiency in tripeptidyl peptidase I (TPP1) leads to late-infantile NCL, measurements of enzyme activity are of great interest for potential drug screenings.

TPP1 activity assay was performed in collaboration with Dr. Staropoli (Massachusetts General Hospital). Dr. Staropoli was in charge of sample preparation and activity measurement.

Cells from one confluent well of a 6-well plate were washed with PBS, scraped into acetate buffer supplemented with the protease inhibitors pepstatin A and E64 and homogenized with 10 passes through a 27-G syringe. TPP1 activity was measured fluorometrically using the Ala-Ala-Phe-7-Amido-4-methylcoumarin substrate (AAF-MCA) as described previously, with some modifications (Page *et al.*, 1993, Lukacs *et al.*, 2003, Ezaki *et al.*, 2000). 20  $\mu$ g of total protein from the scraped cells were incubated in 150  $\mu$ l acetate buffer containing a final concentration of 62.5  $\mu$ M AAF-MCA for 20 h at 37°C. The reaction was stopped by the

addition of 100  $\mu$ l 0.5 M EDTA (pH 12.0). Fluorescence was measured using a Molecular Devices *SpectraMax M2* spectrophotometer with an extinction wavelength of 355 nm and an emission wavelength of 460 nm.

### Acetate buffer

|   |            |
|---|------------|
| Sodium acetate  | 0.1 M      |
| Sodium chloride   | 0.15 M     |
| Pepstatin A   | 10 $\mu$ M |
| Trans-epoxysuccinyl-L-leucylamido-(4-guanidino)butane (E64) | 10 $\mu$ M |

Buffer was adjusted to pH 4.0.

## 2.5 Microscopy

### 2.5.1 Immunofluorescence

The following specifications refer to one well of a 4-well plate.

#### 2.5.1.1 General staining procedure

Media was removed, cells were washed once with PBS and fixed with 4% PFA for 10 min at RT. PFA was aspirated, cells were washed three times with PBS and incubated for 2 h at RT in 250  $\mu$ l blocking solution. Following blocking, primary antibodies (Table 2.7) were diluted in blocking solution and cells were incubated with 250  $\mu$ l primary antibody solution overnight at 4°C. The next day, cells were washed three times for 10 min in PBS. Secondary antibodies were diluted in blocking solution and cells were incubated for 1 h at RT in 250  $\mu$ l secondary antibody solution. Secondary antibody solution was aspirated and sample was washed three times for 10 min in PBS. During all steps involving secondary antibodies, the sample was protected from light.

Cells grown on coverslips were then fixed on microscope slides using *Prolong<sup>®</sup> Gold Antifade Reagent* with 4',6-Diamidino-2-phenylindol (DAPI). Slides were allowed to dry for 24 h at RT and coverslips were then sealed with nail polish.

Nuclei from cells that were not grown on coverslips were stained using Hoechst. 0.75  $\mu$ l of Hoechst solution were mixed with 1 ml PBS and cells were incubated in 500  $\mu$ l Hoechst solution for 2 min at RT. Cells were washed three times with PBS and imaged within 24 h.

---

**Blocking solution**

|              |             |
|--------------|-------------|
| PBS (1X)     | 96,8% (v/v) |
| Donkey Serum | 3% (v/v)    |
| Triton-X100  | 0.2% (v/v)  |

**2.5.1.2 5-bromo-2'-deoxyuridine staining**

Since 5-bromo-2'-deoxyuridine (BrdU) is incorporated into the DNA of cells, a special protocol was performed in order to detect BrdU in treated cells (ref. 2.2.8).

Media was aspirated, cells were washed once with PBS and fixed for 10 min at RT with 4% PFA. Cells were then washed three times with PBS and incubated for 10 min at -20°C in ice-cold acid ethanol (95% EtOH and 5% glacial acetic acid). Following incubation, cells were washed twice with 250 µl 1.5 N HCl and then incubated in 250 µl 1.5 N HCl for 30 min at 37°C. The sample was washed four times with PBS and immunofluorescence was performed according to the protocol described in 2.5.1.

**2.5.1.3 Imaging**

Fluorescence microscopy for qualitative assessment of pluripotency was performed using a *Leica DM IRE2* and the imaging software *Leica FW 4000*. Fluorescence microscopy for qualitative assessment of NPCs was performed using a *Zeiss Axioskop2 mot plus*. Images were captured using the *AxioVision Rel. 4.6* software. For qualitative experiments, only representative images were taken. These were in general, three to four images per marker protein per iPSC clone or NPC line.

Qualitative confocal microscopy was performed using the *Leica TCS SP5*. Images were captured and processed using the *LAS AF* software. In general, three to four representative images were taken per marker per iPSC clone or NPC line. Settings were kept the same for one marker protein within all iPSC clones and NPC lines. In order to obtain reproducible results, iPSCs from one confluent well of a 6-well plate were grown on Matrigel<sup>TM</sup> coated coverslips 72 h prior to fixation. NPCs were plated at a density of 100.000 cells/well onto 4-well plates and allowed to recover for 24 h prior to fixation. Representative images from iPSC clones were taken from the middle of a colony since the edges usually tend to differentiate which could have led to misinterpretation of results.

Fluorescence microscopy for quantitative assessment of BrdU- and TUNEL-positive cells was performed using a *Nikon Eclipse TE2000-U* and the imaging software *NIS-Elements BR 3.2*. For quantification of BrdU-positive cells in iPSC colonies, images of five colonies were taken (approximately 800-1000 cells). In order to determine the percentage of BrdU-positive cells, all Hoechst-positive cells within these images were counted and this number was set to 100%. Afterwards, the number of BrdU-positive cells was determined and set relative to the total number of cells.

### **2.5.2 Electron microscopy**

In order to confirm morphological changes observed in confocal images of different cell types and to obtain more detailed information about structures of cell compartments, electron microscopy (EM) was performed. This work was performed in collaboration with Dr. Staropoli (Massachusetts General Hospital). Dr. Staropoli was in charge of sample preparation and imaging.

IPSCs from one confluent well of a 6-well plate (Matrigel<sup>TM</sup> coated) or NPCs from one confluent 10 cm dish were fixed directly with gentle rocking for 15 min at RT with a glutaraldehyde fixative, gently scraped, pelleted at 500xg, and washed twice with cacodylate buffer. To make a cell block, the cells were centrifuged and resuspended in 60°C warm agar (2%) in a warm water bath to keep the agar fluid. The cells were then centrifuged again and the agar was allowed to solidify in an ice water bath. The tissue containing tip of the centrifuge tube was cut off resulting in an agar block with the cells embedded within it. This agar block was subsequent routinely processed in a *Leica Lynx* automatic tissue processor. Briefly, the tissue was post-fixed in osmium tetroxide, stained *En Bloc* with uranyl acetate, dehydrated in graded ethanol solutions, infiltrated with propylene oxide/Epon mixtures, embedded in pure Epon, and polymerized overnight at 60°C. One micron sections were cut, stained with toluidine blue, and examined by light microscopy. Representative areas were chosen for electron microscopic study and the Epon blocks trimmed accordingly. Thin sections were cut with an *LKB 8801* ultramicrotome and diamond knife, stained with lead citrate, and examined in a *FEI Morgagni<sup>TM</sup>* transmission electron microscope. Images were captured with an AMT digital CCD camera.



---

**Glutaraldehyde fixative**

|                          |              |
|--------------------------|--------------|
| Glutaraldehyde           | 2.5% (v/v)   |
| Paraformaldehyde         | 2% (v/v)     |
| Calcium chloride         | 0.025% (v/v) |
| Sodium cacodylate buffer | 0.1 M        |

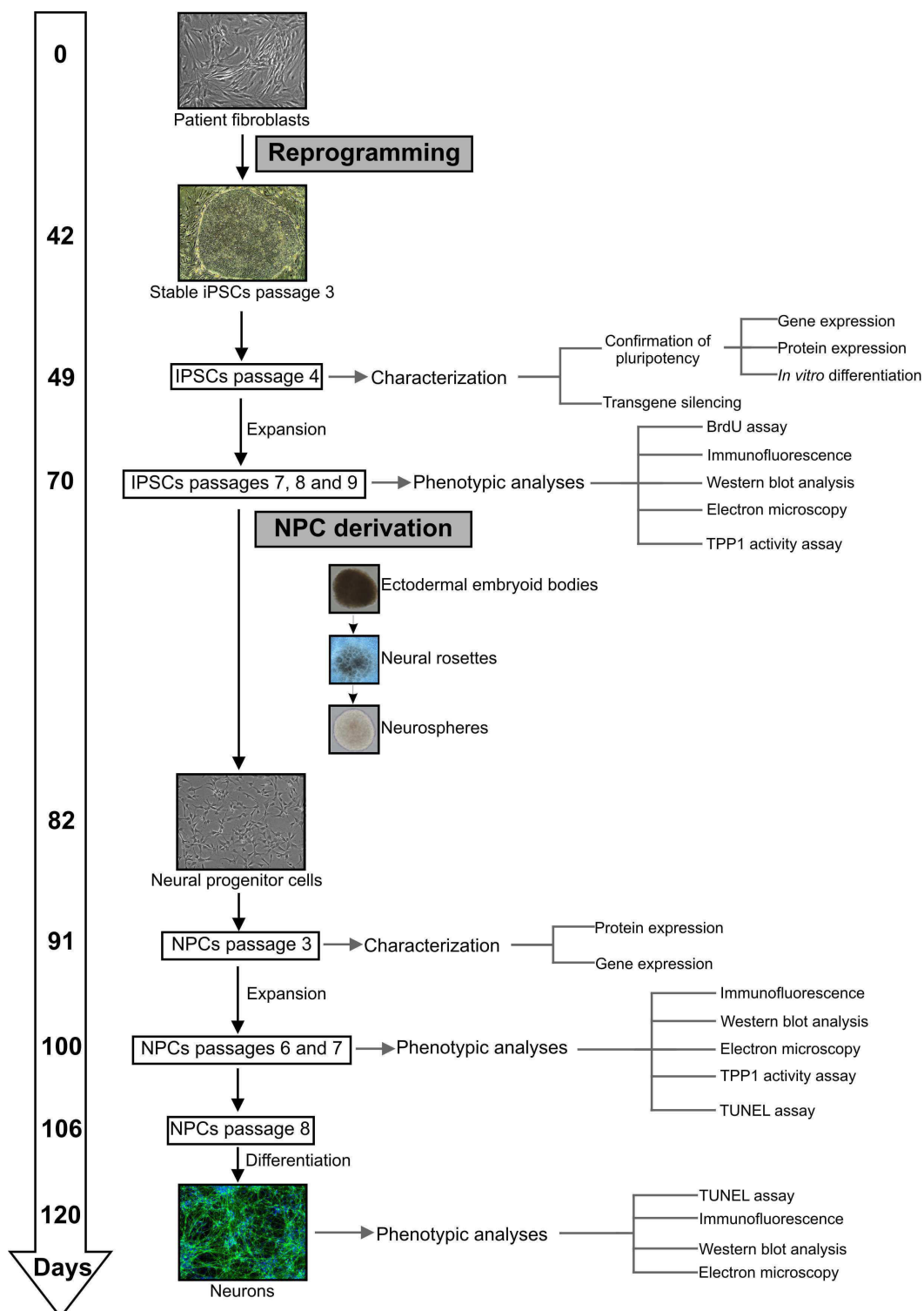
Buffer was adjusted to pH 7.4.

**2.5.3 Statistics**

All data are shown as mean including the standard error of the mean (SEM) for experiments that were run with a sample size  $\geq 3$ . Data were collected and analyzed using the *GraphPad Prism5* software. For Western blot analysis, data were analyzed using the unpaired t-test. Data collected from the BrdU incorporation and the TPP1 enzyme activity assay were analyzed using a one-way ANOVA including a *post-hoc* analysis according to Bonferroni. For all data, statistical significance was assumed when P value was  $< 0.05$ .

### 3 Results

The following scheme shows the experimental outline of the disease modeling.



Scheme 3.1: Experimental outline of the disease modeling

Scheme 3.1 indicates important stages of the disease modeling at which analyses were performed. The given timeline provides an estimate for the duration of the disease modeling from the fibroblast to the neuronal stage.

### 3.1 Induced pluripotent stem cells

#### 3.1.1 Patient tissue-derived cell lines

The project was a collaboration between the laboratories of Prof. Storch (Dresden), Prof. Schöler (Münster), and Dr. Cotman (Boston) with the aim to combine patient-derived iPSCs, generated in the Schöler laboratory, with iPSCs generated in the Cotman laboratory.

We thus recruited two patients that were affected by the common mutation within the CLN3 gene and one patient that was a carrier for the common mutation. Table 3.1 lists the combined tissue assembly. It also indicates the genotype and the iPSC as well as NPC lines that were generated from these tissues and used within this work.

**Table 3.1: Assembled fibroblast lines, their reprogrammed derivatives and derived neural progenitors**

| Fibroblast Line          | Genotype  | iPSC Line   | NPC Line   |
|--------------------------|---|---|--|
| CLN3-1DD                 | Homozygous, 1.02 kb deletion  | CLN3 iPSC 1A DD<br>CLN3 iPSC 1B DD <sup>†</sup>           | CLN3 iPS 1A DD NPC<br>CLN3 iPS 1B DD NPC <sup>†</sup>              |
| CLN3-2DD <sup>#</sup>    | Homozygous, 1.02 kb deletion  | CLN3 iPSC 2A DD<br>CLN3 iPSC 2B DD                        | CLN3 iPS 2A DD NPC   |
| CLN3het-3DD <sup>#</sup> | Heterozygous, 1.02 kb deletion  | CLN3 iPSC 3A DD het <sup>†</sup><br>CLN3 iPSC 3B DD het   | CLN3 iPS 3A DD het NPC <sup>†</sup>                                |
| CLN3-1FB                 | Homozygous 1.02 kb deletion   | CLN3 iPSC 1A<br>CLN3 iPSC 1B                              |  |
| CLN3-2FB                 | Allele 1 (Intron 13): c.1056+3 A>C<br>Allele 2 (Exon 15): c.1247 A>G, p.Asp416Gly | CLN3 iPSC 2A <sup>†</sup><br>CLN3 iPSC 2B                 | CLN3 iPS 2A NPC <sup>†</sup>                                       |
| TPP1-1DD <sup>*</sup>    | Allele 1 (Intron 5): c.509-1 G>C<br>Allele 2 (Exon 6): c.622 C>T, p.Arg208X       | TPP1 iPSC 1A DD<br>TPP1 iPSC 1B DD                        | TPP1 iPS 1A DD NPC<br>TPP1 iPS 1B DD NPC                           |
| TPP1-1FB                 | Allele 1 (Intron 5): c.509-1 G>C<br>Allele 2 (Exon 6): c.622 C>T, p.Arg208X       | TPP1 iPSC 1A<br>TPP1 iPSC 1B <sup>†</sup><br>TPP1 iPSC 1C | TPP1 iPS 1A NPC<br>TPP1 iPS 1B NPC <sup>†</sup><br>TPP1 iPS 1C NPC |
| Control BJ1-4            | Normal  | Control BJ iPSC <sup>**</sup>                             |  |
| Control FS DD            | Normal  | Control FS iPSC <sup>***</sup>                            |  |
| Control GM08330          | Normal  | Control GM iPSC <sup>***†</sup>                           | Control GM NPC <sup>†</sup>  |

<sup>#</sup>Donor of fibroblast line CLN3het-3DD is parent of affected donor of fibroblast line CLN3-2DD

<sup>\*</sup>Fibroblast line was published by Steinfeld *et al.*, 2002

<sup>\*\*</sup>Fibroblast lines and derived iPSC lines were published by Sheridan *et al.*, 2011

<sup>\*\*\*</sup>iPSC line was derived and donated by Prof. Schöler

<sup>†</sup>Representative images of organelle assessment are shown from these lines

---

Table 3.1 lists the fibroblast lines which were established from patient skin biopsies. The fibroblast lines CLN3-1DD, 2DD and CLN3het-3DD were established from skin biopsies which were taken from patients participating in the study conducted in Dresden. Together with the fibroblast line TPP1-1DD, which was donated by Prof. Steinfeld, these samples were then reprogrammed into iPSCs for the purpose of this thesis. They were used together with the iPSC lines generated in the Cotman laboratory in Boston for the disease modeling. Overall, for the JNCL disease model we collected tissue samples from three patients homozygous for the common mutation, one patient with a unique compound heterozygous mutation within the CLN3 gene, and tissue samples from a carrier for the common mutation. Since two iPSC clones from each patient were studied, a total of 10 clones derived from five patients with mutations within the CLN3 gene were analyzed. In terms of modeling LINCL, tissue samples from two unrelated donors affected by the same mutation within the TPP1 gene were collected. Due to the fact that samples from only two patients could be collected, it was decided to analyze from one of these patients three iPSC clones. Thus, five iPSC clones for the LINCL disease model were studied. The control iPSC lines were not age matched because of ethical reasons.

NPC lines that were successfully derived from patient iPSCs are also listed in Table 3.1. Overall five NPC lines were studied for JNCL as well as for LINCL. In order to study more control lines, commercially available NPC lines were used. Their origin and source are given in Table 2.12 (page 33).

The following part describing the characterization of the generated iPSCs only refers to iPSCs generated from CLN3-1 DD, 2DD, CLN3het-3DD and TPP1-1DD since the other iPSC lines were generated within the Cotman laboratory and have been characterized by the CORE facility of the Center for Human Genetic Research.

### **3.1.2 Characterization of induced pluripotent stem cell clones**

#### *3.1.2.1 Transgene silencing and endogenous gene expression*

The reprogramming process is quite ineffective. Given that out of 100.000 plated cells only 10 will give rise to iPSC colonies, the efficiency is as low as 1 colony/10.000 cells. However, 10-15 iPSC clones derived from one fibroblast line are sufficient for the later disease modeling. It is thus necessary to assess the quality of the different iPSC clones in terms of

gene expression and pluripotency. Since the latter is very time and cost intensive, the first selection for good clones is made by analysis of exogenous and endogenous gene expression. It is very important for further studies that gene expression is not driven by any residual viral transgene activity since this could lead to misinterpretation of the results and unwanted events like unregulated growth or spontaneous differentiation of the colony. In fully reprogrammed iPSCs the retroviral transgenes are silenced and the pluripotent state is maintained by endogenous gene expression only (Hotta *et al.*, 2008). Hence, exogenous gene expression of *POU5F1* (also known as *OCT4*), *SOX2*, *KLF4* and *MYC* was first analyzed, using primers which were specific to the viral transgenes.

Figure 3.1 shows the qPCR results for the iPSC clones which showed sufficient transgene silencing and were thus chosen for further characterization.

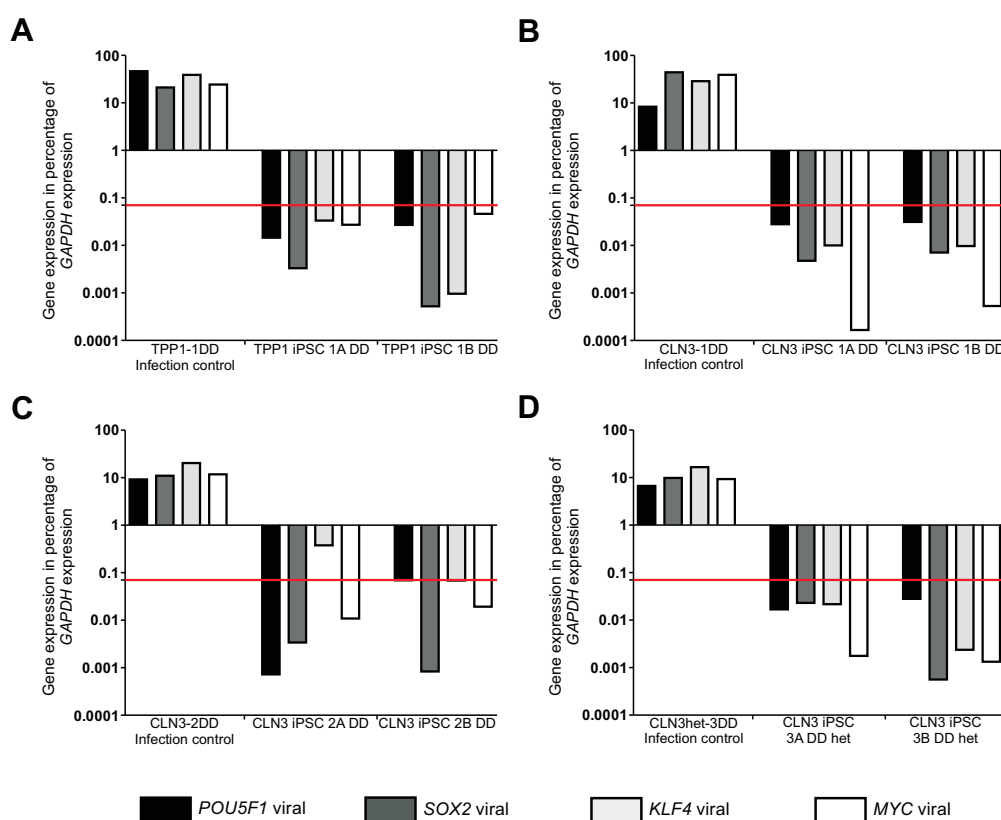


**Figure 3.1: Silencing of retroviral transgenes in human iPSCs**

Diagrams A-D show the quantitative gene expression analysis of retroviral transgenes which was performed in order to identify iPSC clones that sufficiently silenced exogenous gene expression. The red line marks the threshold of *POU5F1* and *MYC* expression which mainly determined silencing criteria. Gene expression was normalized to *GAPDH* expression and was then calculated as percentage of *GAPDH* expression. Freshly infected fibroblasts were used as positive controls for retroviral transgene expression. (All samples were run in duplicate.)

---

Diagrams **A-D** of Figure 3.1 show the exogenous gene expression of the four reprogramming transcription factors which were encoded by the viral transgenes. Figure 3.1 **A** displays the results of the TPP1 line 1DD, diagrams **B** and **C** of Figure 3.1 show the results of the CLN3 lines 1DD and 2DD which were homozygous for the common mutation and diagram **D** of Figure 3.1 shows the results of the CLN3 line CLN3het-3DD which was a carrier of the common mutation within the CLN3 gene. The first group of columns in diagrams **A-D** of Figure 3.1 represents the exogenous gene expression of four factor infected fibroblasts at 48 h after the third infection. As shown, the exogenous gene expression is very variable and does not reflect the ability to give rise to fully reprogrammed iPSCs.

The second and third group of columns shows the exogenous gene expression of iPSC clones at passage 4. The red line indicates the threshold of *POU5F1* and *MYC* expression which should not be exceeded. This threshold was proven in the Schöler laboratory to be a good indicator for sufficient silencing (unpublished data). Clones were thus chosen according to these silencing criteria. This threshold was also reached by the exogenous gene expression of *SOX2* and *KLF4* with exception of the CLN3 iPSC 2A DD clone. Nevertheless, this clone was still chosen for further experiments since the gene expression of *KLF4* was downregulated when compared to the infection control.

In order to maintain the pluripotent state, iPSCs need to re-activate the endogenous gene expression of *POU5F1*, *SOX2*, *KLF4* and *MYC*. Figure 3.2 shows the results of the qPCR which was performed using primer specific to the human genes in order to monitor endogenous gene expression levels in iPSC clones of passage 4. Endogenous gene expression levels of *LIN28A* were analyzed as well since this gene is prominently upregulated in human ESC lines and was not exogenously introduced. It is thus suitable as an additional marker gene for pluripotency.

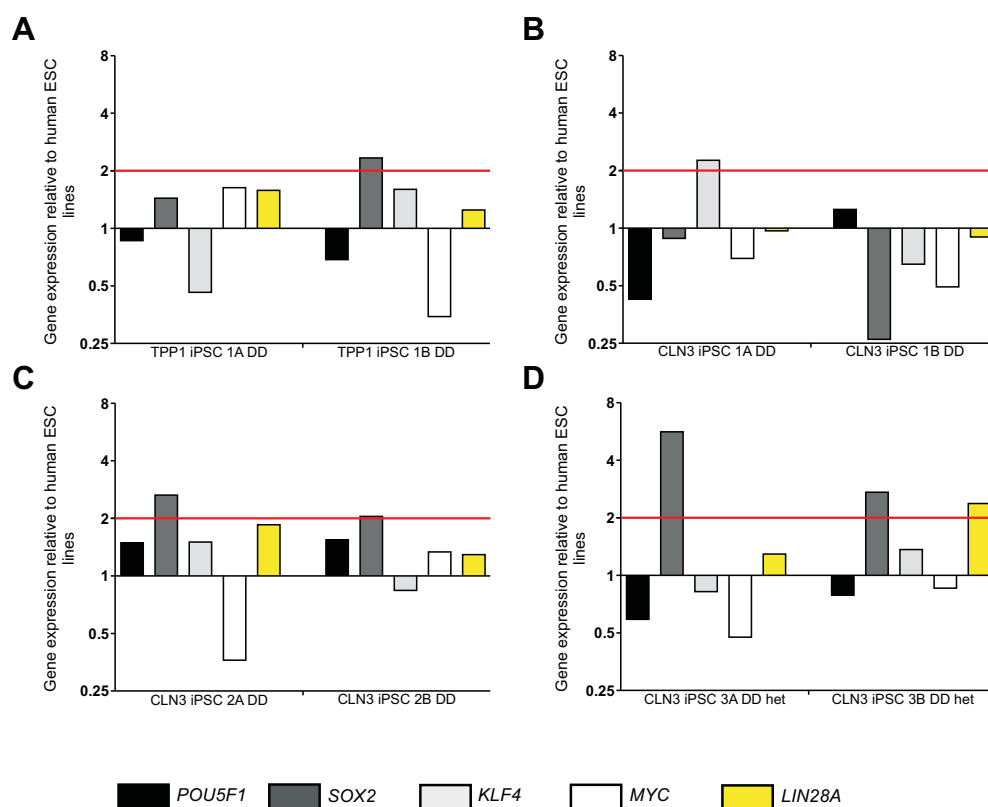


**Figure 3.2: Endogenous expression of pluripotency genes in human iPSCs**

Diagrams A-D show the quantitative expression of pluripotency genes. The red line marks the threshold of *POU5F1* and *MYC* expression which should not be exceeded. Gene expression was normalized to *GAPDH* expression and determined relative to gene expression levels of human ESC lines according to the  $\Delta\Delta C_t$  method. (All samples were run in duplicate.)

Diagrams A-D of Figure 3.2 display the endogenous gene expression of the pluripotency genes *POU5F1*, *SOX2*, *KLF4*, *MYC* and *LIN28A*. The red line marks a two-fold upregulation of gene expression when compared to ESC lines (RNA from the human ESC lines H9 and H1 was kindly provided by the Schöler laboratory). The gene expression of *POU5F1* and *MYC* should be within this range and was the main criteria for the iPSC clone selection, because upregulation of *POU5F1* may cause differentiation into primitive endoderm and mesoderm and *MYC* is a known oncogene which may lead to misinterpretation of the results (Hotta *et al.*, 2008). As shown in the figure (Figure 3.2), endogenous gene expression was very variable among the different iPSC lines and clones. But gene expression was within a normal range in all iPSC clones tested and none of them showed a higher expression for *POU5F1* and *MYC* than given by the threshold. The qPCR results thus confirmed that these clones were suitable for further experiments.

### 3.1.2.2 Confirmation of pluripotency

After selection of iPSC clones that showed sufficient retroviral transgene silencing and endogenous expression of pluripotency genes, these clones were further analyzed for pluripotency at the protein level. Standard procedures for verification of pluripotency include alkaline phosphatase (AP) assay, immunostainings for known marker proteins and differentiation into the three germ layers, namely meso-, endo- and ectoderm.

Figure 3.3 demonstrates the pluripotency of patient fibroblast-derived iPSC clones during expansion. For simplicity, representative images from only one clone per patient fibroblast line are shown.

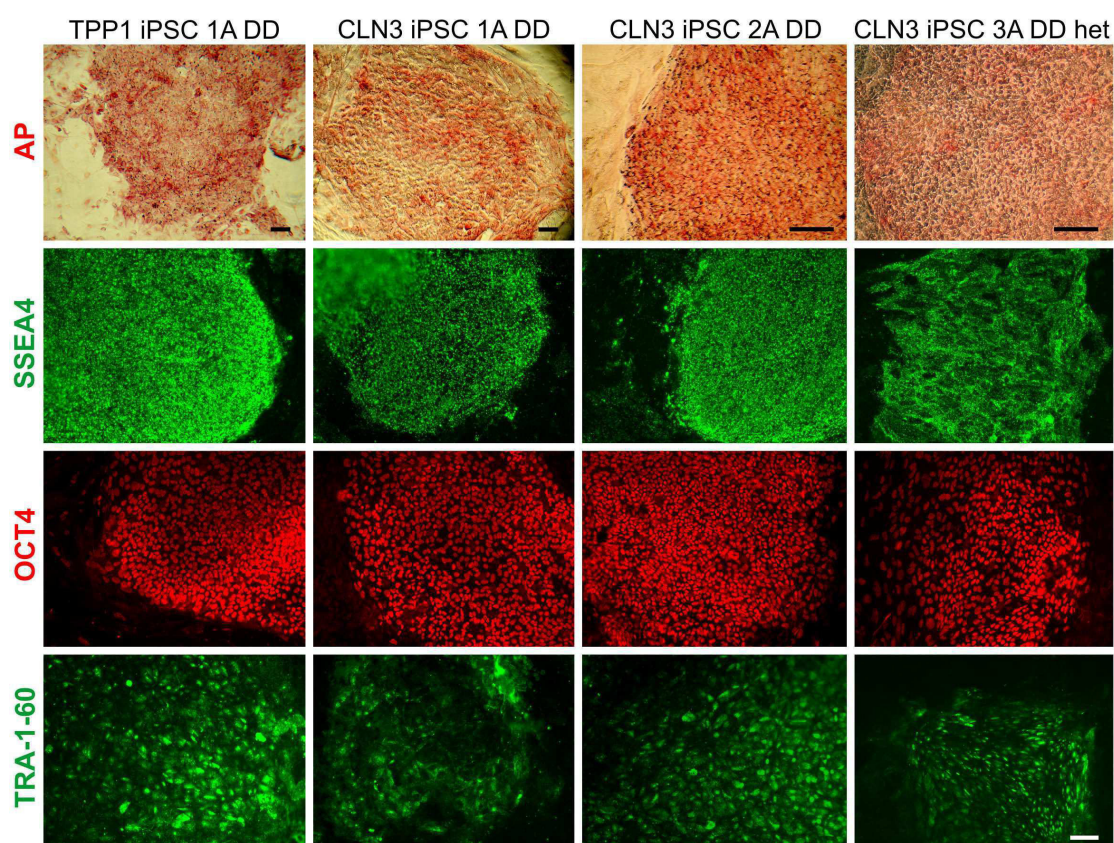


**Figure 3.3: AP and immunostainings for pluripotency marker proteins in patient-derived iPSCs**

The iPSC clones showed enzyme activity for alkaline phosphatase (AP) and were stained positive for known pluripotency marker proteins such as SSEA4, OCT4 and TRA-1-60. Representative images from one clone per patient fibroblast-derived iPSC line during expansion are shown. Scale bars, 100  $\mu$ m.

The first row of Figure 3.3 shows images of the AP assay. AP is an enzyme which is highly active in ESCs. During the assay, colonies that express this enzyme, will turn purple due to the enzymatic conversion of the substrate provided within this assay. As shown, all clones



turned purple during the assay which provided evidence of AP activity. As a further demonstration of pluripotency, iPSC clones were stained for proteins which are known to be expressed in pluripotent ESCs: SSEA4, OCT4 and TRA-1-60. All iPSC clones were stained positive for the pluripotency markers which, together with the AP assay, confirmed the pluripotent state of the iPSCs during expansion.

Next, iPSCs were allowed to form embryoid bodies (EBs) which were then differentiated into the three germ layers. Figure 3.4 shows representative images from one clone per patient fibroblast-derived iPSC line. After two weeks of spontaneous differentiation, iPSC clones were stained positive for known marker proteins of mesoderm (alpha-smooth muscle actin,  $\alpha$ -SMA), endoderm ( $\alpha$ -Fetoprotein), and ectoderm (neuron-specific class III beta-tubulin, TUJ1), which further confirmed their pluripotent nature.

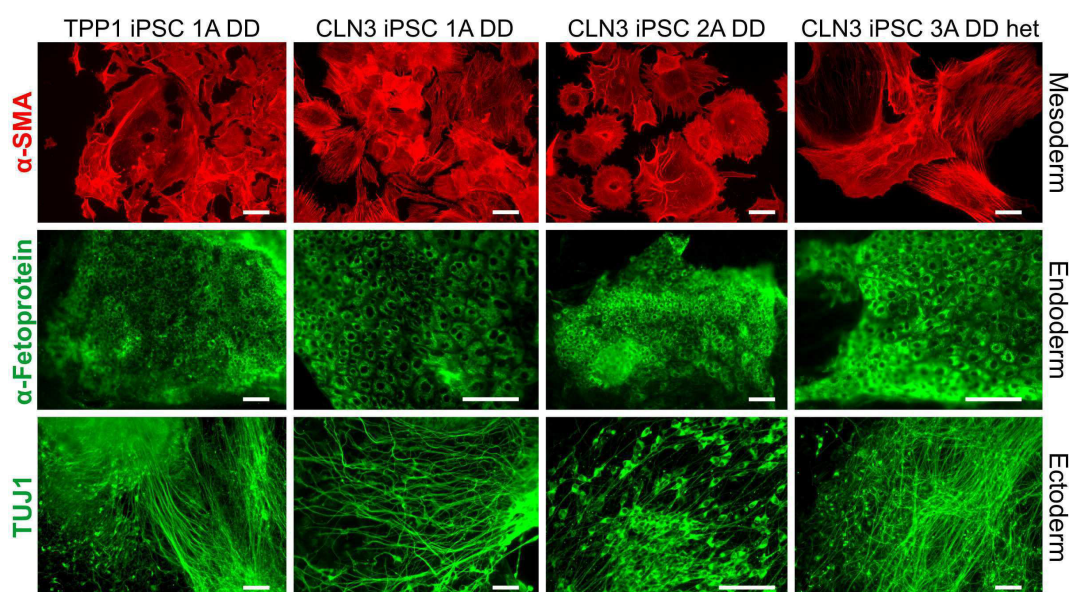


**Figure 3.4: Differentiation of patient-derived iPSCs into cells from the three germ layers**

After two weeks of differentiation, iPSC clones gave rise to cells from the three germ layers, as confirmed by stainings against  $\alpha$ -SMA (mesoderm),  $\alpha$ -Fetoprotein (endoderm) and TUJ1 (ectoderm). Representative images from one clone per patient fibroblast-derived iPSC line during differentiation are shown. Scale bars, 100  $\mu$ m.

### 3.1.2.3 Genotyping of generated induced pluripotent stem cell clones

After confirmation of the pluripotent stem cell nature of the iPSC clones which were meant to be used for the studies of disease modeling, the genotype of the clones derived from JNCL patients was confirmed again.

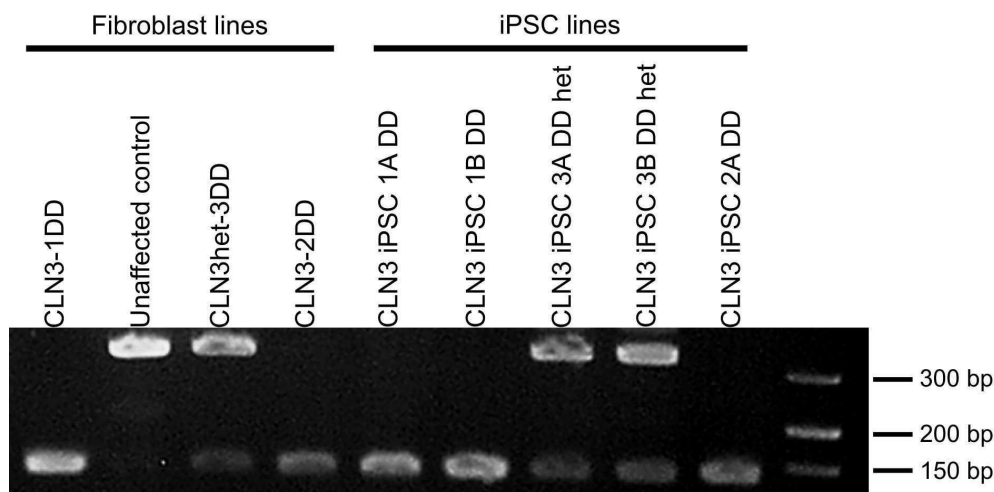


**Figure 3.5: Genotyping of iPSC clones derived from JNCL affected patients**

PCR confirmed the genotype of patient fibroblast-derived iPSCs. Primers were designed to bind within exons 6 and 9 of the CLN3 gene, resulting in a 360 bp product in unaffected control samples and a 143 bp product in samples from patients carrying the 1.02 kb deletion.

Figure 3.5 shows the results of the genotyping PCR. Primers were designed to bind within exon 6 and 9 of the CLN3 gene which results in a 360-bp amplification product in unaffected samples and a 143-bp amplification product in samples carrying the 1.02-kb deletion. As expected, the two JNCL affected patient-derived fibroblast lines gave rise to a PCR amplification product of 143 bp confirming the homozygosity of the samples for the 1.02-kb deletion within the CLN3 gene. The carrier line for the 1.02-kb deletion showed two bands, one at 143 bp and the other one at 360 bp, which confirmed the heterozygosity of the sample. An unrelated, unaffected fibroblast line was chosen as control and showed only one band at 360 bp. The iPSC clones derived from the patient fibroblast lines reflected these results which confirmed their genotype and made them thus suitable for the disease modeling.

### 3.1.3 Assessment of growth rate

iPSC colonies were in general passaged every five to seven days. However, frequency of passaging was depending on the amount of colonies that were left after the cleaning procedure as well as on the colony size. In order to obtain a more accurate estimate on the growth of the different iPSC colonies, Bromodeoxyuridine (BrdU) incorporation assays were performed. BrdU is an analogue of thymidine and is incorporated into the DNA during the s-phase of the cell cycle. Therefore, it can be used to label proliferating cells. Figure 3.6 shows the results of the BrdU incorporation assay in iPSCs.

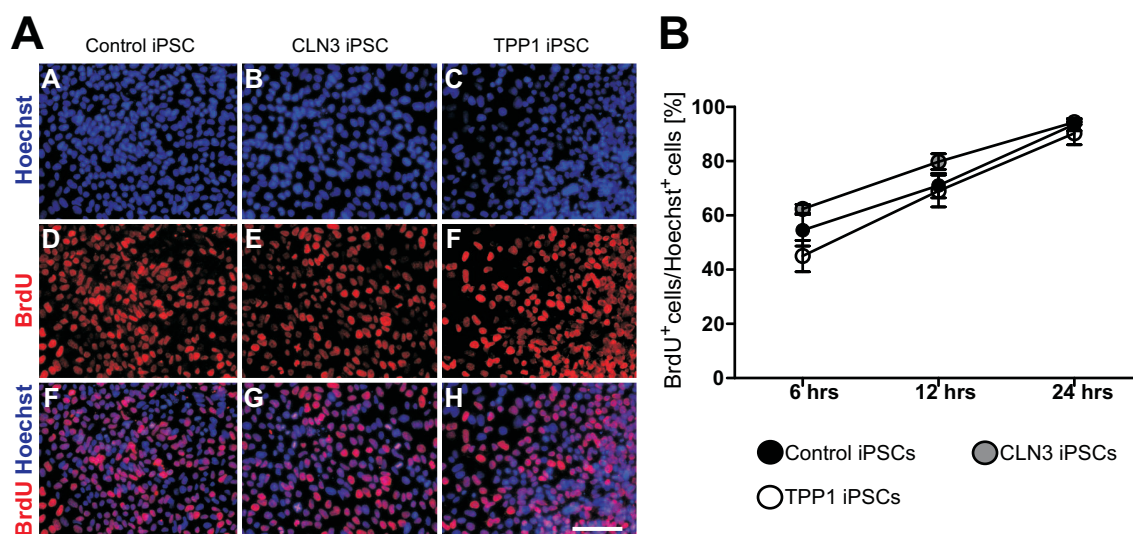


**Figure 3.6: Assessment of iPSC growth rate**

iPSC colonies were treated with 10  $\mu$ M BrdU and fixed after 6, 12 and 24 hours post-treatment. **A** Representative images from one iPSC clone per genotype are showing BrdU stainings in iPSC colonies at 12 hours post-treatment. Scale bar, 100  $\mu$ m. **B** Quantitative analysis of BrdU positive cells after 6, 12 and 24 hours post-treatment. Graph shows mean with SEM (n = 4, control and TPP1 iPSCs; n = 5, CLN3 iPSCs).

The BrdU incorporation assay revealed growth variations between the different lines at 6 and 12 hours post-treatment. After 6 hours only  $45 \pm 5.8\%$  of the TPP1-deficient iPSCs were positive for BrdU in contrast to  $54.5 \pm 5.8\%$  of control and  $62.4 \pm 1.6\%$  of CLN3 patient-derived iPSCs. However, this difference in growth did not reach statistical significance. At 12 hours post-treatment, the percentage of BrdU-positive cells was almost the same in TPP1-deficient and control-derived iPSCs with  $69.0 \pm 5.9\%$  and  $71.0 \pm 4.5\%$  respectively. However, the percentage of BrdU-positive cells in CLN3 patient-derived iPSCs was  $79.8 \pm 2.9\%$ . At 24 hours post-treatment the different iPSC lines showed almost the same percentage of BrdU-positive cells with  $93.5 \pm 2.3\%$  in control,  $94.4 \pm 1.0\%$  in *CLN3* mutant and  $90.3 \pm 4.2\%$  in TPP1-deficient iPSCs. Overall, the iPSC colonies derived from control and patient fibroblasts showed a comparable growth pattern.

### 3.1.4 Phenotypic studies of cell organelles and compartments

#### 3.1.4.1 Immunofluorescence

The reprogramming process resets fibroblasts to an ESC-like state. Thus, possible disease related phenotypes may not be obvious in iPSCs. Several studies in mouse cerebellar cells and yeast reported phenotypes in mitochondria, Golgi and within the lysosomal compartments

(Fossale *et al.*, 2004, Cao *et al.*, 2011, Codlin *et al.*, 2009). This led to the question whether these phenotypes are already aberrant in patient fibroblast-derived iPSCs.

Figure 3.7 shows representative confocal images of immunostainings for mitochondria (mortalin, GRP75), *cis*-Golgi (Golgin A2, GM130), the endoplasmic reticulum (ER; protein disulfide isomerase, PDI), and lysosomes (lysosomal-associated membrane protein 1, LAMP-1) in patient fibroblast-derived iPSCs.

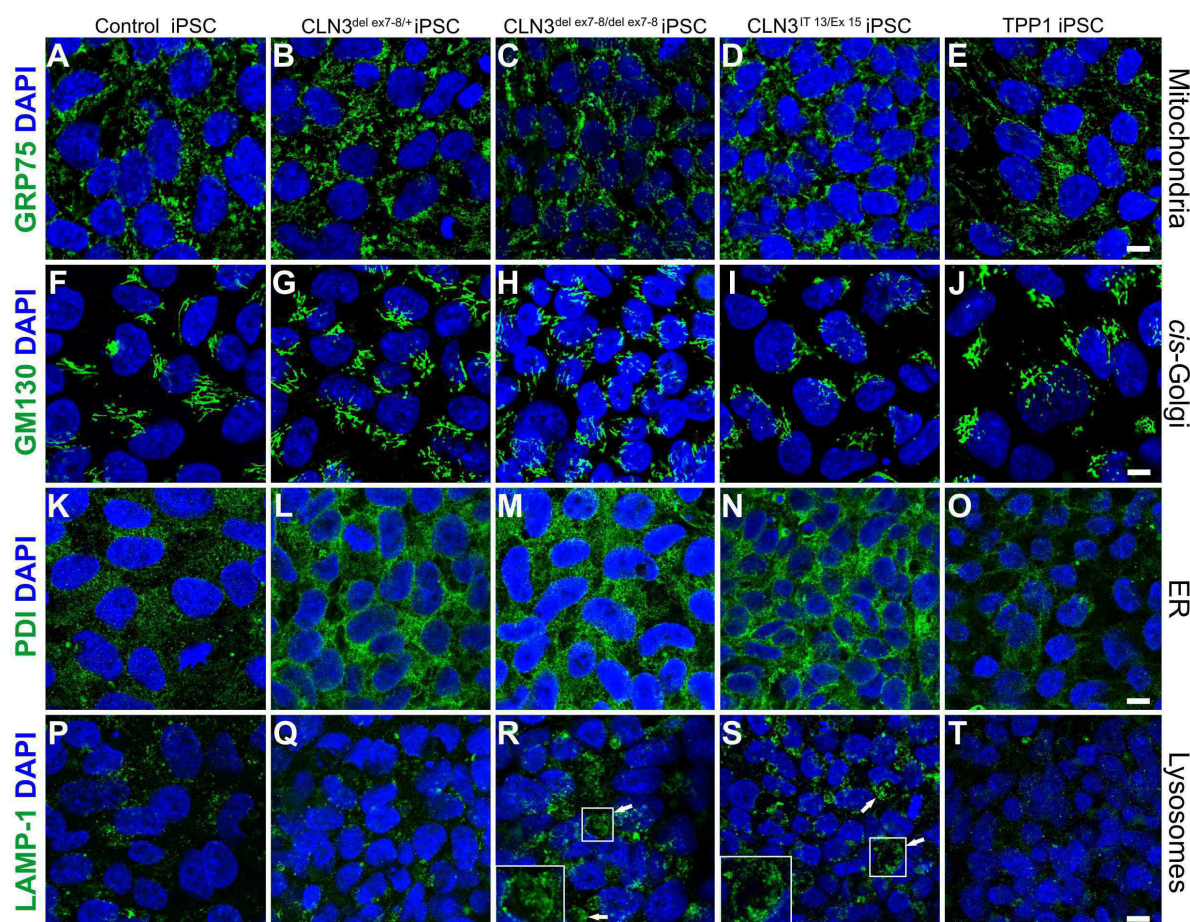


**Figure 3.7: Assessment of cell organelles and compartments in patient-derived iPSCs**

iPSC clones were stained for markers of mitochondria (GRP75, A-E), *cis*-Golgi (GM130, F-J), the ER (PDI, K-O) and lysosomes (LAMP-1, P-T). The most obvious phenotype was the presence of LAMP-1 positive vacuoles within the *CLN3* mutant iPSC clones (arrows, R and S). Representative confocal images are shown from one iPSC clone per genotype. Cell nuclei are counterstained with DAPI (blue). Scale bars, 10  $\mu$ m.

*CLN3*<sup>del ex7-8/+</sup> iPSC, iPSC line derived from donor fibroblasts heterozygous for the 1.02 kb deletion; *CLN3*<sup>del ex7-8/del ex7-8</sup> iPSC, iPSC line derived from donor fibroblasts homozygous for the 1.02 kb deletion; *CLN3*<sup>IT 13/Ex 15</sup> iPSC, iPSC line derived from fibroblasts carrying a compound heterozygous mutation within the *CLN3* gene; TPP1 iPSC, iPSC line derived from *TPPI* mutant fibroblasts.

---

Immunostainings for mitochondria (GRP75), *cis*-Golgi (GM130) and the ER (PDI) did not reveal an obvious phenotype that might have been genotype specific. Differences in shape, position and distribution of mitochondria, Golgi and the ER most likely reflected variations within the different iPSC clones. However, immunostainings for the lysosomal marker protein LAMP-1 showed remarkable amounts of marker positive vacuoles within the JNCL-derived iPSC clones. These vacuoles were abundant in all clones that were derived from fibroblasts which were either homozygous for the common deletion ( $CLN3^{\text{del ex7-8/del ex7-8}}$  iPSCs) or which were affected by a compound heterozygous mutation within the CLN3 gene ( $CLN3^{\text{IT 13/Ex 15}}$  iPSCs).

This observation led to further investigations of possible phenotypes by Western blot and electron microscopy.

#### 3.1.4.2 Western blot analysis

Although mitochondrial morphology was comparable between control and diseased iPSC lines, Western blot analysis was performed in order to investigate mitochondrial protein content. Since the subunit c of the mitochondrial complex is found to be the most abundant storage material in cells of LINCL and JNCL patients, this analysis was of great interest. Figure 3.8 shows the Western blot results and the protein levels which were quantified by densitometry.

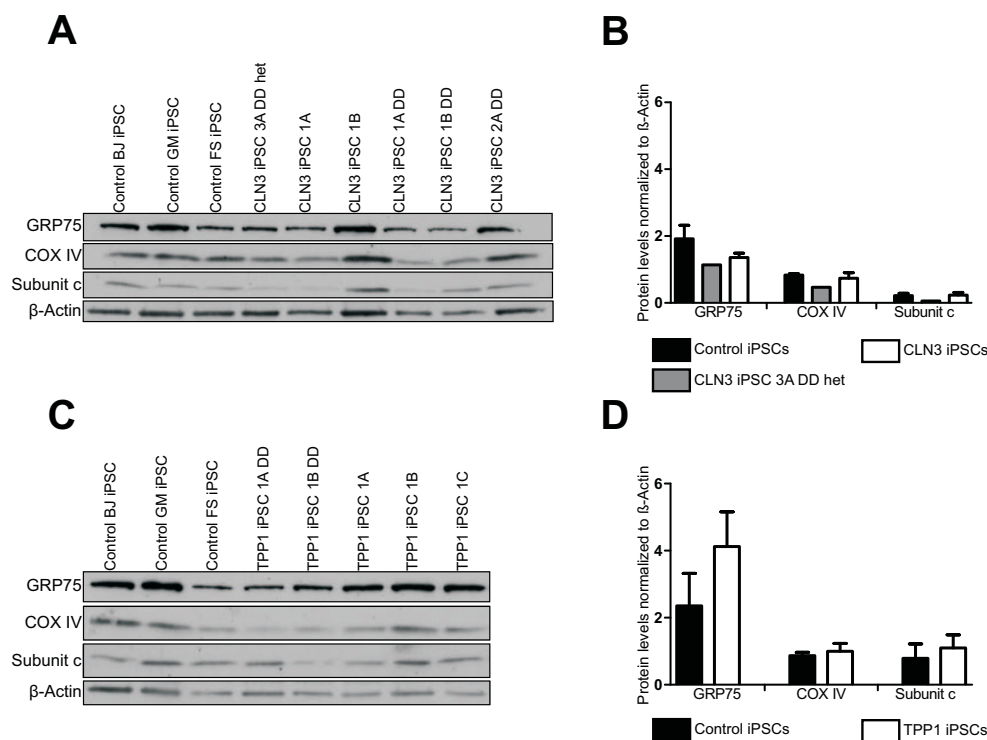


**Figure 3.8: Western blot analysis of mitochondrial proteins in iPSCs**

**A** Western blot results for the mitochondrial proteins GRP75 (75 kDa), COX IV (17 kDa) and the subunit c (4 kDa) of the mitochondrial ATPase complex in iPSCs derived from control and JNCL patient fibroblasts.  $\beta$ -Actin (43 kDa) was used as loading control. **B** Quantitative analysis of Western blot results from control and JNCL patient-derived iPSCs. Protein levels were normalized to  $\beta$ -Actin. Bar graph shows mean with SEM ( $n = 3$ , control iPSCs;  $n = 5$ , CLN3 iPSCs). **C** Western blot results for the mitochondrial proteins GRP75 (75 kDa), COX IV (17 kDa) and the subunit c (4 kDa) of the mitochondrial ATPase complex in iPSCs derived from control and LINCL patient fibroblasts.  $\beta$ -Actin (43 kDa) was used as loading control. **D** Quantitative analysis of Western blot results from control and LINCL patient-derived iPSCs. Protein levels were normalized to  $\beta$ -Actin. Bar graph shows mean with SEM ( $n = 3$ , control iPSCs;  $n = 5$ , TPP1 iPSCs).

The results of the Western blot analysis confirmed the findings obtained by immunofluorescence. The protein content of GRP75, cytochrome c oxidase subunit IV (COX IV) and subunit c was not significantly altered in the mutant iPSC lines when compared to control iPSCs.

Since immunofluorescence revealed large LAMP-1 positive vacuoles within the JNCL patient-derived iPSCs, Western blot analysis was performed to investigate the overall content of LAMP-1 protein. Because lysosomes are part of the autophagy pathway, Western blot

analysis was also performed for the early endosome antigen 1 (EEA-1) in order to investigate potential defects in autophagy which were reported for the JNCL mouse model (Cao *et al.*, 2006).

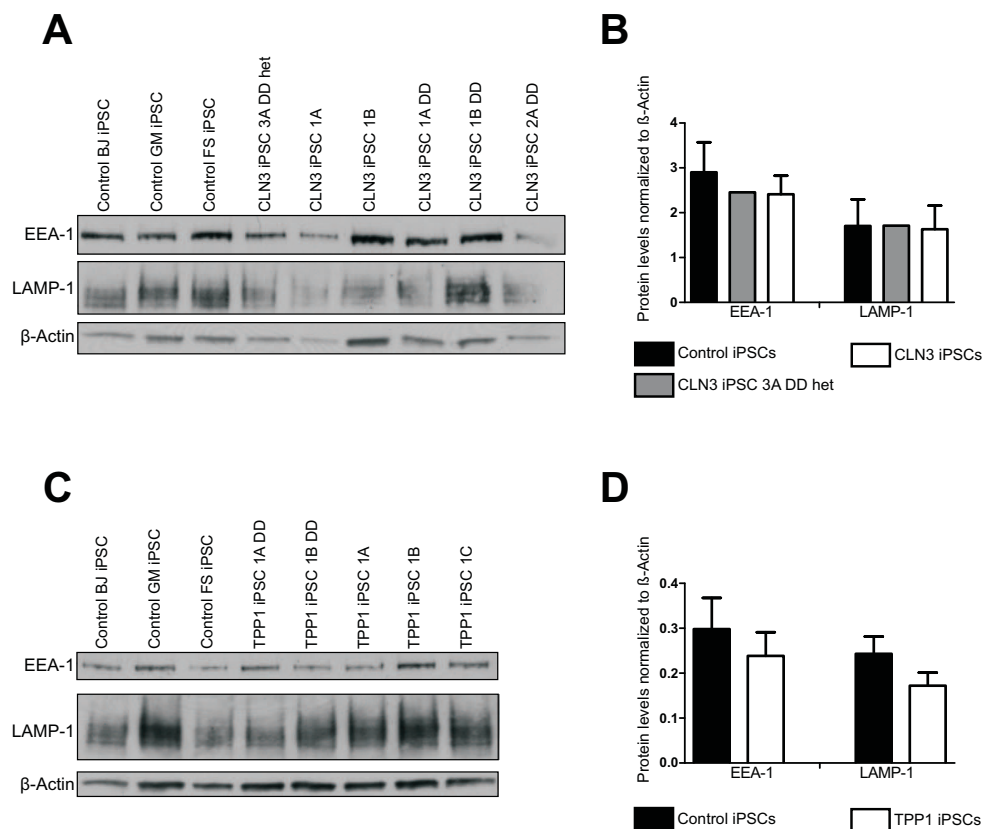


**Figure 3.9: Western blot analysis of autophagy related proteins EEA-1 and LAMP-1 in iPSCs**

**A** Western blot results for the early endosomal marker EEA-1 (170 kDa) and the lysosomal marker protein LAMP-1 (~120 kDa) in iPSCs derived from control and JNCL patient fibroblasts.  $\beta$ -Actin (43 kDa) was used as loading control. **B** Quantitative analysis of Western blot results from control and JNCL patient-derived iPSCs. Protein levels were normalized to  $\beta$ -Actin. Bar graph shows mean with SEM (n = 3, control iPSCs; n = 5, CLN3 iPSCs). **C** Western blot results for the early endosomal marker EEA-1 (170 kDa) and the lysosomal marker protein LAMP-1 (~120 kDa) in iPSCs derived from control and LINCL patient fibroblasts.  $\beta$ -Actin (43 kDa) was used as loading control. **D** Quantitative analysis of Western blot results from control and LINCL patient-derived iPSCs. Protein levels were normalized to  $\beta$ -Actin. Bar graph shows mean with SEM (n = 3, control iPSCs; n = 5, TPP1 iPSCs).

Western blot results did not reveal any significant differences in EEA-1 and LAMP-1 protein levels in iPSCs derived from control and patient fibroblasts. Protein levels were comparable between control and JNCL patient-derived iPSCs (Figure 3.9 **A** and **B**), suggesting that the large LAMP-1 positive vacuoles, that were found in stainings of JNCL patient-derived iPSCs,

were not due to an abundant amount of LAMP-1 protein but rather to improper maturation of late endosomes to lysosomes. These findings led to further investigations of the nature of vacuoles using electron microscopy (EM).

### 3.1.4.3 Electron microscopy

Figure 3.10 shows representative EM images of iPSC colonies derived from control, JNCL and LINCL patient fibroblasts.

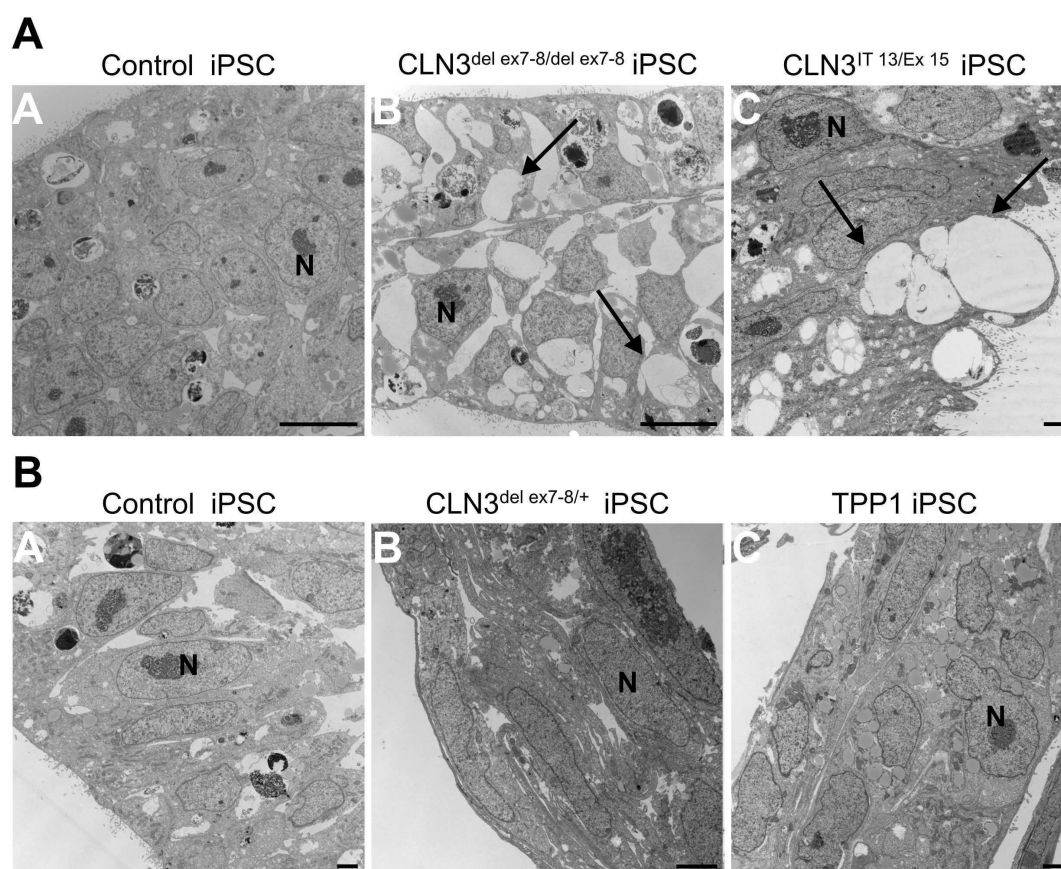


**Figure 3.10: Electron microscopy images of control and patient-derived iPSCs**

**A** Representative EM images showing iPSC colonies derived from control (A) and JNCL patient fibroblasts (B, C). iPSC colonies derived from JNCL patients showed large vacuoles (arrows) within the cytoplasm that were not apparent within the control iPSC colonies. Scale bars, 10  $\mu\text{m}$  (A and B), 2  $\mu\text{m}$  (C). **B** Representative EM images showing iPSC colonies derived from control (A), heterozygous donor (B) and LINCL patient fibroblasts (C). EM images did not reveal any obvious differences between these samples. Scale bars, 2  $\mu\text{m}$ .

N, nucleus; CLN3<sup>del ex7-8/+</sup> iPSC, iPSC line derived from donor fibroblasts heterozygous for the 1.02 kb deletion; CLN3<sup>del ex7-8/del ex7-8</sup> iPSC, iPSC line derived from donor fibroblasts homozygous for the 1.02 kb deletion; CLN3<sup>IT 13/Ex 15</sup> iPSC, iPSC line derived from fibroblasts carrying a compound heterozygous mutation within the CLN3 gene; TPP1 iPSC, iPSC line derived from *TPP1* mutant fibroblasts.



---

EM imaging revealed large vacuoles within the iPSC colonies that were homozygous for the common deletion within the CLN3 gene ( $CLN3^{\text{del ex7-8/del ex7-8}}$  iPSC) and within the colonies that were derived from donor fibroblasts carrying the compound heterozygous deletion within the CLN3 gene ( $CLN3^{\text{IT 13/Ex 15}}$  iPSC, Figure 3.10 A B and C). Although the vacuoles were very frequent and a couple of them were as large as the cell nucleus itself, no cargo or storage material could be detected within the vacuoles. Neither the iPSC line derived from a fibroblast line that was heterozygous for the common deletion within the CLN3 gene ( $CLN3^{\text{del ex7-8/+}}$  iPSC) nor the TPP1-deficient iPSC lines showed comparable vacuoles within the cytoplasm of the iPSC colonies (Figure 3.10 B B and C). These results suggest that the vacuoles observed on the EM images at least partly correspond to the ones seen by LAMP-1 immunostaining (Figure 3.7 A R and S).

### 3.1.5 Tripeptidyl peptidase I enzyme activity in human induced pluripotent stem cells

Mutations within the TPP1 gene affect the tripeptidyl peptidase I (TPP1) enzyme and thus lead to a decrease in TPP1 enzyme activity. In clinical screenings, TPP1 activity is determined by using patients leukocytes (Sohar *et al.*, 1999, Sohar *et al.*, 2000) or, more recently, dried blood spots (Lukacs *et al.*, 2003). Since this activity assay would be a valuable tool for future drug screenings, the application as an *in vitro* cell culture assay is of great interest. For this reason, TPP1 activity assay was performed on iPSC cultures derived from control, JNCL and LINCL patient fibroblasts. The assay is based on the fact that Ala-Ala-Phe-7-Amido-4-methylcoumarin is cleaved by TPP1 and the release of cleavage products can be measured spectrofluorometrically. In order to avoid effects of other lysosomal endopeptidases, E64 and pepstatin A are added during the assay.

Figure 3.11 shows the results of the TPP1 enzyme activity assay in iPSC cultures.

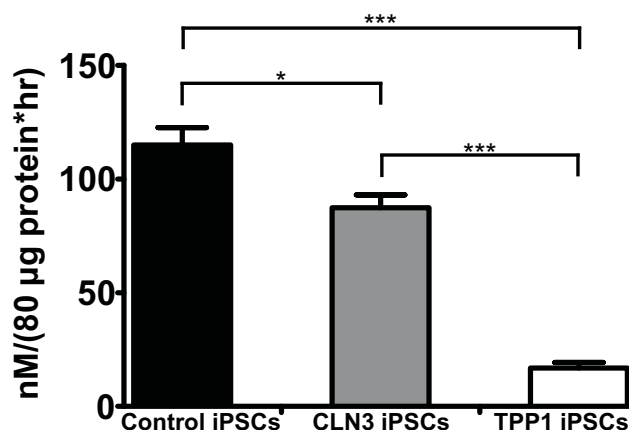


**Figure 3.11: TPP1 enzyme activity assay in patient fibroblast-derived iPSCs**

The assay revealed a highly significant decrease in TPP1 enzyme activity in iPSCs derived from LINCL patient fibroblasts. Bar graph shows mean with SEM. (n = 4, independent samples, one way ANOVA with *post-hoc* Bonferroni multiple comparison test, \* P<0.05 and \*\*\* P<0.001)

The assay demonstrated a highly significant decrease in TPP1 enzyme activity in iPSCs which were derived from LINCL patient fibroblasts ( $16.8 \pm 2.4$  nM/(80 µg protein\*hr)) when compared to control ( $114.9 \pm 7.6$  nM/(80 µg protein\*hr)) and *CLN3* mutant iPSCs ( $87.3 \pm 5.6$  nM/(80 µg protein\*hr)). This decrease in activity was also significant when comparing TPP1-deficient iPSCs to *CLN3* mutant iPSCs which demonstrates that the assay is indeed genotype specific. The slight decrease in TPP1 activity in *CLN3* mutant iPSCs compared to control iPSCs might be due to biological variations within the samples but will require further analyses. Taken together, these results showed that the TPP1 enzyme activity assay in iPSCs could be proven to be a valuable *in vitro* assay for future drug screenings.

## 3.2 Neural progenitor cells

### 3.2.1 Derivation of neural progenitor cells from induced pluripotent stem cells

The next step after generation and phenotypical characterization of patient fibroblast-derived iPSCs, was to derive neural progenitor cells (NPCs) which would, upon differentiation, give rise to a high yield of mature neurons. Since the NCLs are neurodegenerative disorders, NPCs as well as the finally differentiated neurons are the cells of interest for the disease modeling.

To date, two main approaches for derivation of NPCs from iPSCs are available in the literature. One is using intermediate steps such as EB and neural rosette formation whereas the other one is using a monolayer approach. Since the latter one seemed to derive NPCs in a

---

shorter time and appeared to be less complex, thus leading to fewer pitfalls, this protocol was tested first.

The monolayer approach is based on a protocol that was published by Chambers and colleagues (Chambers *et al.*, 2009; Chambers *et al.*, 2011). In brief, a single cell suspension of cleaned iPSC colonies is plated onto Matrigel<sup>TM</sup> coated plates and neural induction is achieved through dual inhibition of BMP and TGF- $\beta$  signaling. Within 9-11 days neuroectoderm should have formed, providing a pure population of NPCs. Use of the original protocol did not result in any iPSC-derived NPC population. Thus, attempts were made in order to modify this protocol for the control and mutant iPSCs that have been generated during this study. For example, the initial plating density of the iPSC single-cell suspension was varied. In addition, the neuroectoderm was split at days 9-15 because it might have been that the neural induction was simply delayed. Furthermore, in the original protocol, the neuroectoderm-derived NPCs are plated onto Matrigel<sup>TM</sup> coated plates. Since cells that were plated onto Matrigel<sup>TM</sup> did not appear to be NPCs, different coatings were used, such as CELLstart<sup>TM</sup> and PLO/L. Overall, this protocol only resulted in one NPC line that was derived from an iPSC control line.

Since the monolayer approach did not result in iPSC-derived NPCs, the other derivation approach, including EB and neural rosette formation, was tested. The protocol was provided by the Schöler group and its modification is given in detail under 2.2.9. The original protocol was suitable until the neural rosette formation step. Instead of four days, plated EBs, derived from TPP1-deficient iPSCs, gave rise to rosette-like structures after six to seven days, thus leading to a delay in rosette picking. Furthermore, the original protocol suggested plating the NPCs on Matrigel<sup>TM</sup> or CELLstart<sup>TM</sup>. None of the generated NPC lines could be propagated on CELLstart<sup>TM</sup> for more than four passages. Matrigel<sup>TM</sup> worked out well for the control and TPP1-deficient NPC lines but did not result in any NPC cultures derived from *CLN3* mutant iPSCs. However, PLO/L turned out to be a suitable surface coating for NPCs derived from control, *CLN3* mutant and TPP1-deficient iPSCs. All NPC lines used during this study were generated according to this modified protocol.

### **3.2.2 Confirmation of neural progenitor identity**

Before using the derived NPCs as disease model, confirmation of their neural progenitor identity was necessary. Selection criteria included morphology and expression of NPC specific markers at both the protein and gene expression levels.

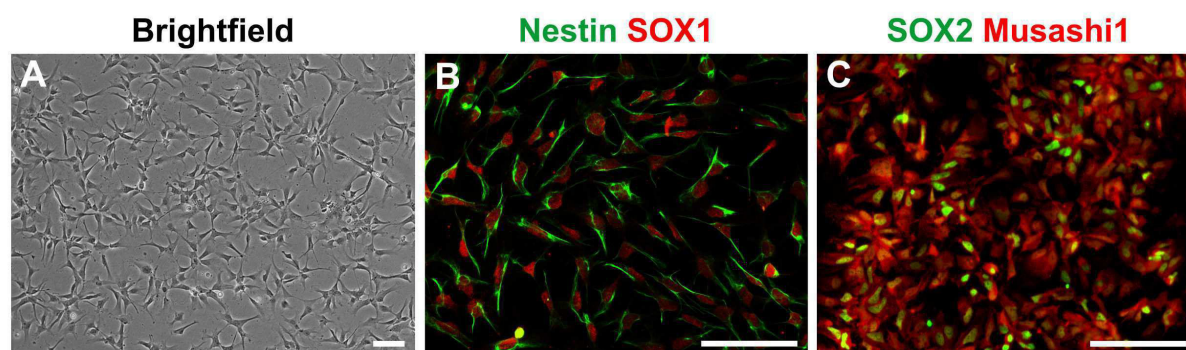


**Figure 3.12: Human iPSC-derived neural progenitor cells**

iPSC-derived NPCs displayed characteristic morphology (A) and showed expression of known NPC marker proteins such as Nestin and SOX1 (B) as well as SOX2 and Musashi1 (C). Scale bars, 100  $\mu\text{m}$ .

Figure 3.12 shows the morphology and the results of immunostainings for known marker proteins of iPSC-derived NPCs. The progenitor cells displayed the characteristic polarized shape of NPCs (Figure 3.12 A) and they showed high expression on the protein level for the known neural progenitor markers Nestin, SOX1, SOX2 and Musashi1 (Figure 3.12 B and C). Since SOX1 and SOX2 are transcription factors, their staining is expected to be nuclear whereas Nestin belongs to the intermediate filament protein family and is thus expected to give a cytoplasmic staining. Musashi1 is an RNA binding protein and therefore found to give both a nuclear and cytoplasmic staining pattern.

To further confirm the neural identity of iPSC-derived NPCs, gene expression levels were analyzed. Analyses were focused on downregulation of pluripotency and upregulation of neural progenitor specific genes as well as downregulation of genes regulating non-neural lineage fates.

Figure 3.13 and Figure 3.14 show the qPCR results for NPCs derived from iPSCs which were generated from patients affected by either JNCL or LINCL, respectively. Since gene expression levels may be variable between NPCs derived from different donor iPSCs, commercially available NPC lines (refer to Table 2.12) were included for the validation of gene expression levels. The control lines EnStemA and hNP-1 were generated from the human H9 ESC line whereas hNSC 21 was generated from human iPSCs.

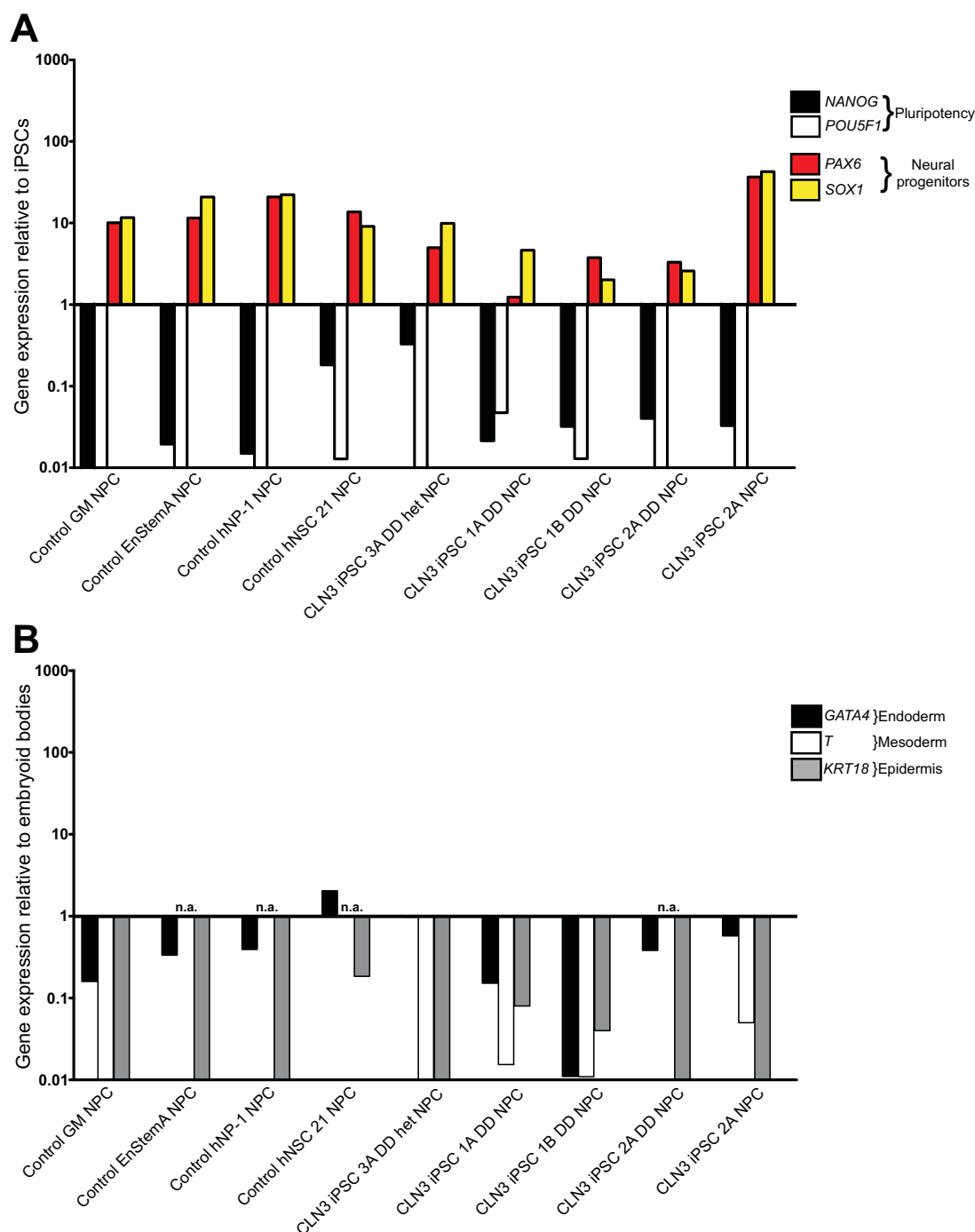


**Figure 3.13: Gene expression levels of NPCs derived from control and *CLN3* mutant iPSCs**

Diagram **A** shows the gene expression levels of the pluripotency genes *NANOG* and *POU5F1* as well as the expression levels of the neural lineage specific genes *PAX6* and *SOX1* in human NPCs. Gene expression was analyzed relative to *GAPDH* and gene expression levels of iPSCs derived from control human fibroblasts according to the  $\Delta\Delta Ct$  method. Diagram **B** shows the gene expression levels of the mesoderm specific gene *T*, the endoderm specific gene *GATA4* and of *KRT18*, a gene specifically expressed in the epidermis, in human NPCs. Gene expression was analyzed relative to *GAPDH* and embryoid bodies derived from human control iPSCs using the  $\Delta\Delta Ct$  method. (All samples were run in duplicate.)

n.a., no amplification

---

The qPCR results revealed strong variations within the expression levels of the different NPC lines. Nevertheless, pluripotency regulating genes such as *NANOG* and *POU5F1* were downregulated whereas the neural progenitor specific genes *PAX6* and *SOX1* were upregulated in all NPC lines when compared to expression levels of control iPSCs (Figure 3.13 A).

In order to assess relative expression levels of genes regulating non-neural lineage differentiation, expression levels were compared to those from embryoid bodies which were derived from human control iPSCs. As already seen in relative gene expression levels of pluripotency and neural lineage regulating genes, expression of *T*, *GATA4* and *KRT18* was strongly variable between the different NPC lines (Figure 3.13 B). Although the expectation was that the three genes would be downregulated within the samples, the commercial available NPC line hNSC 21 showed an upregulation of *GATA4* when compared to relative expression levels of embryoid bodies. No amplification of *T*, which encodes Brachyury, a protein involved in mesodermal differentiation, was detected in the NPC lines derived from the human ESC line H9 (EnstemA and hNP-1), hNSC 21 and in NPCs derived from CLN3 iPSC 2A DD iPSCs. *KRT18* a gene expressed in human epidermis was downregulated in all samples. This was of great interest since the iPSCs which gave rise to the NPC cultures were generated from human fibroblasts.

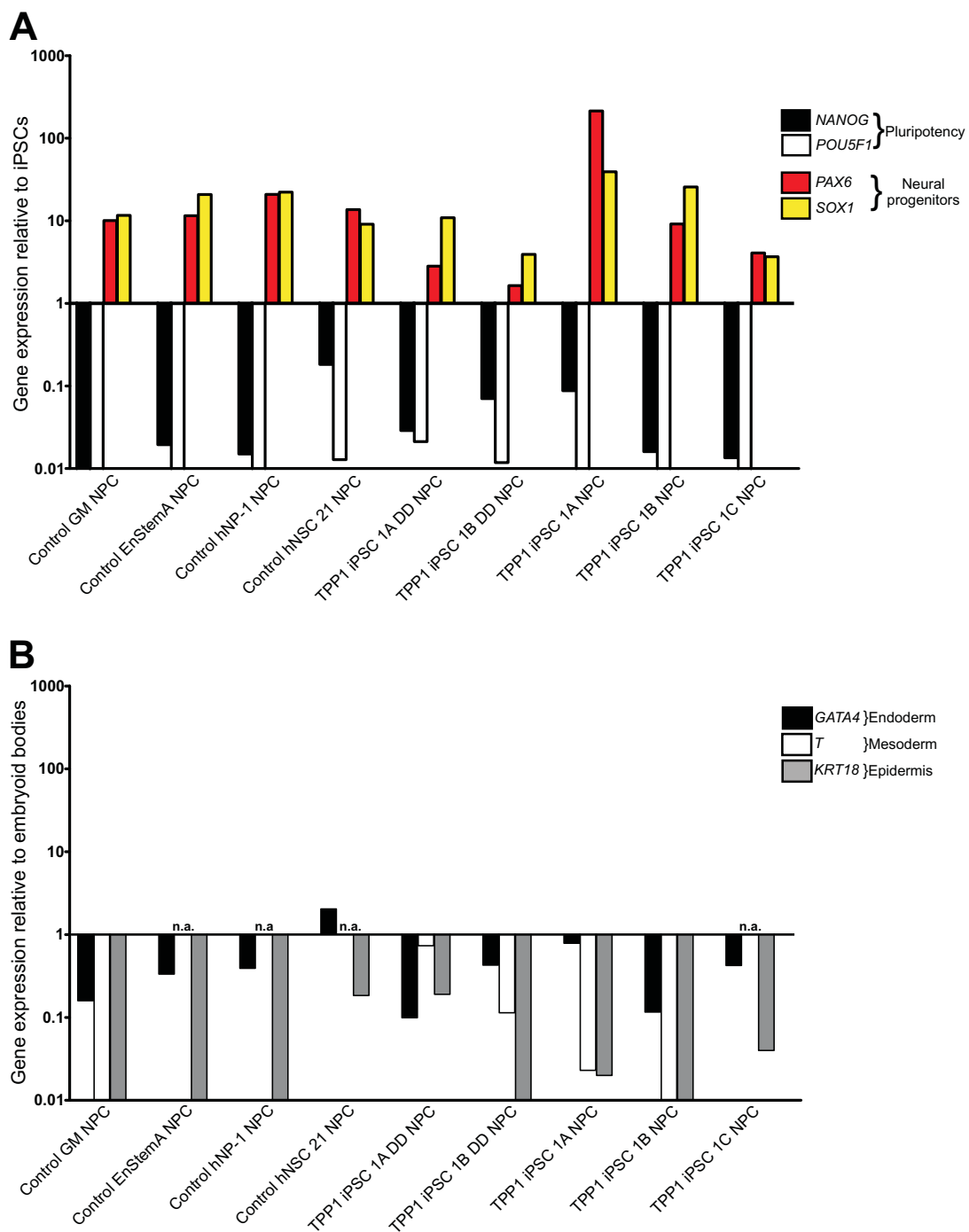


**Figure 3.14: Gene expression levels of NPCs derived from control and TPP1-deficient iPSCs**

Diagram A shows the gene expression levels of the pluripotency genes *NANOG* and *POU5F1* as well as the expression levels of the neural lineage specific genes *PAX6* and *SOX1* in human NPCs. Gene expression was analyzed relative to *GAPDH* and gene expression levels of iPSCs derived from control human fibroblasts using the  $\Delta\Delta C_t$  method. Diagram B shows the gene expression levels of the mesoderm specific gene *T*, the endoderm specific gene *GATA4* and of *KRT18*, a gene specifically expressed in the epidermis, in human NPCs. Gene expression was analyzed relative to *GAPDH* and embryoid bodies derived from human control iPSCs according to the  $\Delta\Delta C_t$  method. (All samples were run in duplicate.)

n.a., no amplification

---

When analyzing gene expression levels of pluripotency and neural stem cell genes in NPCs derived from TPP1-deficient iPSC lines (Figure 3.14 A), strong variation within the expression levels was apparent just like seen before in the *CLN3* mutant NPCs. But still, the pluripotency regulating genes *NANOG* and *POU5F1* were downregulated whereas the neural progenitor specific genes *PAX6* and *SOX1* were upregulated when compared to iPSCs derived from human control fibroblasts.

Also, genes regulating non-neural differentiation were downregulated in NPCs derived from TPP1-deficient iPSCs. No amplification for the transcript of *T* was detectable in NPCs derived from TPP1 iPSC 1C iPSCs.

Together with the results from the immunofluorescence and morphological studies, these data confirmed the neural identity of the iPSC-derived NPCs. For this study, it was not aimed to derive region-specific neurons. Hence, neural induction and NPC derivation was performed without patterning neural rosettes towards neural tissue that is specific to different regions of the central nervous system. Therefore, further gene expression analyses of fore-, mid- and hindbrain marker genes were not performed.

The iPSC-derived NPCs were highly proliferative and were usually passaged twice a week. They could be passaged up to 20 times without showing loss of proliferation or neural identity. The main advantage of the NPC culture is that they can be frozen down without any significant loss of cells and recover within 24 hours after thawing. In comparison, freezing down iPSCs results in a significant loss of cells which leads to a recovery time of about 7 to 10 days. NPCs are thus an ideal cell population for experiments and further differentiation into mature neurons.

### **3.2.3 Phenotypic studies of cell organelles in neural progenitor cells**

#### *3.2.3.1 Immunofluorescence*

After confirmation of neural stem cell identity of iPSC-derived NPCs phenotypic studies of cell organelles were performed. As previously performed on patient fibroblast-derived iPSCs (3.1.4), the emphasis was put on mitochondria, Golgi and the ER.

Figure 3.15 shows representative confocal images of immunostainings for mitochondria (GRP75), *cis*-Golgi (GM130) and the ER (PDI) which were performed on iPSC-derived NPCs.



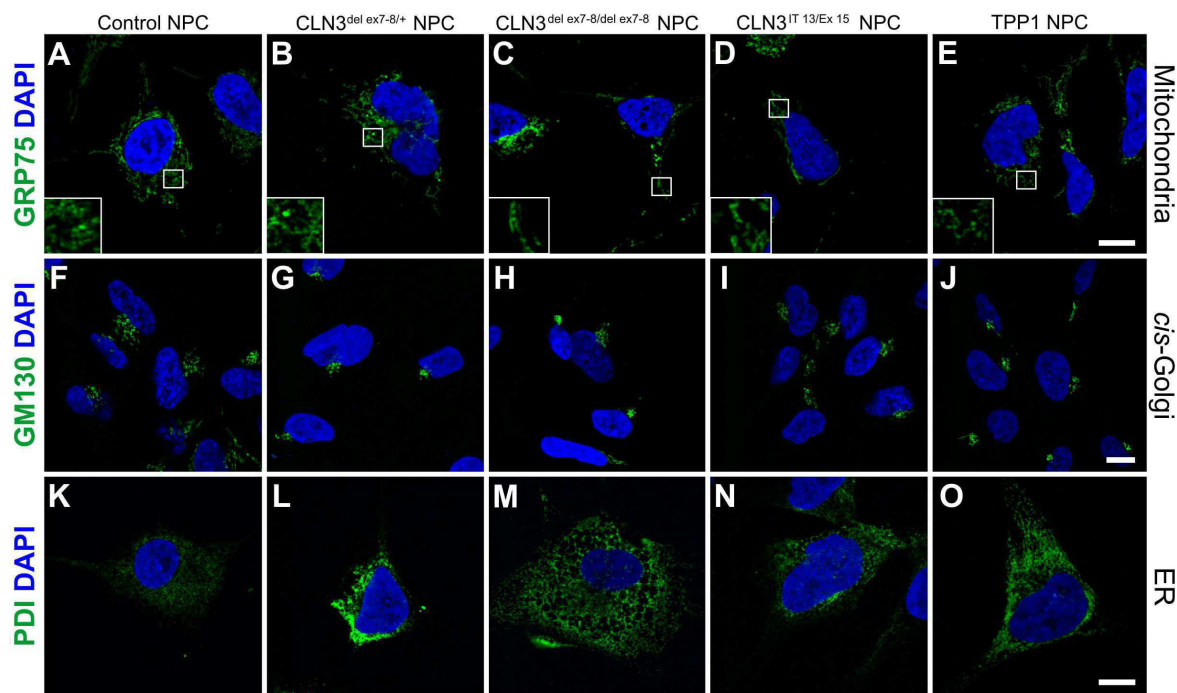


**Figure 3.15: Assessment of cell organelles in iPSC-derived NPCs**

NPCs were stained for markers of mitochondria (GRP75, A-E), *cis*-Golgi (GM130, F-J) and the ER (PDI, K-O). Mitochondria from *CLN3* mutant NPCs (C and D) appeared to be more elongated when compared to control NPCs (A and B). Differences in Golgi and the ER stainings might be due to cell line variations. Representative confocal images are shown from one NPC line per genotype. Cell nuclei are counterstained with DAPI (blue). Scale bars, 10  $\mu$ m.

*CLN3*<sup>del ex7-8/+</sup> NPC, NPC line derived from iPSCs heterozygous for the 1.02 kb deletion; *CLN3*<sup>del ex7-8/del ex7-8</sup> NPC, NPC line derived from iPSCs homozygous for the 1.02 kb deletion; *CLN3*<sup>IT 13/Ex 15</sup> NPC, NPC line derived from iPSCs carrying a compound heterozygous mutation within the *CLN3* gene; *TPP1* NPC, NPC line derived from *TPP1* mutant iPSCs.

Immunofluorescence images of NPCs stained for the mitochondrial marker protein GRP75 (Figure 3.15) showed abnormal mitochondria in *CLN3* mutant (C and D). Compared to control NPCs (A) and NPCs derived from iPSCs heterozygous for the common mutation within the *CLN3* gene (B), the mitochondria appeared to be more elongated and dilated. Furthermore, structural changes in Golgi appearance were observed. While Golgi seemed to be polarized and close to the cell nucleus in control and *CLN3*<sup>Ex 7-8/+</sup> NPCs (A and B), it appeared to be disrupted in some cells of the *CLN3*<sup>IT 13/Ex 15</sup> NPCs (I). Also, some of the Golgi structures observed in the *TPP1*-deficient NPC lines (J) seemed to be more distant from the cell nucleus when compared to control NPCs. But since stainings for the *cis*-Golgi marker GM130 were also very heterogeneous in the control NPC lines, structural differences might be due to cell line variations. The same conclusions can be drawn from immunostainings for

PDI, a marker protein for the ER. Immunostainings for PDI were overall quite heterogeneous so that variations might be due to clonal differences in cell lines.

Immunostainings against LAMP-1 and subunit c were performed in order to address the question whether lysosomal abnormalities or possible storage material can already be seen in NPCs (Figure 3.16).

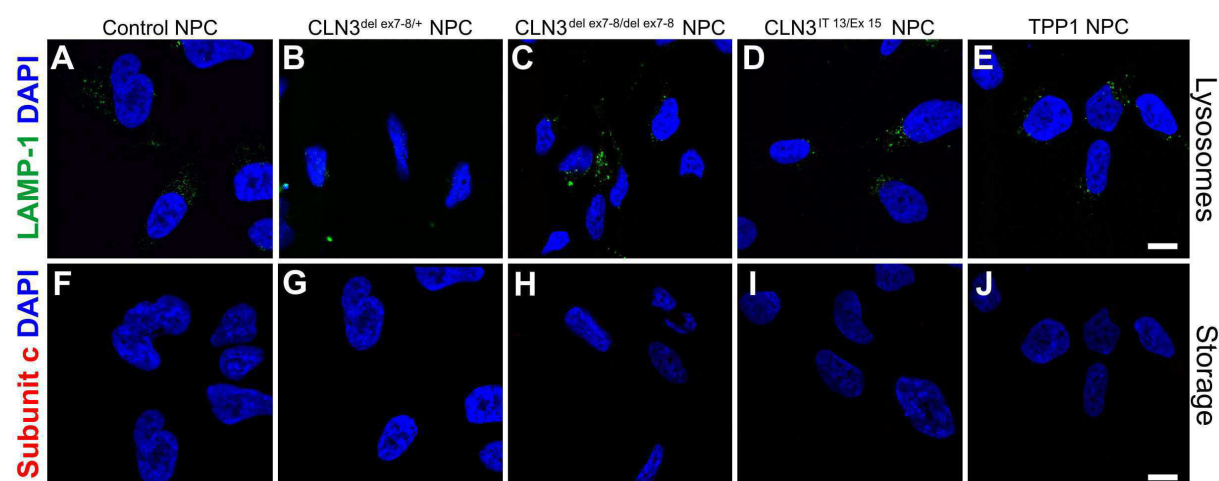


**Figure 3.16: Immunostainings against LAMP-1 and subunit c in iPSC-derived NPCs**

NPCs were stained for markers of lysosomes (LAMP-1, A-E) and the subunit c of the mitochondrial ATPase complex (subunit c, F-J). Neither abnormalities within LAMP-1 staining pattern nor subunit c accumulation were found. Representative confocal images are shown from one NPC line per genotype. Cell nuclei are counterstained with DAPI (blue). Scale bars, 10  $\mu$ m.

CLN3<sup>del ex7-8/+</sup> NPC, NPC line derived from iPSCs heterozygous for the 1.02 kb deletion; CLN3<sup>del ex7-8/del ex7-8</sup> NPC, NPC line derived from iPSCs homozygous for the 1.02 kb deletion; CLN3<sup>IT 13/Ex 15</sup> NPC, NPC line derived from iPSCs carrying a compound heterozygous mutation within the CLN3 gene; TPP1 NPC, NPC line derived from *TPP1* mutant iPSCs.

Figure 3.16 shows representative immunofluorescence images from stainings against LAMP-1 (A-E) and subunit c (F-J). LAMP-1 positive vesicles found in control and mutant NPCs were overall of the same size and appeared to have the same distribution within the cell. However, a couple of cells within the CLN3<sup>del ex7-8/del ex7-8</sup> NPCs showed a few LAMP-1 positive vesicles that were slightly larger than those found within the control NPCs. Immunostainings for the subunit c of the ATPase complex resulted in no apparent signal in control and mutant NPCs. The very weak signal was hard to capture and sometimes indistinguishable from the background signal.

---

Taken together, the results from immunofluorescence experiments suggested genotype specific differences in mitochondria. Thus, Western blot analyses were performed in order to investigate possible changes in mitochondrial protein content.

### 3.2.3.2 Western blot analysis

As previously done for iPSC cultures, two mitochondrial associated proteins were analyzed: GRP75 which belongs to the heat shock protein 70 family and which is essential for transportation of mitochondrial proteins from the cytoplasm to the mitochondria (Schneider *et al.*, 1994), as well as COX IV a component of the terminal oxidase in the mitochondrial electron transport chain. Since accumulation of subunit c is one of the hallmarks in LINCL and JNCL, Western blot analyses for possible subunit c storage material were performed as well, although immunostainings were negative.

Figure 3.17 shows the Western blot results for GRP75, COX IV and subunit c. In order to compare protein levels between NPCs derived from different sources, commercially available control NPCs (refer to Table 2.12) were included in the Western blot analyses. Protein content was analyzed by densitometry and normalized to protein levels of  $\beta$ -Actin.

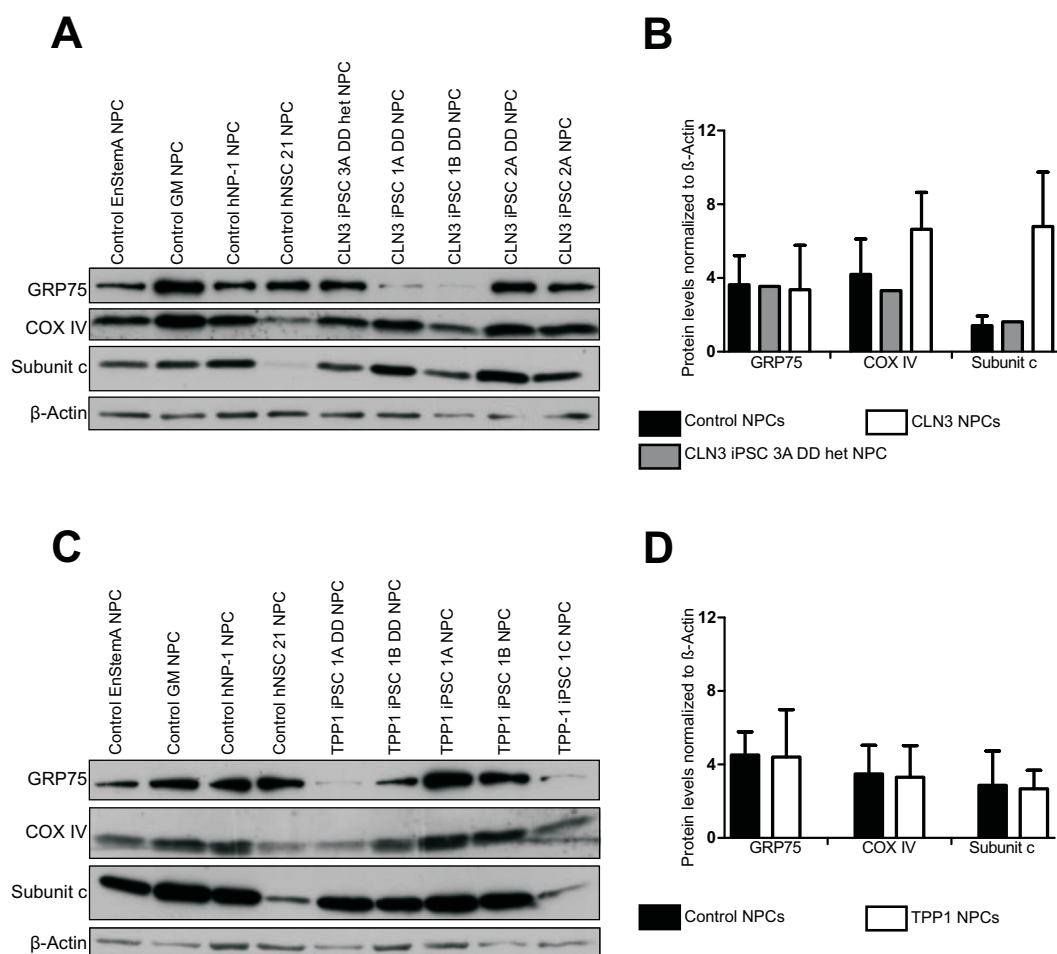


**Figure 3.17: Western blot analysis of mitochondrial proteins in iPSC-derived NPCs**

**A** Western blot results for the mitochondrial proteins GRP75 (75 kDa), COX IV (17 kDa) and the subunit c (4 kDa) of the mitochondrial ATPase complex in NPCs derived from control and *CLN3* mutant iPSCs.  $\beta$ -Actin (43 kDa) was used as loading control. **B** Quantitative analysis of Western blot results from control and *CLN3* mutant NPCs. Protein levels were normalized to  $\beta$ -Actin. Bar graph shows mean with SEM ( $n = 4$ ). **C** Western blot results for the mitochondrial proteins GRP75 (75 kDa), COX IV (17 kDa) and the subunit c (4 kDa) of the mitochondrial ATPase complex in NPCs derived from control and TPP1-deficient iPSCs.  $\beta$ -Actin (43 kDa) was used as loading control. **D** Quantitative analysis of Western blot results from control and TPP1-deficient NPCs. Protein levels were normalized to  $\beta$ -Actin. Bar graph shows mean with SEM ( $n = 4$ , control NPCs;  $n = 5$ , TPP1 NPCs).

---

Western blot analysis of GRP75 and COX IV revealed that protein levels were comparable between control and *CLN3* mutant as well as TPP1-deficient NPC lines. Although protein levels in subunit c did not show a statistically significant change in *CLN3* mutant NPCs when compared to control NPCs, there was a trend towards increased levels in *CLN3* mutant NPC lines. However, a comparable trend in accumulation of subunit c was not observed in TPP1-deficient NPC lines.

Since mitochondrial protein content was not altered in mutant NPC lines, the increase in subunit c protein levels observed in *CLN3* mutant NPC lines is not due to an increase in mitochondrial mass but might rather be due to an accumulation of storage material which might still not be enough to be captured by immunofluorescence.

Although immunostainings did not reveal any obvious changes in size or distribution of LAMP-1 positive lysosomes, Western blot analyses were performed in order to investigate total LAMP-1 protein content. Since formation of storage material suggests a dysfunction of the autophagy pathway (Cao *et al.*, 2006), investigation of possible alterations in total protein content of the early endosomal marker EEA-1 was of great interest as well.

Figure 3.18 shows the Western blot results for LAMP-1 and EEA-1 in control, *CLN3* mutant, and TPP1-deficient NPC lines. Protein content was analyzed by densitometry and normalized to  $\beta$ -Actin protein levels.

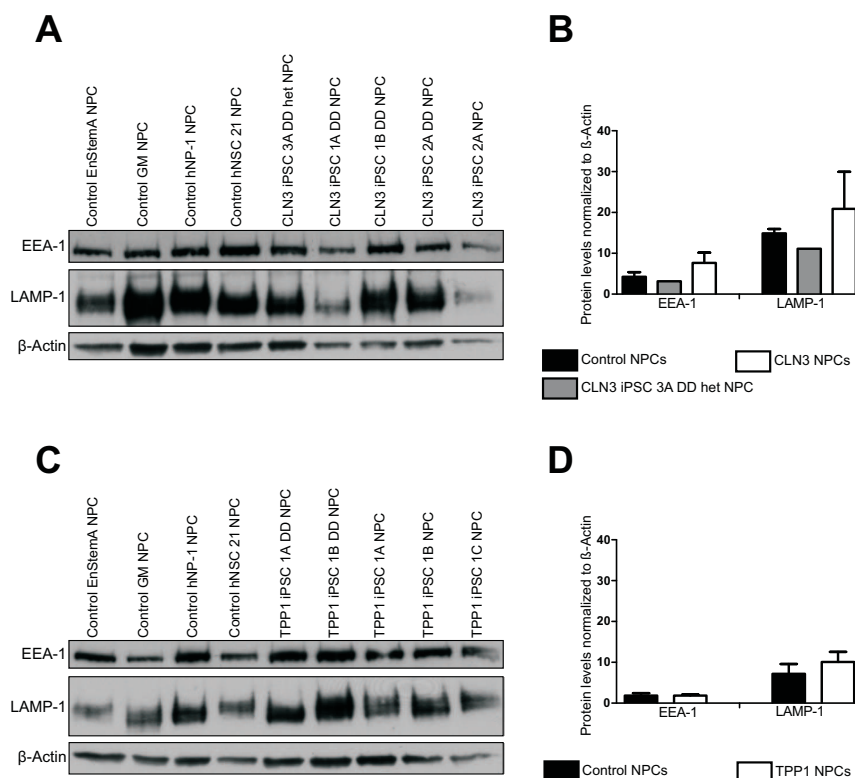


**Figure 3.18: Western blot analysis of autophagy related proteins EEA-1 and LAMP-1 in human NPCs**

**A** Western blot results for the early endosomal marker EEA-1 (170 kDa) and the lysosomal marker protein LAMP-1 (~120 kDa) in NPCs derived from control and *CLN3* mutant iPSCs.  $\beta$ -Actin (43 kDa) was used as loading control. **B** Quantitative analysis of Western blot results from control and *CLN3* mutant NPCs. Protein levels were normalized to  $\beta$ -Actin. Bar graph shows mean with SEM (n = 4). **C** Western blot results for the early endosomal marker EEA-1 (170 kDa) and the lysosomal marker protein LAMP-1 (~120 kDa) in NPCs derived from control and TPP1-deficient iPSCs.  $\beta$ -Actin (43 kDa) was used as loading control. **D** Quantitative analysis of Western blot results from control and TPP1-deficient NPCs. Protein levels were normalized to  $\beta$ -Actin. Bar graph shows mean with SEM (n = 4, control NPCs; n = 5, TPP1 NPCs).

Although protein levels of EEA-1 and LAMP-1 were slightly elevated in *CLN3* mutant NPCs in comparison to control NPC lines, changes were not significant (Figure 3.18 **A** and **B**). TPP1-deficient NPC lines showed comparable protein levels of EEA-1 and LAMP-1 to controls (Figure 3.18 **C** and **D**). Overall, the Western blot results confirmed the immunofluorescence findings which showed no differences in size, distribution or number of LAMP-1 positive vesicles.

Taken together, Western blot analyses suggest that *CLN3* mutant NPCs accumulate subunit c as possible storage material, although not apparent by immunofluorescence images. TPP1-deficient NPC lines did not reveal any obvious phenotype by Western blot analysis.

### 3.2.3.3 Electron microscopy

In order to obtain more detailed information about organelle structures within the NPC lines, transmission electron microscopy was performed.

Figure 3.19 shows representative EM images from control, *CLN3* mutant and *TPP1*-deficient NPC lines.

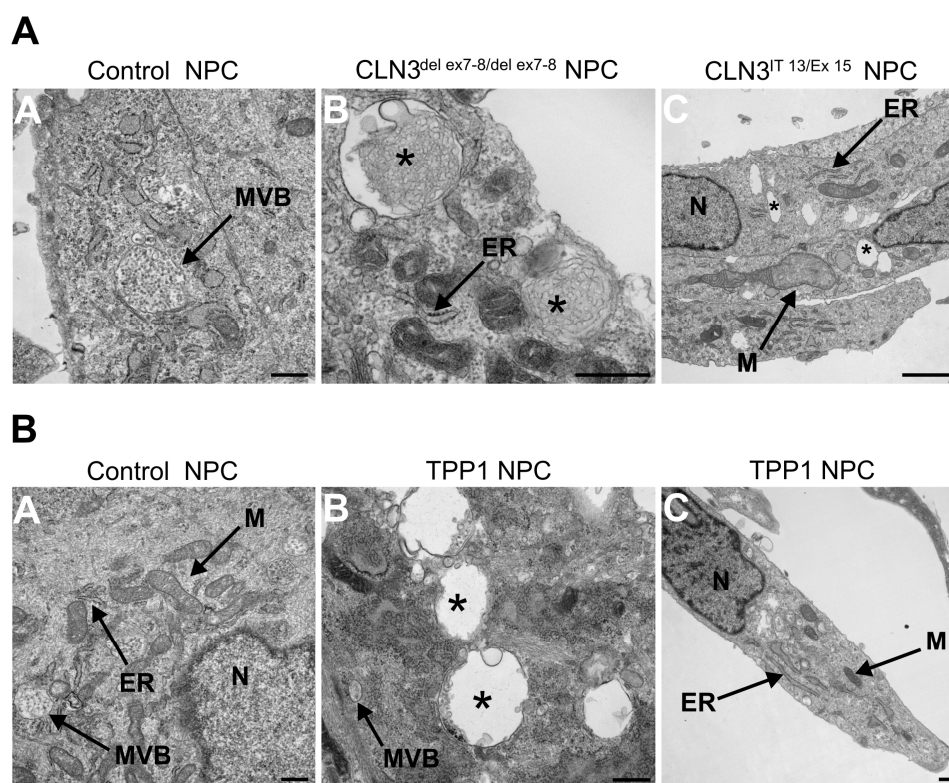


**Figure 3.19: Electron microscopy images of control, *CLN3* mutant and *TPP1*-deficient NPCs**

**A** Representative EM images showing control (A) and *CLN3* mutant NPCs (B, C). NPCs derived from *CLN3* mutant iPSCs showed vacuoles within the cytoplasm that were not apparent in control NPCs (asterisk). Vacuoles within the *CLN3*<sup>del ex7-8/del ex7-8</sup> NPCs showed frequent membrane-bound storage material that is obviously different from multivesicular bodies (MVB) observed within the cytoplasm of control-derived NPCs. Vacuoles within the *CLN3*<sup>IT 13/Ex 15</sup> NPCs appeared to be empty. Mitochondria in *CLN3*<sup>IT 13/Ex 15</sup> NPCs displayed a distended morphology with disrupted cristae (M, arrow). Morphology of the ER (ER, arrows) appeared normal. Scale bars, 500 nm (A and B), 2  $\mu$ m (C). **B** Representative EM images showing control (A) and *TPP1*-deficient NPCs (B and C). EM images showed large empty vacuoles within the cytoplasm of the *TPP1*-deficient NPC lines (asterisk). Mitochondria did not display any obvious morphological changes (M, arrow). The ER showed a dilated morphology (ER, arrow). Scale bars, 500 nm.

ER, endoplasmic reticulum; N, nucleus, M, mitochondria; MVB, multivesicular body; \*, designates large vacuoles. *CLN3*<sup>del ex7-8/del ex7-8</sup> NPC, NPC line derived from iPSCs homozygous for the 1.02 kb deletion; *CLN3*<sup>IT 13/Ex 15</sup> NPC, NPC line derived from iPSCs carrying a compound heterozygous mutation within the *CLN3* gene; *TPP1* NPC, NPC line derived from *TPP1* mutant iPSCs.

---

Electron microscopy revealed vacuoles within the cytoplasm of the *CLN3* mutant NPC lines that were not apparent in control NPCs (Figure 3.19 A A-C). These vacuoles appeared to be mostly empty in the  $CLN3^{IT\ 13/Ex\ 15}$  NPCs, which was already seen within the parent iPSC colonies (Figure 3.10 A C). However, EM images from  $CLN3^{del\ ex7-8/del\ ex7-8}$  NPCs revealed vacuoles containing frequent membrane-bound storage material which was often curvilinear and clearly different from multivesicular bodies, which represent late endosomal intermediates, observed within the cytoplasm of control-derived NPCs (Figure 3.19 A). This storage material was neither seen in any of the control samples nor in the parent iPSC colonies. Furthermore, the curvilinear profile suggests that the storage material might be other than the subunit c of the mitochondrial ATPase complex which is in accordance with the lack of signal in the immunofluorescence (Figure 3.16 H and I).

Another obvious phenotype is shown within the  $CLN3^{IT\ 13/Ex\ 15}$  NPCs (Figure 3.19 A C). The mitochondria appear to be elongated and partially distended showing disrupted cristae when compared to control NPCs. This phenomenon was also seen in the *CLN3* iPSC 1A DD NPC line which is homozygous for the 1.02 kb common mutation within the *CLN3* gene.

Vacuolation within the cytoplasm was also seen within the TPP1-deficient NPC lines (Figure 3.19 B B and C). However, these vacuoles were free of any apparent storage material. Nevertheless, these empty vacuoles were not observed in EM images from the parent iPSC colonies suggesting *de novo* formation of pre-storage vesicles. In contrast to *CLN3* mutant NPCs, some multivesicular bodies were found as well within the cytoplasm of TPP1-deficient NPCs. However, these bodies showed malformation when compared to multivesicular bodies found in control-derived NPCs. Unlike the findings within the  $CLN3^{IT\ 13/Ex\ 15}$  NPCs, mitochondria appeared to be normal. However, in contrast to the *CLN3* mutant NPC lines, the ER was remarkably dilated in comparison to control NPCs (Figure 3.19 B C). In some fields it appeared to be as thick as mitochondria.

Although storage material was not observed in all of the mutant NPC lines, they all showed vacuoles within the cytoplasm that were not apparent in control NPCs. These findings lead to the assumption that iPSC-derived NPCs start to recapitulate the phenotypes seen in patient brain samples. Also, EM images confirmed the findings revealed by immunofluorescence which showed elongated mitochondria within the *CLN3* mutant cell lines.



### 3.2.4 Tripeptidyl peptidase I enzyme activity in neural progenitor cells

As patient-derived NPCs are thought to play a major part in future drug screenings, a robust read-out is of great interest. Since the TPP1 enzyme activity assay showed reproducible results in iPSC lines, the same assay was performed on iPSC-derived NPCs. As this assay was thought to be a proof of principle, only one NPC line for each genotype was chosen for the assay but run in quadruplicates.

Figure 3.20 shows the results of the TPP1 enzyme activity assay performed on iPSC-derived NPCs.

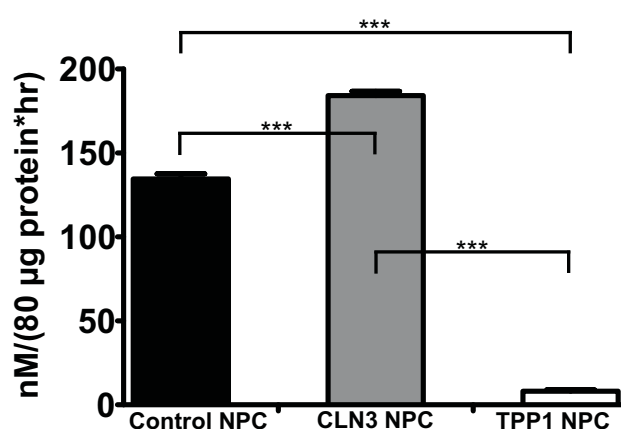


**Figure 3.20: TPP1 activity assay in iPSC-derived NPCs**

The assay revealed a highly significant decrease in TPP1 enzyme activity in NPCs that were derived from TPP1-deficient iPSCs. Bar graph shows mean with SEM. (One sample per genotype was run in quadruplicate, one way ANOVA with *post-hoc* Bonferroni multiple comparison test, \*\*\* P<0.001)

The TPP1 enzyme activity assay showed a highly significant decrease in TPP1-deficient NPCs ( $8.1 \pm 0.8$  nM/(80 µg protein\*hr)) when compared to control ( $134.5 \pm 3.0$  nM/(80 µg protein\*hr)) and *CLN3* mutant NPCs ( $184.1 \pm 2.1$  nM/(80 µg protein\*hr)). These results were in accordance with the findings in the parent iPSC lines. However, for further investigations more biological replicates would be needed.

In summary the TPP1 enzyme activity assay showed genotype-specific results in NPCs and might therefore be a valuable tool for potential applications in drug screenings.

### 3.2.5 Assessment of cell death in neural progenitor cells

As revealed by immunostainings and EM images, *CLN3* mutant NPCs showed alterations in mitochondria and vacuoles containing storage material. EM images of TPP1-deficient NPCs revealed a dilated ER and empty, possibly pre-storage, vacuoles. Furthermore, the TPP1 activity assay showed a significant decrease in enzyme activity in the TPP1-deficient cell line. In order to address the question whether these phenotypes have an impact on cell survival of the progenitor cells, TUNEL assays were performed (Figure 3.21).

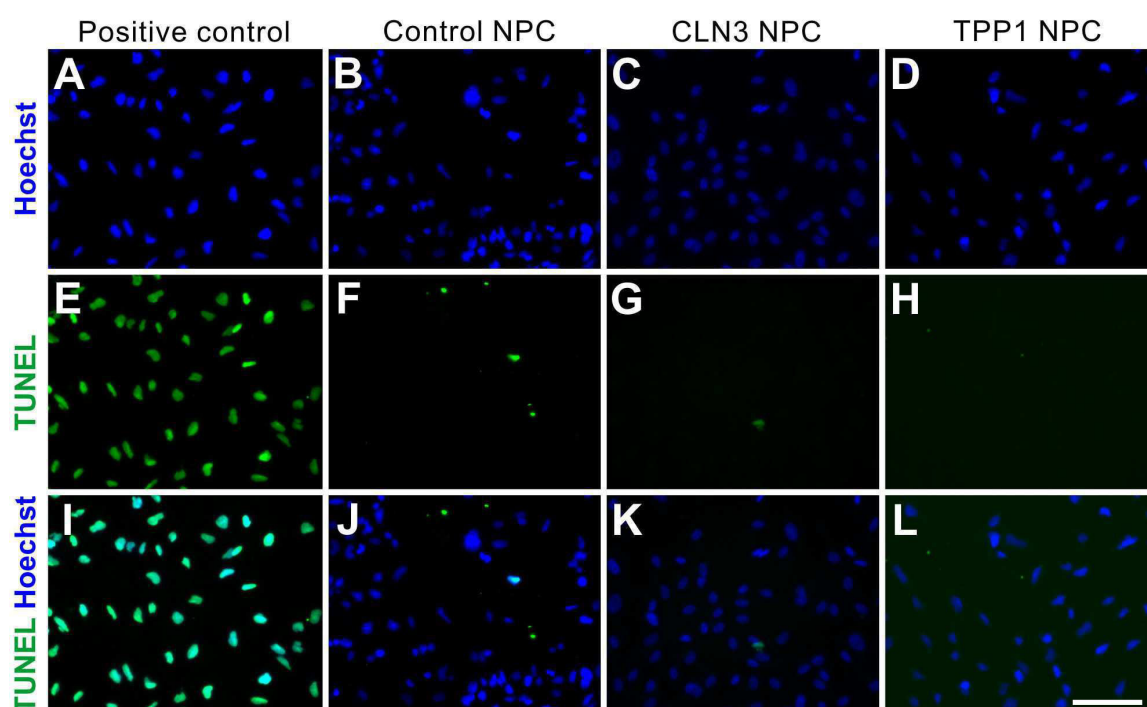


**Figure 3.21: TUNEL assay in iPSC-derived NPCs**

Representative images from one NPC line per genotype are showing TUNEL-positive cells in the positive control as well as in control, *CLN3* mutant and TPP1-deficient NPCs. Scale bar, 100  $\mu$ m.

Figure 3.21 clearly demonstrates that apoptotic events, which could have been measured by TUNEL-positive cells, were nearly absent in the NPC cultures.

## 3.3 Mature neurons

### 3.3.1 Differentiation of neural progenitor cells into mature neurons

After generation and phenotypical characterization of iPSC-derived NPCs, differentiation of derived NPCs into mature neurons was of great interest. Since neurons are the ones which are

the most affected cell type in LINCL and JNCL, their *in vitro* differentiation and subsequently phenotypical characterization was one of the major goals.

Although the protocol that was used to drive NPCs towards differentiation was quite effective for control-derived and TPP1-deficient NPCs, it resulted in a poor yield of immature and mature neurons in *CLN3* mutant NPC cultures, as shown below (Figure 3.22).

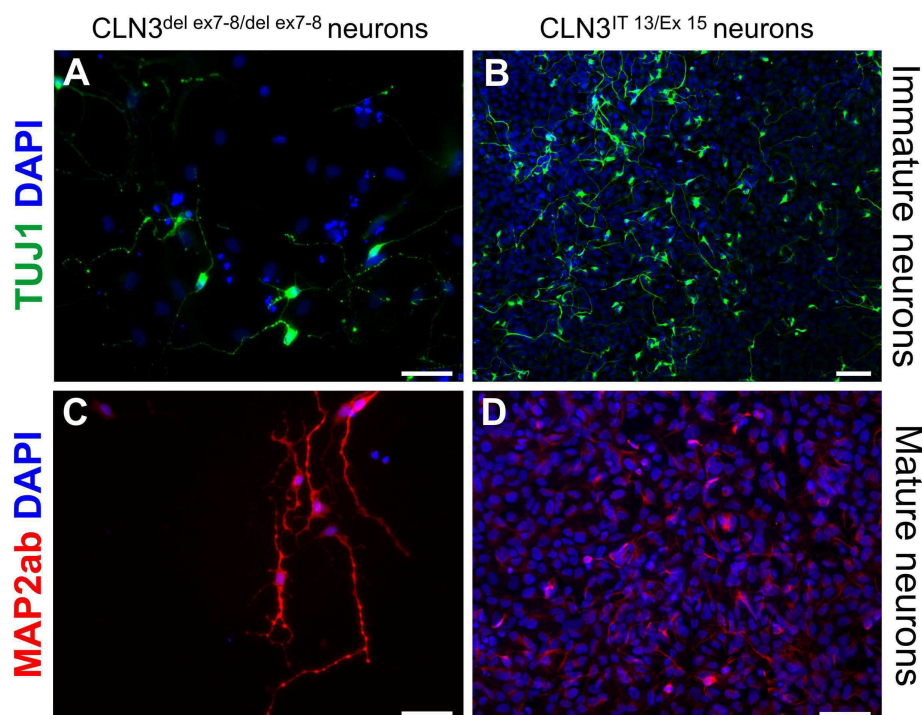


**Figure 3.22: Impaired differentiation potential of *CLN3* mutant neurons**

NPC monolayer cultures derived from *CLN3* mutant iPSCs were differentiated for 14 days and stained for markers of immature (TUJ1, green) as well as mature neurons (MAP2ab, red). Representative images from one line per genotype are shown. Cell nuclei are counterstained with DAPI (blue). Scale bars, 100  $\mu$ m.

*CLN3*<sup>del ex7-8/del ex7-8</sup> neurons, neurons derived from NPCs homozygous for the 1.02 kb deletion; *CLN3*<sup>IT 13/Ex 15</sup> neurons, neurons derived from iPSCs carrying a compound heterozygous mutation within the *CLN3* gene.

Figure 3.22 demonstrates the impaired differentiation potential of the monolayer culture of *CLN3* mutant NPCs. NPCs, that were homozygous for the common deletion within the *CLN3* gene, gave rise to neuron-specific class III beta-tubulin (TUJ1)-positive immature and microtubule-associated protein 2 (MAP2ab)-positive mature neurons. However, after 14 days of differentiation very few cells were left on the tissue culture plate, suggesting cell death during differentiation. In contrast, NPCs carrying a compound heterozygous mutation within the *CLN3* gene gave rise to a few immature TUJ1-positive neurons. However, after 14 days of

differentiation, MAP2ab-positive neurons were almost absent and the culture did not appear to be neuronal when analyzed by bright-field microscopy. Even longer differentiation periods such as three and four weeks did not increase the number of neurons derived from *CLN3* mutant NPCs. Therefore, a different differentiation approach was chosen. Instead of deriving neurons from the monolayer NPC culture, they were derived from neurospheres (for detailed information refer to 2.2.9.2). This culture system was previously shown to harbor a higher differentiation potential than monolayer cultures in general (Lojewski, 2009; unpublished data). Using this approach, *CLN3* mutant NPCs successfully gave rise to TUJ1-positive immature and MAP2ab-positive mature neurons.

Figure 3.23 shows representative images of finally differentiated NPCs into immature and mature neurons.

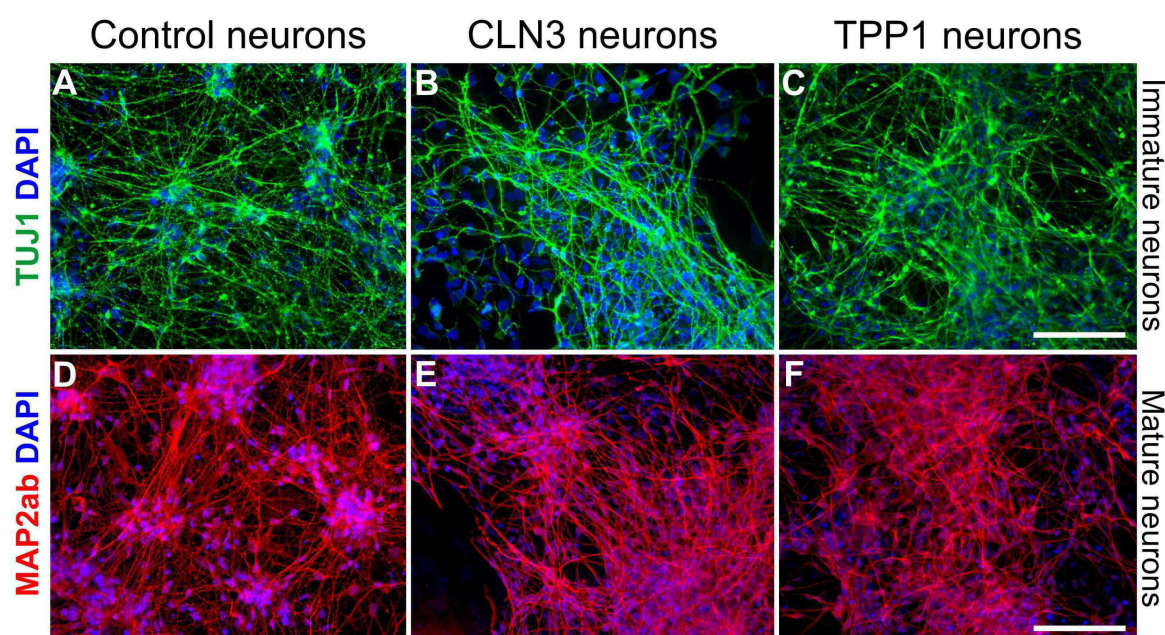


**Figure 3.23: Differentiation of iPSC-derived NPCs into mature neurons**

NPCs derived from control (A and D), *CLN3* mutant (B and E) and TPP1-deficient (C and F) iPSCs were differentiated for 14 days and stained for markers of immature (TUJ1, green) as well as mature neurons (MAP2ab, red). Representative images from one line per genotype are shown. Cell nuclei are counterstained with DAPI (blue). Scale bars, 100  $\mu$ m.

NPCs derived from control, *CLN3* mutant and TPP1-deficient iPSCs were plated onto PLO/L coated plates and allowed to differentiate for 14 days. The differentiation protocol was designed to derive high yields of neurons (unpublished data, Schöler laboratory).

As shown in Figure 3.23 A-F, NPCs derived from control, *CLN3* mutant and TPP1-deficient iPSCs are able to give rise to a high yield of immature TUJ1-positive and mature, MAP2ab-positive, neurons. Differentiation of *CLN3* mutant neurospheres, resulted thus in a neuronal network that was comparable to control and TPP1-deficient neurons that were derived from NPC monolayer cultures.

### 3.3.2 Assessment of cell death in neuronal cultures

As mentioned earlier, after 14 days of differentiation, only a few neurons, that were derived from monolayer cultures of NPCs homozygous for the common mutation within the *CLN3* gene, were left on the tissue culture plate. To address the question whether apoptotic events in neurons led to cell death in these cultures, TUNEL assays were performed (Figure 3.24).

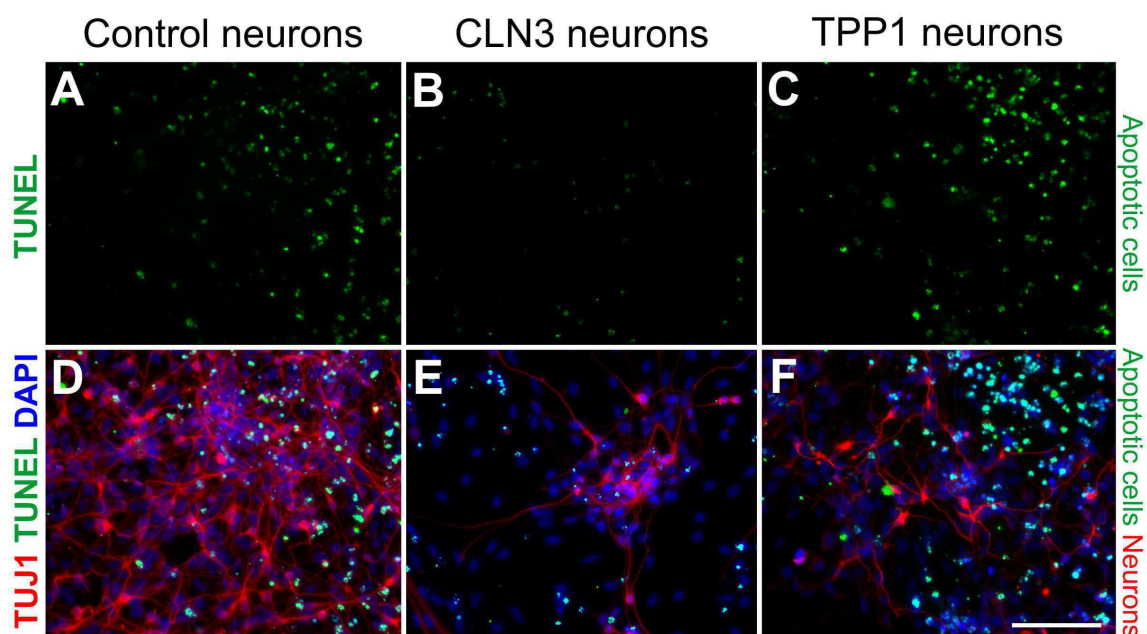


**Figure 3.24: TUNEL assay in neuronal cultures**

NPCs derived from control (A and D), *CLN3* mutant (B and E) and TPP1-deficient (C and F) iPSCs were differentiated for 7 days. After performing the TUNEL reaction, cells were stained for the neuronal marker protein TUJ1 (green). Representative images from one line per genotype are shown. Cell nuclei are counterstained with DAPI (blue). Scale bar, 100  $\mu$ m.

Figure 3.24 shows representative images of the TUNEL assay that was performed on neuronal cultures that were differentiated for 7 days. This time point was chosen because 14 days appeared to be too late in order to capture apoptotic events. As shown by the images,

apoptotic cells were present in differentiating NPC cultures of control and mutant cell lines. However, there was no co-localization of TUNEL- and TUJ1-positive cells.

### 3.3.3 Phenotypic studies of cell organelles and compartments in neuronal cultures

#### 3.3.3.1 Immunofluorescence

After 14 days of differentiation, neuronal cultures were analyzed for organellar morphology. These included mitochondria and *cis*-Golgi. Figure 3.25 shows representative confocal images of differentiated NPCs, derived from control, *CLN3* mutant and TPP1-deficient iPSCs, that were co-stained for the mitochondrial marker protein GRP75 and MAP2ab.

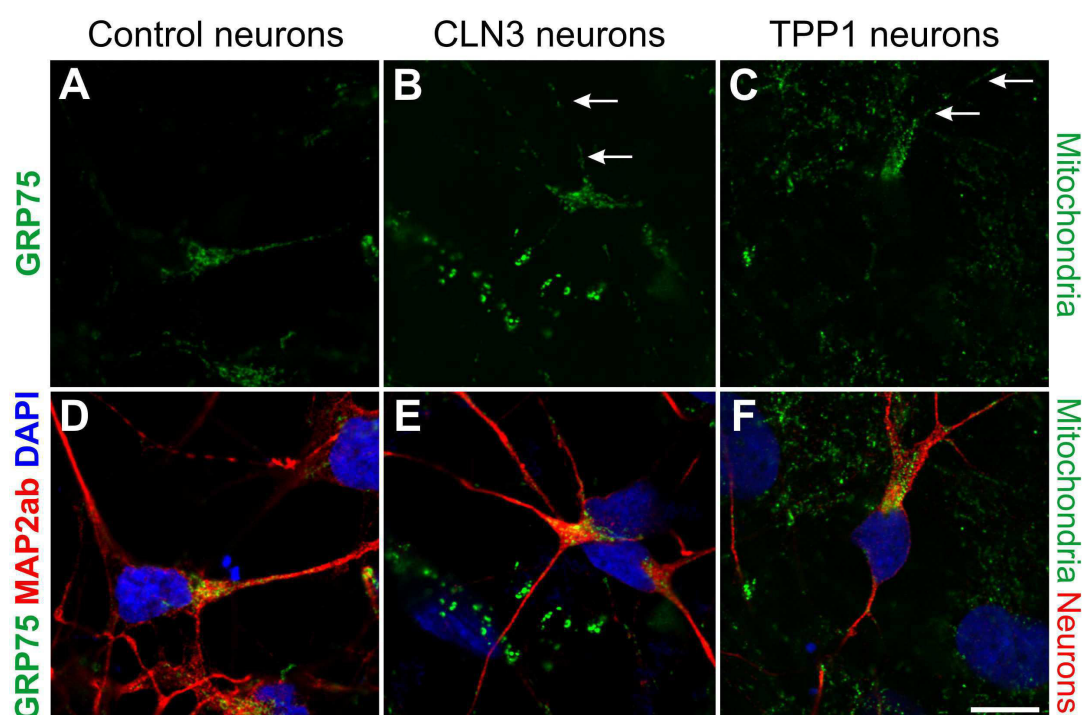


**Figure 3.25: GRP75 immunostaining in mature neurons**

Control (A and D), *CLN3* mutant (B and E) and TPP1-deficient (C and F) NPCs were differentiated for 14 days and co-stained for markers of mitochondria (GRP75, green) and mature neurons (MAP2ab, red). Mitochondria in mutant neurons appeared to be disrupted along the neurites (arrows). Representative confocal images for each genotype are shown. Cell nuclei are counterstained with DAPI (blue). Scale bar, 10  $\mu$ m.

Mitochondria in mature neurons derived from control and mutant NPCs showed the same cytosolic organization. The samples showed clusters of mitochondria near the cell nucleus and elongated ones along the neurites. However, mitochondria along the neurites of neurons that

were derived from *CLN3* mutant and TPP1-deficient NPCs, appeared to be disrupted and discontinued (Figure 3.25 B and C, arrows).

Since immunostainings for the *cis*-Golgi marker protein GM130 in NPCs revealed disrupted structures in *CLN3* mutant and TPP1-deficient cell lines (Figure 3.15 F-J), Golgi organization within neuronal cultures was of great interest.

Figure 3.26 shows representative confocal images of GM130 and MAP2ab co-stainings in neuronal cultures derived from control, *CLN3* mutant and TPP1-deficient NPCs.

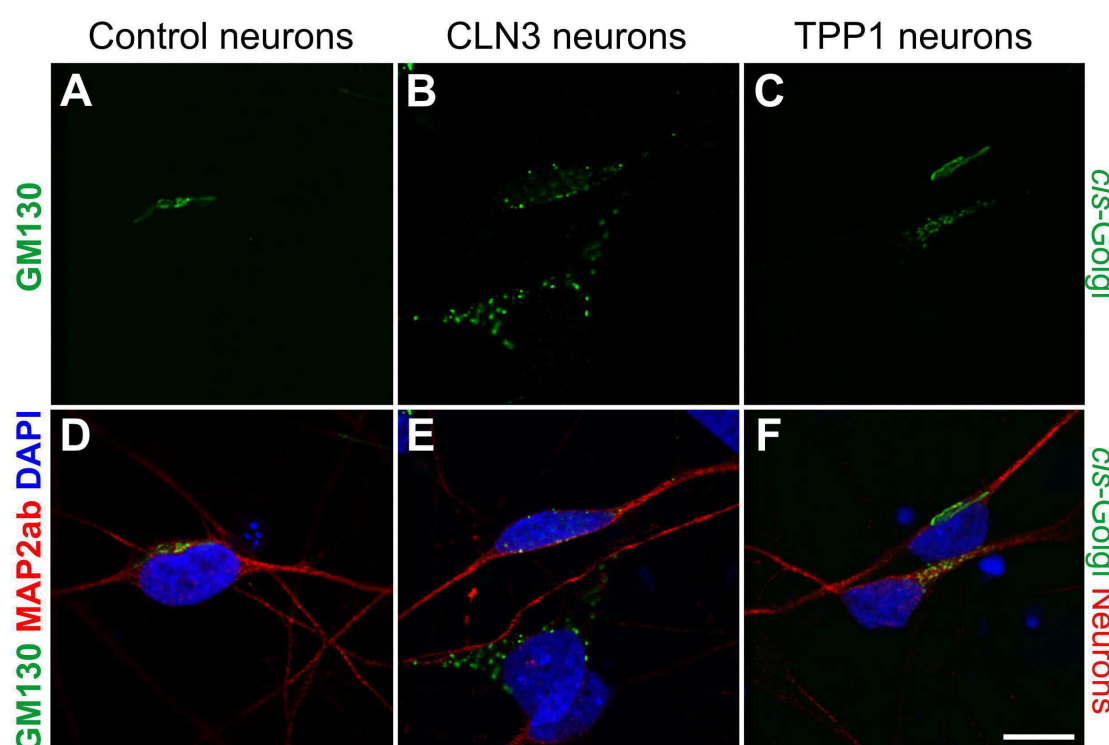


**Figure 3.26: GM130 immunostaining in mature neurons**

Control (A and D), *CLN3* mutant (B and E) and TPP1-deficient (C and F) NPCs were differentiated for 14 days and co-stained for markers of *cis*-Golgi (GM130, green) and mature neurons (MAP2ab, red). Golgi structures in mutant cell lines (B and C) appeared rather punctate and unorganized when compared to control neurons (A). Representative confocal images for each genotype are shown. Cell nuclei are counterstained with DAPI (blue). Scale bar, 10  $\mu$ m.

Immunostainings for the *cis*-Golgi marker protein GM130 in neuronal cell cultures revealed distinct phenotypes in the mutant cell lines. In neurons derived from control NPCs, Golgi was well organized and polarized to one site of the cell nucleus (A and D). In neurons derived from *CLN3* mutant NPCs, however, GM130 immunostaining revealed punctate structures surrounding the cell nucleus (B and E). This phenomenon was also seen in neurons derived

from TPP1-deficient NPCs (C and F), although some of them showed a well organized and polarized Golgi structure as seen in neurons derived from control NPCs.

Taken together, mitochondria and Golgi structures seem to have a distinct phenotype in *CLN3* mutant and TPP1-deficient neurons that was already apparent in their parent NPC lines.

Studies suggested dysfunction within the autophagy pathway in cultures of *CLN3* mutant cells (Cao *et al.*, 2006). Furthermore, it is well known that subunit c is a major constituent of storage material found in tissue samples from NCL patients and animal models (Palmer *et al.*, 1992). Hence, investigations of lysosomes and possible storage in neurons derived from mutant NPCs were performed.

Figure 3.27 shows representative confocal images of LAMP-1/MAP2ab co-stainings in neurons derived from control, *CLN3* mutant and TPP1-deficient NPC lines.

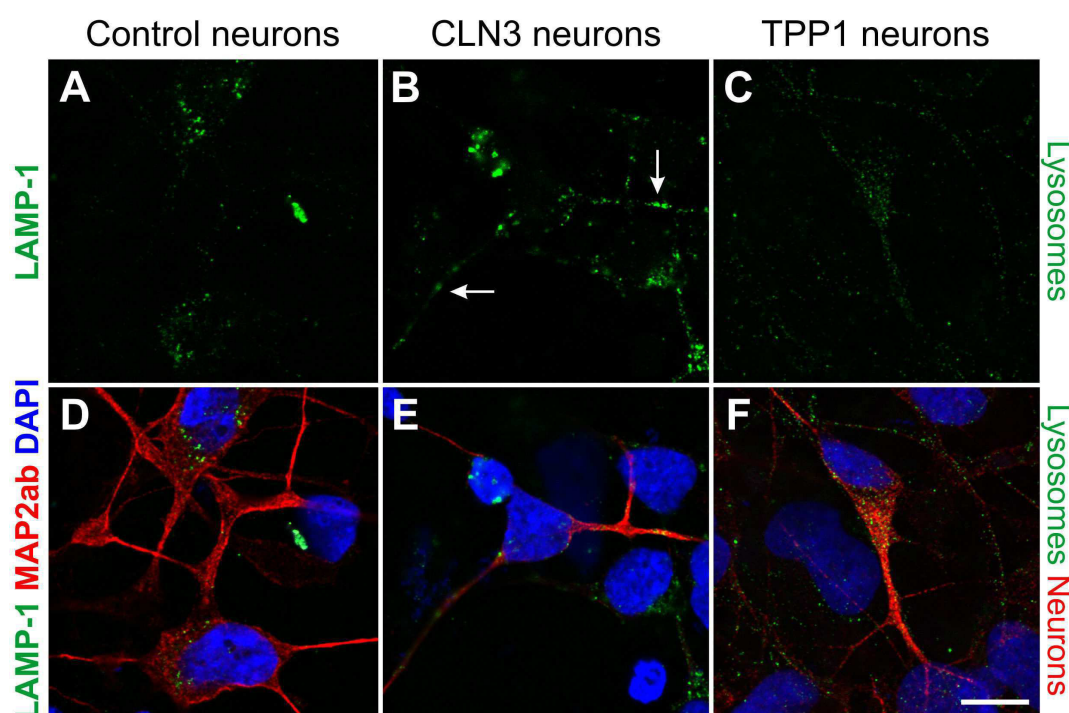


**Figure 3.27: LAMP-1 immunostainings in mature neurons**

Control (A and D), *CLN3* mutant (B and E) and TPP1-deficient (C and F) NPCs were differentiated for 14 days and co-stained for markers of lysosomes (LAMP-1, green) and mature neurons (MAP2ab, red). In contrast to control-derived neurons, *CLN3* mutant neurons showed LAMP-1 positive vesicles along the neurites (arrows). Representative confocal images for each genotype are shown. Cell nuclei are counterstained with DAPI (blue). Scale bar, 10  $\mu$ m.



Immunostainings for LAMP-1 in mature neurons derived from control NPCs (A and D) revealed LAMP-1 positive vesicles that were located near the cell nucleus. However, LAMP-1 positive vesicles found in *CLN3* mutant NPCs were rather distributed along the neurites (B and E, arrows). Neurons derived from TPP1-deficient NPC lines showed a very distinctive staining pattern for LAMP-1 positive vesicles (C and F). Vesicles found within the neurons were not only smaller than those found in control and *CLN3* mutant-derived neurons but were also distributed quite evenly throughout the entire neuron, i.e., soma and neurite.

Finally, investigations about possible storage material e.g. accumulation of subunit c in neurons derived from *CLN3* mutant and TPP1-deficient NPCs were performed. Figure 3.28 shows the results of immunostainings for subunit c in neurons derived from control and mutant NPCs.

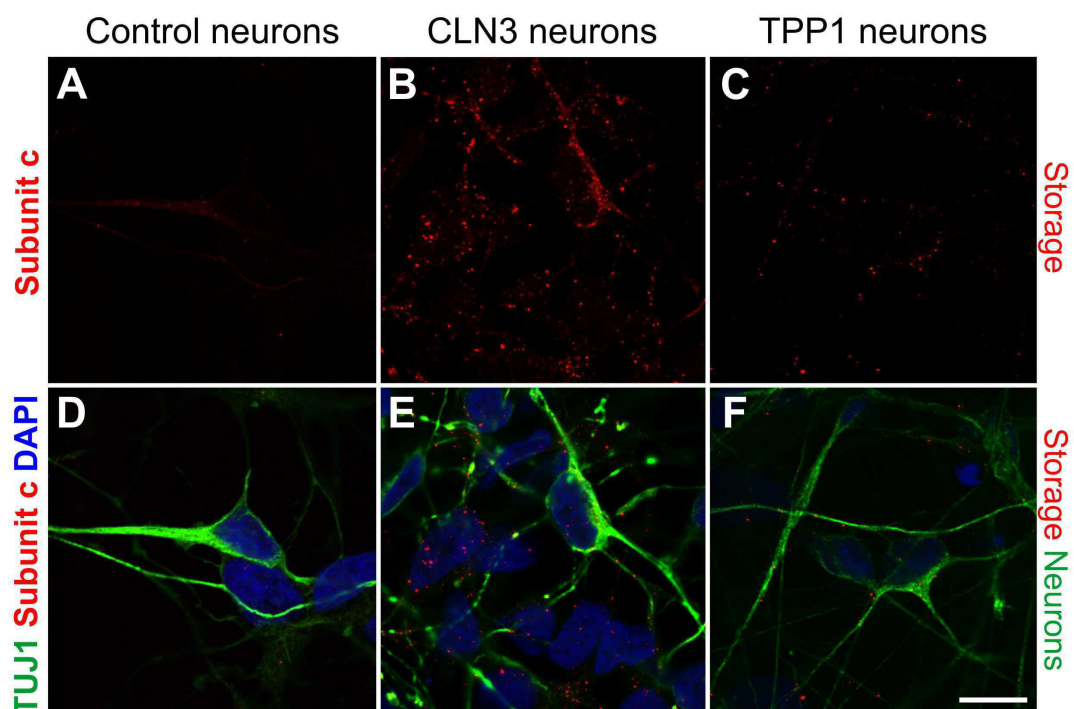


**Figure 3.28: Subunit c immunostaining in NPC-derived neurons**

Control (A and D), *CLN3* mutant (B and E) and TPP1-deficient (C and F) NPCs were differentiated for 14 days and co-stained for subunit c (red) and neurons (TUJ1, green). Subunit c staining was abundant within the mutant cell lines. Representative confocal images for each genotype are shown. Cell nuclei are counterstained with DAPI (blue). Scale bar, 10  $\mu$ m.

---

Confocal images of immunostainings for subunit c in TUJ1-positive neurons derived from control NPC lines (A and D) did show very few puncta within the neurites and cell nuclei. In contrast to the staining pattern found in control-derived neurons, subunit c staining was abundant in neuronal cultures derived from *CLN3* mutant NPCs (B and E). Staining revealed not only more subunit c positive vesicles but they were also larger in size when compared to the control. Although subunit c staining in TPP1-deficient neurons (C and F) was less abundant than in *CLN3* mutant ones, more positive vesicles were found in comparison to control-derived neurons. The subunit c positive vesicles, which were larger in size compared to those found in control neurons, were mostly distributed along the neurites and the soma. Overall, immunofluorescence results clearly demonstrated a distinctive phenotype within the mutant cell lines that is genotype-specific. The abundant staining of subunit c in mutant neurons leads to the assumption of storage material which would recapitulate findings in human tissue samples and in mouse models.

In order to quantify potential differences on the protein level, Western blot analysis was performed on neuronal cell cultures.

### 3.3.3.2 Western blot analysis

Western blot analysis was performed to get more information about possible genotype-related differences on the protein level. Since *CLN3* mutant NPCs could only give rise to mature neurons when grown as neurospheres, it was not possible to obtain enough protein for Western blot analysis. Thus, investigations on the protein level were only performed on neurons derived from control and TPP1-deficient NPCs.

Figure 3.29 shows Western blot results of neurons derived from control and TPP1-deficient NPCs.

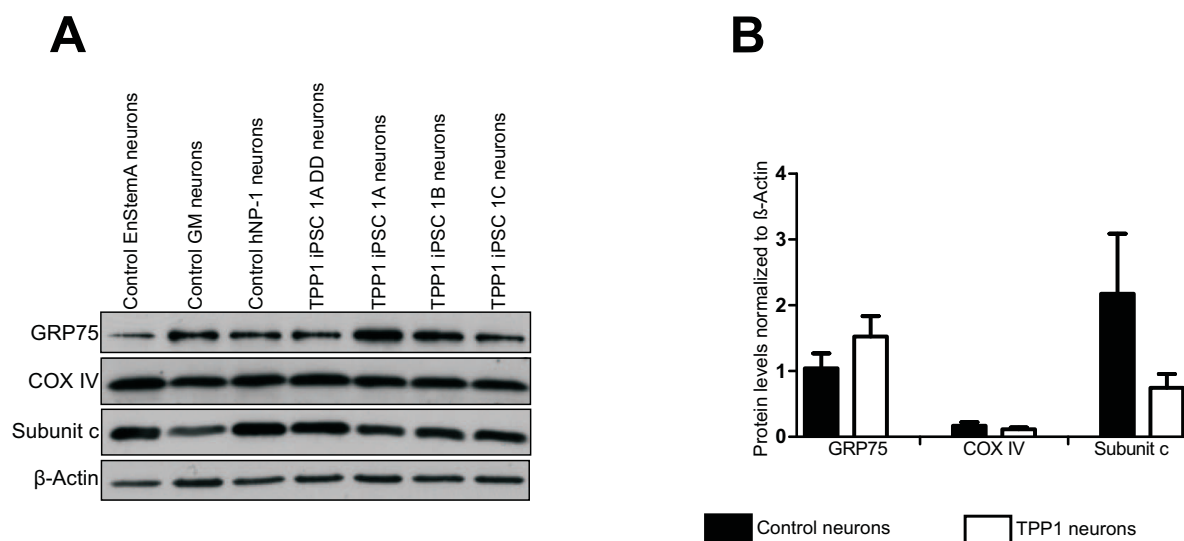


**Figure 3.29: Western blot analysis of mitochondrial proteins in neuronal cultures**

**A** Western blot results for the mitochondrial proteins GRP75 (75 kDa), COX IV (17 kDa) and the subunit c (4 kDa) of the mitochondrial ATPase complex in neurons derived from control and TPP1-deficient NPCs.  $\beta$ -Actin (43 kDa) was used as loading control. **B** Quantitative analysis of Western blot results from control and TPP1-deficient neuronal cultures. Protein levels were normalized to  $\beta$ -Actin. Bar graph shows mean with SEM (n = 3, control neurons; n = 4, TPP1 neurons).

According to the Western blot quantification, there was no significant difference on the protein level in neither of the mitochondrial associated proteins GRP75 and COX IV nor on subunit c protein levels.

Since immunostainings against LAMP-1 revealed positive vesicles that were evenly distributed throughout the entire neuron in TPP1-deficient cell cultures, Western blot analysis was performed to see if more LAMP-1 protein could be found in these cultures compared to control neuronal cell cultures. Because LAMP-1 is associated with the autophagy pathway, Western blot was performed as well for the early endosomal marker EEA-1 in neuronal cultures derived from control and TPP1-deficient NPCs (Figure 3.30).

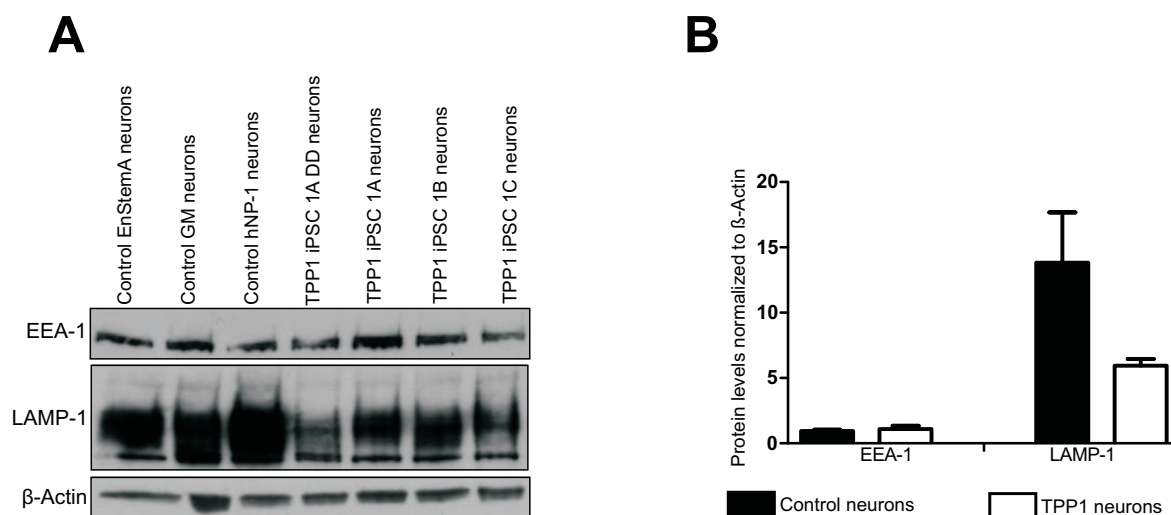


**Figure 3.30: Western blot analysis of EEA-1 and LAMP-1 in neuronal cultures**

**A** Western blot results for the autophagy related proteins EEA-1 (170 kDa) and the LAMP-1 (~120 kDa) in neurons derived from control and TPP1-deficient NPCs.  $\beta$ -Actin (43 kDa) was used as loading control. **B** Quantitative analysis of Western blot results from control and TPP1-deficient neurons. Protein levels were normalized to  $\beta$ -Actin. Bar graph shows mean with SEM ( $n = 3$ , control neurons;  $n = 4$ , TPP1 neurons).

Western blot results did not reveal any significant difference on the protein level for EEA-1 or LAMP-1 in neurons that were derived from control and TPP1-deficient cell lines. However, there was a trend of more LAMP-1 protein in neurons derived from control NPCs compared to those ones derived from TPP1-deficient NPCs ( $p = 0.0619$ ). This might reflect the size of the LAMP-1 positive vesicles found in control neurons which were larger compared to vesicles found in TPP1-deficient neurons by immunostaining.

In summary, Western blot results did not show any significant differences at the protein level for organelles or autophagy-related structures in control or TPP1-deficient neuronal cell cultures.

### 3.3.3.3 Electron microscopy

Transmission electron microscopy was performed in order to obtain more detailed information about organelle structure and to verify possible phenotypes observed in neuronal cultures by immunofluorescence.

Figure 3.31 shows representative EM images from control, *CLN3* mutant and TPP1-deficient neurons.

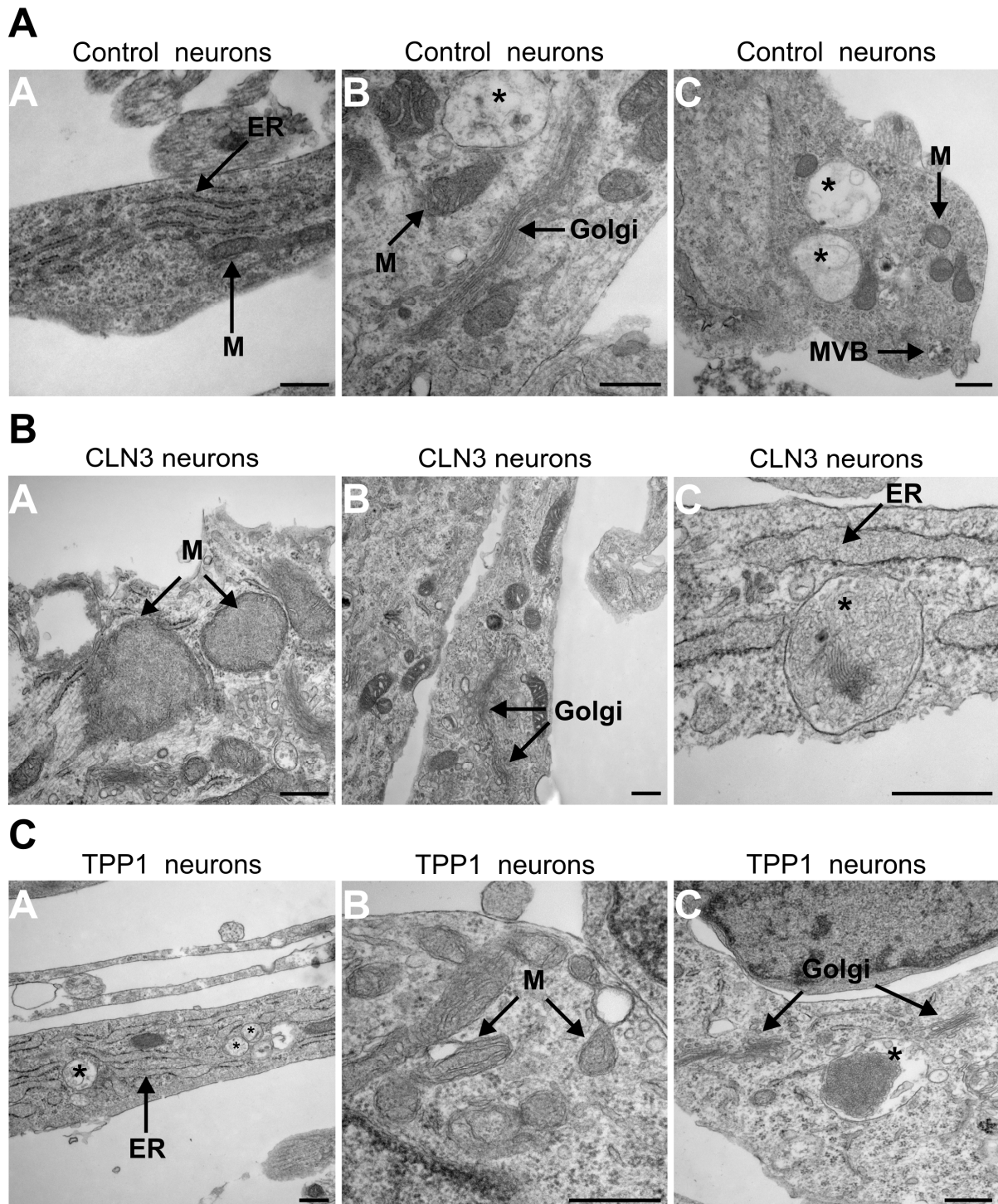


**Figure 3.31: Electron microscopy images of control, *CLN3* mutant and TPP1-deficient neurons**

**A** Representative EM images showing control-derived neurons. Neurons showed a long, narrowed ER (ER, arrow) as well as organized and well-stacked Golgi apparatus (Golgi, arrow). Mitochondrial shape varied within a normal range from bean-like to roundish (M, arrows). Small multivesicular bodies (MVB) as well as large, possibly immature multivesicular bodies (asterisk) were found within the cytoplasm. Scale bars, 500 nm. **B** Representative EM images showing *CLN3* mutant neurons. Some mitochondria were found to be distended and lacking internal structure (M, arrows). The Golgi apparatus appeared to be distended and not well-stacked (Golgi, arrows). In addition, multiple Golgi-related vesicles were found. The ER showed an abnormally elongated and distended morphology (ER, arrow). Numerous vacuoles containing curvilinear storage material were found within the cytoplasm. In some of these vacuoles, storage material displaying fingerprint profile was found (C, asterisk). Scale bars, 500 nm. **C** Representative EM images showing TPP1-deficient neurons. The ER appeared to be distended and elongated (ER, arrow). Some mitochondria showed an altered morphology and were abnormally vacuolated (M, arrows). The Golgi apparatus appeared to be distended and abundant (Golgi, arrows). Vacuoles (asterisks) within the cytoplasm often showed curvilinear storage material (C, asterisk). Scale bars, 500 nm.

ER, endoplasmic reticulum; Golgi, Golgi apparatus; M, mitochondria; MVB, multivesicular body; \*, designates vacuoles.

Electron microscopy revealed an enlarged and quite distended ER in *CLN3* mutant (Figure 3.31 **B C**) and TPP1-deficient neurons (Figure 3.31 **C A**) when compared to the ER in control-derived neurons (Figure 3.31 **A A**). Mitochondria found within neurons showed various morphologies. Some were bean-like shaped (Figure 3.31 **A B**) whereas others were roundish (Figure 3.31 **A C**). Most mitochondria in *CLN3* mutant neurons showed a normal morphology with intact cristae. However, some mitochondria appeared to be distended, lacking any internal structures (Figure 3.31 **B A**) when compared to control-derived neurons. Furthermore, the Golgi apparatus appeared to be distended in *CLN3* mutant neurons (Figure 3.31 **B B**) and not as well stacked as the Golgi apparatus found in control-derived neurons (Figure 3.31 **A B**). In addition, multiple Golgi-related vesicles, that were not apparent in the control-derived neurons, were found in *CLN3* mutant neurons (Figure 3.31 **B B**). Although, vacuoles containing frequent membrane-bound storage material, that was often curvilinear, were already apparent in EM images of *CLN3* mutant NPCs, some of the *CLN3* mutant neurons showed storage material with a fingerprint-like profile (Figure 3.31 **B C**).

Similar to *CLN3* mutant and control-derived neurons, EM images of TPP1-deficient neurons revealed mitochondria of various shapes. However, some mitochondria in TPP1-deficient neurons showed an altered, vacuolated morphology (Figure 3.31 **C B**). Furthermore, TPP1-deficient neurons showed abundant Golgi structures that were distended (Figure 3.31 **C C**).

---

Similar to TPP1-deficient NPCs, mutant neurons showed vacuoles within the cytoplasm. However, in contrast to the vacuoles found within the NPCs, these ones were not empty. EM images revealed frequent membrane bound storage material that was often curvilinear (Figure 3.31 C C).

Taken together, EM images confirmed the findings of the immunofluorescence experiments that showed altered morphologies of mitochondria and Golgi apparatus in mutant-derived neurons. Furthermore, electron microscopy revealed storage material with fingerprint-like profile exclusively in *CLN3* mutant neurons, suggesting a higher amount of subunit c within the storage material found in vacuoles within the *CLN3* mutant neurons. This finding is in accordance with the immunostainings that showed more subunit c signal within the *CLN3* mutant neurons than within the TPP1-deficient neurons (Figure 3.28).

### 3.3.4 Astrocytes in neuronal cultures

Although this work was focused on NPCs and mature neurons, recent reports on astrocytic activation that precedes neuronal death in model systems of NCL (Oswald *et al.*, 2005; Macauley *et al.*, 2011), led to the question whether astrocytes derived from *CLN3* mutant and TPP1-deficient NPCs show any morphological alterations when compared to control-derived astrocytes.

Figure 3.32 shows representative images of astrocytes derived from control, *CLN3* mutant and TPP1-deficient NPCs.

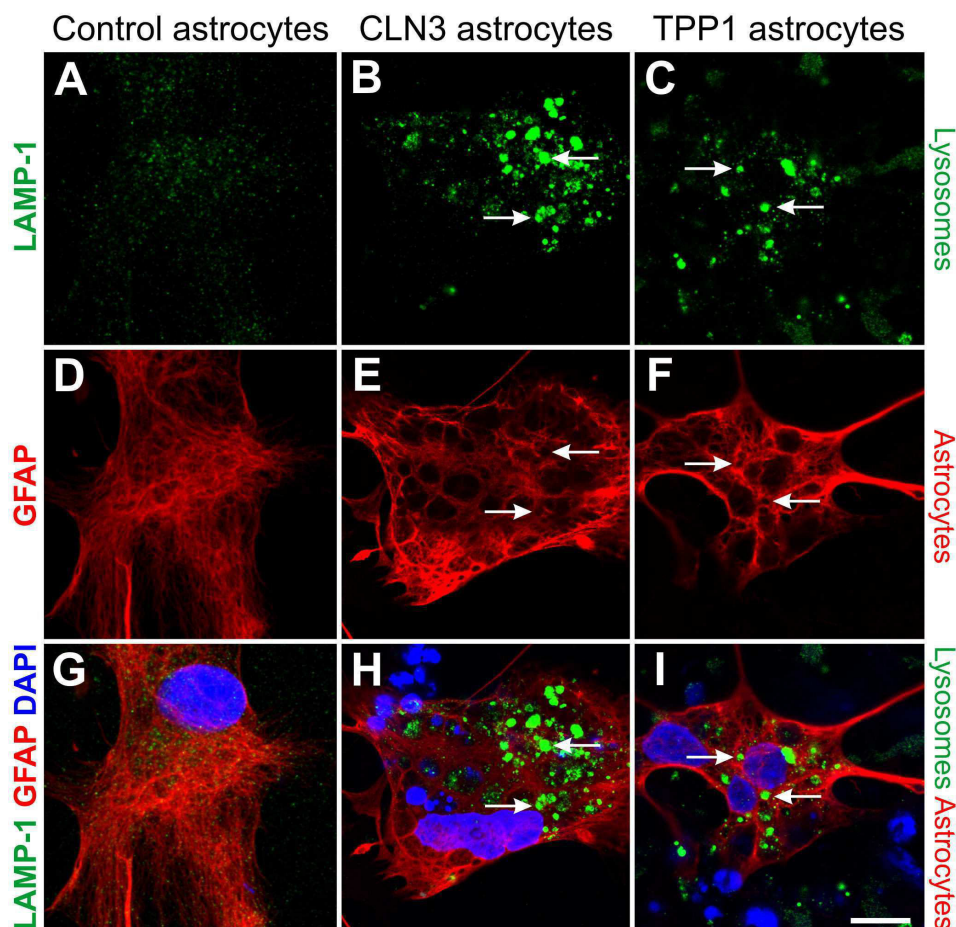


**Figure 3.32: LAMP-1 immunostaining in astrocytes**

Control (A, D and G), *CLN3* mutant (B, E and H) and TPP1-deficient (C, F and I) NPCs were differentiated for 14 days and co-stained for markers of lysosomes (LAMP-1, green) and astrocytes (GFAP, red). In contrast to control-derived astrocytes, *CLN3* mutant and TPP1-deficient astrocytes show alterations in their filament structure. In addition, mutant astrocytes show an accumulation of large LAMP1-positive vesicles within the cytoplasm (white arrows). Representative confocal images for each genotype are shown. Cell nuclei are counterstained with DAPI (blue). Scale bar, 10  $\mu$ m.

Immunostainings for the astrocytic marker protein glial fibrillary acidic protein (GFAP) revealed filament alterations in mutant astrocytes. The GFAP-positive astrocytes derived from *CLN3* mutant and TPP1-deficient NPCs appeared to be porous when compared to control-derived astrocytes. In order to address the question whether these pores are the result of enlarged lysosomal vacuoles, co-stainings with LAMP-1 were performed. Indeed, LAMP-1-positive vesicles found in mutant astrocytes were enlarged and accumulated in the cytoplasm. However, only a few LAMP-1-positive vesicles were found to be localized within the “pores”.



---

## 4 Discussion

Since their first description, induced pluripotent stem cells (iPSCs) have revolutionized the field of medical research. Their pluripotent nature enables researchers to study any cell type of the human body while overcoming legal and ethical obstacles that are associated with the use of embryonic stem cells. Patient-derived iPSCs offer the singular opportunity to model a particular disease *in vitro*. This great potential of disease modeling can be used for detailed *in vitro* studies such as phenotypic analyses, drug screenings, and genetic correction. In terms of personalized medicine, these cells harbor the potential for a new mode of drug discovery.

The present thesis described the generation of patient-derived iPSCs and their use in modeling neuronal ceroid lipofuscinoses as shown here in the case of classic late infantile (CLN2) and juvenile neuronal ceroid lipofuscinosis (CLN3). This is, to our knowledge, the first report on the generation of iPSCs and the subsequent derivation of neural progenitor cells and neurons from patients suffering from a form of neuronal ceroid lipofuscinosis.

### 4.1 Modeling neuronal ceroid lipofuscinosis

Neuronal ceroid lipofuscinosis (NCL) is a neurodegenerative disorder. Therefore, in order to establish human disease models for the two most common forms of NCLs, juvenile and late infantile NCL, access to neurons or their progenitor cells is required. Since brain tissue samples from living patients is almost unavailable, an intermediate cell culture, that provides neural progenitor cells (NPCs) which can be expanded and further differentiated into mature neurons, is required. iPSCs are such intermediates.

To date, the most validated protocol for the generation of patient-derived iPSCs involves a four-factor reprogramming approach of patient-derived fibroblasts. Therefore, skin fibroblasts were taken from patients suffering from either LINCL or JNCL and were infected with retroviruses encoding for OCT4, SOX2, KLF4 and MYC. Since the method used for generation of patient-derived iPSCs uses a standard protocol that was established in the Schöler laboratory for several other disease models, the demonstration of pluripotency was narrowed down to a minimum (Zaehres *et al.*, 2010). In particular, the elaborate *in vivo* teratoma formation assay which involves teratoma formation in immunodeficient mice, was replaced by formation of embryoid bodies and subsequent differentiation into cells derived

---

from the three germ layers. This approach was already reported to be a sufficient demonstration of pluripotency (Sheridan *et al.*, 2011) and, quite recently, has been proposed to entirely replace the teratoma formation assay (Sheridan *et al.*, 2012). Retroviral silencing, expression of endogenous pluripotency marker genes and proteins as well as differentiation into cells of the three germ layers demonstrated the successful generation of iPSCs from patients suffering from either LINCL or JNCL. So far, no reports on iPSCs derived from any of the known NCLs are currently available and only a few reports are published about derivation of iPSCs from patients suffering of a lysosomal storage disorder such as mucopolysaccharidosis type IIIB (Lemonnier *et al.*, 2011), Gaucher disease (Park *et al.*, 2008; Mazzulli *et al.*, 2011) and Hurler syndrome (Tolar *et al.*, 2011). In addition, one needs to consider that some patient-derived fibroblasts can not give rise to iPSCs. For example, iPSCs from patients suffering from Fanconi anemia could only be generated after correction of the genetic defect in the patient-derived fibroblasts (Raya *et al.*, 2009).

The reprogramming of somatic cells into iPSCs resets these cells towards an ESC-like state. Thus, disease-related phenotypes which are expected in finally differentiated cells may not be obvious in iPSCs. The majority of the current disease models involving iPSCs focuses on the cells mainly affected by the disease, i.e., neurons or their progenitor cells. However, Lemonnier and colleagues used patient-derived iPSCs to model the lysosomal storage disorder mucopolysaccharidosis type IIIB and reported a disease-related phenotype which was already apparent in the patient-derived iPSCs (Lemonnier *et al.*, 2011). The authors found, in immunofluorescence as well as in EM images, intracellular vacuoles and a disorganization of the Golgi complex structure. However, the investigators stated that the patient-derived iPSCs were not impaired in their neuroectodermal differentiation potential. Thus, iPSCs derived from LINCL and JNCL patients were phenotypically analyzed. Reports on mitochondrial abnormalities (Fossale *et al.*, 2004), impairments within the Golgi system (Fossale *et al.*, 2004; Codlin *et al.*, 2009; Kama *et al.*, 2011; Padilla-Lopez *et al.*, 2012), altered trafficking within the autophagy pathway (Cao *et al.*, 2006; Chang *et al.*, 2011) and the characteristic feature of the NCLs, lysosomal storage of the subunit c of the mitochondrial ATPase complex, led to the assessment of mitochondria, Golgi, ER, lysosomes, early endosomes and subunit c storage. As these phenotypes may be markers of disease progression, these organelles and compartments were assessed not only during the iPSC stage but also in the neural progenitors and later on in the mature neurons.

The next step towards the disease modeling was to establish NPC populations from patient-derived iPSCs. NPCs are of great interest for researchers. In contrast to iPSCs, they can be

easily frozen down and thawed. Moreover, unlike mature neurons, NPCs can be expanded for multiple passages and are ready to be differentiated into mature cell types at any time, thus providing a valuable source for neuronal and glial cells. To date, two main approaches are used to derive NPCs from iPSC cultures. The first uses a monolayer protocol (Chambers *et al.*, 2009; Chambers *et al.*, 2011), and the second one derives NPCs via formation of neural rosettes (Elkabetz *et al.*, 2008a; Lie *et al.*, 2012). Although the latter one is more sophisticated, it has been widely used for ESCs and iPSCs and has therefore been optimized during the past years (Lie *et al.*, 2012). In order to establish NPC lines from LINCL and JNCL patient-derived iPSCs, the rosette forming protocol was used since this approach provided more reliable NPC cultures than the monolayer protocol. As it was aimed to generate mature neurons independently of further fate specification, patterning of neural rosettes towards fore-, mid- or hindbrain fate (refer to Figure 1.3) was not performed.

The final step in the disease modeling of LINCL and JNCL was to derive mature neurons from NPCs, the cell type predominantly affected in NCLs. Since the objective was not to derive a specific neuronal sub-type, the iPSC-derived NPCs were not pre-patterned and the final differentiation protocol was designed for general differentiation only (unpublished data, Schöler laboratory). The goal of the disease modeling was to follow potential disease markers over the course of iPSC differentiation, i.e. phenotypical analyses during the ESC-like state, the neural progenitor state, and the mature neuronal state. Thus, as with iPSCs, iPSC-derived NPCs and neurons were as well analyzed for mitochondria, Golgi, ER, lysosomes and the subunit c of the mitochondrial ATPase complex.

The following table provides an overview of the phenotypes found during the different stages of the disease models. A potential phenotype found by immunofluorescence was only considered a true phenotype when EM analysis of at least two biological different samples could confirm the phenotype.

**Table 4.1: Phenotypes of the disease models**

| Form of NCL | Induced pluripotent stem cells                   |  |                                     | Neural progenitor cells  |   |  | Neurons   |  |   |
|-------------|--|--|-------------------------------------|--|---|--|---|--|---|
|             | IF   | EM   | Others                              | IF   | EM  | Others                                   | IF  | EM   | Others  |
| JNCL        | <b>Lysosomes:</b> large LAMP-1-positive vesicles | Large empty <b>vacuoles</b> within the cytoplasm |                                     | <b>Mitochondria:</b> elongated<br><br><b>Lysosomes:</b> some enlarged vesicles | <b>Mitochondria:</b> elongated, dilated<br><br><b>Vacuoles</b> containing curvilinear-shaped storage material | WB: trend towards subunit c accumulation | <b>Mitochondria:</b> discontinued<br><br><b>Lysosomes:</b> enlarged vesicles along neurites<br><br><b>Golgi:</b> disrupted<br><br><b>Storage:</b> abundant subunit c staining | <b>Mitochondria:</b> distended, lack of cristae<br><br><b>Vacuoles</b> containing storage material<br><br><b>ER:</b> distended, elongated<br><br><b>Golgi:</b> distended; multiple Golgi-associated vesicles<br><br><b>Storage:</b> curvilinear and fingerprint profiles | Monolayer culture: impaired differentiation potential<br><br><b>Astrocytes:</b> porous filament structure; accumulation of enlarged LAMP-1 vesicles |
| LINCL       |  |  | Reduced TPP1 enzyme activity levels |  | Empty <b>vacuoles</b> within the cytoplasm<br><br><b>ER:</b> dilated  | Reduced TPP1 enzyme activity levels      | <b>Mitochondria:</b> discontinued<br><br><b>Lysosomes:</b> numerous smaller vesicles<br><br><b>Golgi:</b> disrupted<br><br><b>Storage:</b> subunit c staining                 | <b>Mitochondria:</b> altered, vacuolated morphology<br><br><b>Vacuoles</b> containing storage material<br><br><b>ER:</b> distended, elongated<br><br><b>Golgi:</b> abundant, distended<br><br><b>Storage:</b> curvilinear profiles                                       | WB: trend towards reduced LAMP-1 levels<br><br><b>Astrocytes:</b> porous filament structure; accumulation of enlarged LAMP-1 vesicles               |

EM, electron microscopy; ER, endoplasmic reticulum; IF, immunofluorescence; JNCL, juvenile neuronal ceroid lipofuscinosis; LAMP-1, lysosomal-associated membrane protein 1; LINCL, late infantile neuronal ceroid lipofuscinosis; TPP1, tripeptidyl peptidase I; WB, Western blot

#### 4.1.1 Juvenile neuronal ceroid lipofuscinosis disease model

Phenotypic analysis of JNCL patient-derived iPSCs in terms of mitochondria, Golgi, ER and potential storage material, such as subunit c of the mitochondrial ATPase complex, showed no alterations. However, immunostainings for the lysosomal marker protein LAMP-1 and EM images reproducibly revealed large vacuoles within the iPSC colonies. It is most likely, that some of the vacuoles seen in EM images correspond to the vacuoles detected by immunostaining because LAMP-1 not only localizes to the limiting membrane of lysosomes and late endosomes but was also found to be present on the limiting membrane of late autophagic vacuoles (reviewed by Eskelinen *et al.*, 2003). However, as seen in the EM images, the vacuoles were free of any storage material. This suggests an early phenotype which might be due to the reported defect in the autophagy pathway (Cao *et al.*, 2006). The fact that iPSCs are self-renewing and have a metabolic state that is very similar to ESCs (Prigione *et al.*, 2010a; Prigione *et al.*, 2010b), might explain the absence of storage material

---

in these vacuoles. Although these vacuoles were not apparent in control and TPP1-deficient iPSCs, *CLN3* mutant iPSCs showed no growth rate alterations, as shown by BrdU experiments, or impairments in differentiation into cells from the three germ layers. Moreover no impact on NPC derivation was observed.

In contrast to JNCL patient-derived iPSCs, derived NPCs showed disease-related phenotypes with progression during neuronal differentiation. Immunostainings for the mitochondrial marker protein GRP75 revealed elongated mitochondria in NPCs and neurons from JNCL patient-derived iPSCs. EM images of these lines showed that the mitochondria were not only elongated but also dilated. These results confirm the mitochondrial phenotype found to be prominent in cerebellar cells of *Cln3* <sup>$\Delta$ ex7/8</sup> knock-in mice (Fossale *et al.*, 2004). Similar mitochondrial phenotypes were also found in fibroblasts from patients affected by CLN1 or CLN6 disease (Pezzini *et al.*, 2011). Moreover, EM images of NPCs revealed that many of the mitochondria possessed a reduced number of cristae and some mitochondria found within neurons even entirely lacked internal structures. Fewer cristae might have an impact on the energy metabolism of the cell. The invaginations of the inner membrane enlarge the surface area and thus enable higher and faster ATP production (Zick *et al.*, 2009). A similar mitochondrial phenotype has been described for the English setter dog which is a model for the CLN8 disease. March and colleagues observed enlarged mitochondria with abnormal cristae (March *et al.*, 1995). The authors suggested that this might either be a physiological reaction to metabolic stress or a direct result of the metabolic defect which might possibly be associated with altered trafficking of subunit c of the mitochondrial ATPase complex and thus representing a pathological change. Interestingly, the CLN8 disease is due to a defect in the CLN8 gene which encodes, similar to *CLN3*, a transmembrane protein. However, unlike the CLN3 protein, the CLN8 protein resides within the ER (Jalanko *et al.*, 2009). Nevertheless, unlike findings in CLN1 and CLN6 patient-derived fibroblasts which reported reduced protein levels of COX IV by Western blot (Pezzini *et al.*, 2011), levels of the mitochondrial marker proteins GRP75 and COX IV were not altered when comparing control and mutant NPC lines, suggesting no changes in mitochondrial protein content. The mitochondrial phenotype might have had as well an impact on the differentiation potential of the NPC monolayer culture. It is well known that differentiation requires functional mitochondria and mitochondrial biogenesis in order to meet the energy requirements during differentiation (Cho *et al.*, 2006; Facucho-Oliveira *et al.*, 2007). Hence, a potential mitochondrial dysfunction could therefore be one possible explanation for the unsuccessful neuronal differentiation of the monolayer culture of *CLN3* mutant NPCs. The reason why the neurosphere culture could successfully promote

---

neuronal differentiation might be explained by the supporting environment that resides within the neurosphere niche. It is well known that neurospheres are composed of progenitor cells as well as finally differentiated cells including glia cells (Galli *et al.*, 2003). This unique composition of neurospheres creates a microenvironment that supports itself through release of intrinsic factors (Gritti *et al.*, 2002). This might have overcome mitochondrial dysfunction and therefore could have had a positive effect on the neuronal differentiation capacity. However, further investigations are required to address this question.

In contrast to *CLN3* mutant NPCs, immunostainings for the Golgi marker protein GM130, revealed a punctate, fragmented pattern in mature neurons. EM images confirmed a distended structure and multiple Golgi-associated vesicles were apparent. Fragmentation of the Golgi apparatus have also been reported for other neurodegenerative diseases such as Parkinson's disease (Fujita *et al.*, 2006), amyotrophic lateral sclerosis (Fujita *et al.*, 2000) and Alzheimer's disease (Baloyannis *et al.*, 2004). Moreover, Lemonnier and colleagues reported Golgi fragmentation that was revealed by EM imaging, in neurons derived from iPSCs that were generated from patients suffering from the lysosomal storage disorder mucopolysaccharidosis type IIIB (Lemonnier *et al.*, 2011). Apparently the Golgi apparatus undergoes fragmentation during apoptosis which is partly a result of caspase-mediated cleavage of several Golgi-associated proteins (Fan *et al.*, 2008). Interestingly, Walker and colleagues demonstrated that especially GM130 is rapidly diminished during Fas-mediated apoptosis which is associated with fragmentation of the Golgi apparatus (Walker *et al.*, 2004). The Golgi apparatus was as well reported to be involved in the axoplasmic flow of numerous endogenous proteins and exogenous macromolecules in neurons (Fan *et al.*, 2008). Therefore, it might not be surprising that neurodegenerative processes, demonstrating fragmentation of the Golgi apparatus, are associated with deficiencies in axonal transport (Fan *et al.*, 2008). Whether the apoptotic cascade is the underlying reason for the observed Golgi fragmentation in mature neurons derived from *CLN3* mutant NPCs will require further investigations. However, these results suggest a potential defect in axonal transport and membrane trafficking and is also consistent with at least partial localization of *CLN3* protein in Golgi membranes (Kremmidiotis *et al.*, 1999).

Since several groups reported that altered autophagy contributes to the course of disease in model systems for *CLN3* (Cao *et al.*, 2006), *CLN6* (Thelen *et al.*, 2012) and *CLN10* disease (Koike *et al.*, 2005), endosomes and lysosomes were investigated within the NPC and neuronal cultures. Immunostainings for the lysosomal marker protein LAMP-1 showed that

---

the overall distribution of positive vesicles was not altered in *CLN3* mutant NPC lines and Western blot analysis showed comparable protein content to control lines. The same was true for Western blot analysis of the early endosomal marker protein EEA-1. However, EM images revealed vacuoles within *CLN3* mutant NPCs that were not apparent in NPCs derived from controls. In contrast to the large, empty vacuoles found within the *CLN3* mutant iPSC lines, some vacuoles present in the NPC lines contained membrane-bound storage material that was often curvilinear. Although the most prominent profile of storage material in *CLN3* disease is a fingerprint profile, it has been reported that some cases show mixed profiles (Ju *et al.*, 2006). The profile of storage observed in EM images depends on the main component of stored material (Cotman *et al.*, 2012). Since the EM profile of the storage material was curvilinear, it is very likely that the storage did not exclusively consist of subunit c of the mitochondrial ATPase complex which could explain the lack of signal by immunofluorescence and the trend toward subunit c accumulation by Western blot that did not reach significance in NPC cultures. Other possible storage material could be saposins A and D (Cotman *et al.*, 2012). In addition, it is unknown whether a curvilinear profile of storage material precedes a fingerprint profile which would suggest a progression in storage material formation. Therefore, it was of main interest to address the question whether neurons derived from *CLN3* mutant NPCs would recapitulate the hallmark of JNCL which is an accumulation of subunit c of the mitochondrial ATPase complex that results in a fingerprint profile of stored material that is observed by EM imaging. LAMP-1 immunostainings in mature neurons derived from *CLN3* mutant NPCs revealed enlarged, aggregated vesicles that were mainly situated along the neurites. A similar phenotype was reported in cerebellar cells derived from *Cln3*<sup>Δex7/8</sup> knock-in mice. In this study, the authors demonstrated that the aggregated Lamp-1 positive vesicles contained storage material, namely subunit c of the mitochondrial ATPase complex (Cao *et al.*, 2011). This suggests that the enlargement of the LAMP-1 positive vesicles found in mature neurons might be due to storage material and might therefore reflect a key feature of the lysosomal storage disorder. Immunostainings for subunit c in neuronal cultures derived from control and mutant NPCs revealed abundant subunit c positive vesicles in neurons derived from *CLN3* mutant NPCs. In addition, EM images revealed vacuoles within the cytoplasm of the neurons that always contained storage material. Moreover, in some of these vacuoles the storage material showed not only a curvilinear but also a fingerprint-like profile. Thus, *CLN3* mutant neurons recapitulate the hallmark of JNCL. These results not only show a progression of the disease but also demonstrate the suitability of the disease model.

#### 4.1.2 Late infantile neuronal ceroid lipofuscinosis disease model

TPP1-deficient iPSCs showed no phenotypic alterations by immunofluorescence, EM imaging or Western blot analysis. However, since mutations within the TPP1 gene usually lead to a decrease in TPP1 enzyme activity, the question was if an enzyme activity assay might show genotype-specific alterations between the different iPSC lines. A robust read-out for drug screenings is essential to identify potential candidate drugs. The TPP1 enzyme activity assay is a very robust assay that is widely used in clinical screenings, since reduced enzyme activity is a diagnostic feature of LINCL (Sohar *et al.*, 2000, Lukacs *et al.*, 2003). The assay revealed a significant decrease in TPP1 enzyme activity in LINCL-derived iPSCs when compared to control and *CLN3* mutant iPSCs. These results demonstrate that this is a reliable assay that might be used as a read-out in order to identify drugs which potentially increase TPP1 enzyme activity. This is of great interest because several groups reported that an increase in TPP1 enzyme activity led to a milder course of disease in LINCL mouse models (Chang *et al.*, 2008; Sleat *et al.*, 2008) and a Dachshund model (Vuilleminot *et al.*, 2011). However, important features of iPSCs such as spontaneous differentiation or derivation of NPCs were not impaired by reduced TPP1 enzyme activity.

In contrast to control and *CLN3* mutant NPCs, TPP1-deficient NPCs and later on neurons revealed a disrupted and dilated ER morphology. This phenotype, related to TPP1 deficiency, has not been reported in the literature, so far. However, it is well known that the ER plays a key role in protein synthesis, folding and trafficking. It is also involved in lipid and steroid synthesis as well as in calcium homeostasis (Engin *et al.*, 2010). Therefore, stress that affects the ER, leads to an arrest in protein translation and direction of un- and misfolded proteins towards degradation. Prolonged ER stress can even lead to programmed cell death (Schroder, 2008). That this mechanism plays an important role in CLN8 and CLN1 disease was shown recently. It was reported that ER stress induces apoptosis and therefore neuronal death in mouse models for the CLN8 (Galizzi *et al.*, 2011) and CLN1 disease (Kim *et al.*, 2006). Moreover, it seems as if an accumulation of mutant protein within the ER might as well induce a stress response. In a study, Sasaki and colleagues examined anterior horn neurons from patients suffering from amyotrophic lateral sclerosis using immunohistochemistry and electron microscopy (Sasaki, 2010). EM images of motor neurons from patients with a defect within the superoxide dismutase 1 (SOD-1) gene, revealed a dilated ER that showed an accumulation of amorphous electron-dense material. The author suggested that this material is mutant superoxide dismutase 1 protein and that the accumulation induced ER stress which



---

was demonstrated by a dilated structure in EM images. Since the mutations within the TPP1 gene, that are reported in this thesis, lead to an aberrant splicing and a nonsense mutation, it might be possible that this leads to an accumulation of mutant protein within the ER and that the dilated structure of this organelle, revealed by EM imaging, is a result of possible stress that was induced to the ER. These findings suggest that ER stress might as well play an important role in LINCL.

EM images of TPP1-deficient neurons revealed that some mitochondria showed a vacuolated morphology and the Golgi apparatus was, similar to the Golgi apparatus found in *CLN3* mutant neurons, distended. It appears that alterations in Golgi structure and mitochondria, which often involve organelle dysfunction, are a common feature of neurodegenerative diseases such as amyotrophic lateral sclerosis, Alzheimer's and Parkinson's disease (for reviews refer to Fan *et al.*, 2008; Martin, 2012). These findings suggest that altered mitochondrial and Golgi morphologies might rather be a consequence instead of a cause of NCL.

Similar to JNCL-derived NPCs, TPP1-deficient NPCs showed vacuoles within the cytoplasm by EM imaging. However, in contrast to the findings in JNCL-derived NPCs, vacuoles found within the TPP1-deficient NPC lines were largely free of apparent storage material. That seems odd, because TPP1 deficiency leads to an earlier age of onset in patients than mutations within the *CLN3* gene. A possible reason for the lack of storage material within the TPP1-deficient lines, in comparison to the *CLN3* mutant lines, might be that vacuoles were already apparent within the *CLN3* mutant iPSC lines which might have led to an earlier accumulation of storage material within the NPC lines as compared to the TPP1-deficient lines. In accordance with the lack of apparent storage material by EM, was the fact that subunit c signal was not observed by immunofluorescence. These findings led to the question whether TPP1-deficient neurons would show a progression in disease similar to that observed in the JNCL culture system. TPP1-deficient neurons showed a scattered pattern of LAMP-1 positive vesicles in mature neurons and Western blotting revealed a trend towards reduced LAMP-1 protein levels, whereas protein levels for the early endosomal marker protein EEA-1 were not altered. These results suggest a dysfunction within the lysosomal pathway. The TPP1 protein is a lysosomal enzyme and deficiency in TPP1 might lead to an impaired formation of lysosomes and thus to a disruption of lysosomal homeostasis. Wei and colleagues could demonstrate that a chemical disruption of lysosomal homeostasis induced ER stress, suggesting a cross-talk between the lysosomes and the ER (Wei *et al.*, 2008). These findings underline a possible link between the dilated ER, observed in EM images of TPP1-deficient

---

NPCs and neurons, and the scattered lysosomal pattern in mature neurons derived from TPP1-deficient NPCs. In addition, immunofluorescence revealed a moderate staining for subunit c in neurons derived from TPP1-deficient NPCs. The fact that the subunit c staining was less abundant in TPP1-deficient neurons when compared to *CLN3* mutant neurons is in accordance with the fact that storage material found in tissue samples from LINCL patients may contain to less extent subunit c of the mitochondrial ATPase complex, but more saposins A and D, than storage material found in tissue samples from JNCL patients (Cotman *et al.*, 2012). In accordance with these reports are the findings by EM imaging that showed vacuoles containing storage material which was exclusively curvilinear in TPP1-deficient neurons. These results demonstrate that the disease model for LINCL also showed a progression of the disease during the course of differentiation into mature neurons.

#### **4.2 The established disease models represent early phenotypes**

Studies on neurodegenerative disorders usually involve transgenic animal systems or human tissue that was obtained post-mortem. The advantage of the model system established during this thesis is that fibroblasts are available from live patients. Moreover, the derived iPSCs not only allow for studying NPCs and neuronal subtypes which are usually inaccessible but they also allow to study the earliest events in neurodegeneration. Tissue that was obtained post-mortem usually shows the end stage of a disease. iPSC-derived NPCs and neurons, however, represent a cell system that might show the features of neurodegeneration over time. Discovering the earliest events underlying the disease is very important for future drug discoveries. The disease models for JNCL and LINCL were representing early phenotypes that showed a progression during the course of neuronal differentiation. But, although important cell organelles such as mitochondria, ER and Golgi were affected, neurodegeneration such as apoptotic neurons, were not observed. Therefore, in order to fully recapitulate the phenotypes associated with LINCL and JNCL, it should be considered to age neurons *in vitro*. Neurons studied during this work were differentiated for two weeks. A longer differentiation period such as six to eight weeks might show a more advanced phenotype especially in terms of storage. In addition, agents that induce oxidative stress to the cell such as Rotenone or hydrogen peroxide might not only stress the cells, which would lead to an artificial aging process, but it would also give insights into the question whether mutant neurons are more susceptible to cellular stressors than control-derived neurons.

The disease models of JNCL and LINCL showed a common mitochondrial phenotype consistent with those present in other NCL model systems. Interestingly, impaired mitochondrial function is often associated with neurodegeneration (reviewed by Correia *et al.*, 2012). On the other hand mutations in the lysosomal protein PARK9 lead to an early-onset of Parkinsonism, the Kufor-Rakeb syndrome (Usenovic *et al.*, 2012). Interestingly, *PARK9* is also known as ATP13A2 which was very recently referred to as CLN12 (refer to Table 1.1). This link between the NCLs and other neurodegenerative disorders might render results obtained from this disease model transferable to other diseases.

The lack of obvious neurodegeneration, characterized by neuronal death in neuronal cultures derived from mutant NPCs, suggests that other factors might as well contribute to neuronal death in LINCL and JNCL. Studies in sheep affected by the CLN6 disease showed glial activation which preceded neurodegeneration (Oswald *et al.*, 2005). Pontikis and colleagues reported a localized astrocytosis in the *CLN3*<sup>-/-</sup> knock-out mouse model (Pontikis *et al.*, 2005), providing further evidence for a potential participation of glia cells in the course of NCL disease. Preliminary data on glial cells in neuronal cultures derived from JNCL and LINCL patients, showed an altered morphology of GFAP-positive astrocytes. Moreover, an accumulation of large LAMP-1-positive vesicles within these cells was observed, suggesting an alteration within the autophagy pathway. However, to what extent glia cells might have an influence on the disease model systems for LINCL and JNCL set forth in this thesis, remains to be elucidated.

However, the patient-derived iPSCs and their derivatives recapitulated most of the common features associated with NCLs that are described in the literature. Thus, patient-derived iPSCs and their derivatives are suitable for disease modeling of NCLs and therefore represent a valuable model system for further research.

## 5 Summary

The discovery of resetting human somatic cells via introduction of four transcription factors into an embryonic stem cell-like state that enables the generation of any cell type of the human body has revolutionized the field of medical science. The generation of patient-derived iPSCs and the subsequent differentiation into the cells of interest has been, nowadays, widely used as model system for various inherited diseases.

The aim of this thesis was to generate iPSCs and to subsequently derive NPCs which can be differentiated into neurons in order to model the two most common forms of the NCLs: LINCL which is caused by mutations within the *TPP1* gene, encoding a lysosomal enzyme, and JNCL which is caused by mutations within the *CLN3* gene, affecting a lysosomal transmembrane protein.

It was shown that patient-derived fibroblasts can be successfully reprogrammed into iPSCs by using retroviral vectors that introduced the four transcription factors *POU5F1*, *SOX2*, *KLF4* and *MYC*. The generated iPSCs were subsequently differentiated into expandable NPCs and finally into mature neurons.

Phenotype analysis during the different stages, namely pluripotent iPSCs, multipotent NPCs and finally differentiated neurons, revealed a genotype-specific progression of the disease. The earliest events were observed in organelle disruption such as mitochondria, Golgi and ER which preceded the accumulation of subunit c of the mitochondrial ATPase complex that was only apparent in neurons. However, none of these events led to neurodegeneration *in vitro*.

The established disease models recapitulate phenotypes reported in other NCL disease models such as mouse, dog and sheep model systems. More importantly, the hallmark of the NCLs, accumulation of subunit c in neurons, could be reproduced during the course of disease modeling which demonstrates the suitability of the established system. Moreover, the derived expandable NPC populations can be used for further applications in drug screenings. Their robust phenotypes such as low levels of *TPP1* activity in LINCL patient-derived NPCs or cytoplasmic vacuoles, containing storage material, observed in *CLN3* mutant NPCs, should serve as possible phenotypic read-outs.

---

## 6 References

- Aasen, T., Raya, A., Barrero, M. J., Garreta, E., Consiglio, A., Gonzalez, F., Vassena, R., Bilic, J., Pekarik, V., Tiscornia, G., Edel, M., Boue, S. and Izpisua Belmonte, J. C. (2008). Efficient and rapid generation of induced pluripotent stem cells from human keratinocytes. *Nat Biotechnol* **26**(11): 1276-1284.
- An, M. C., Zhang, N., Scott, G., Montoro, D., Wittkop, T., Mooney, S., Melov, S. and Ellerby, L. M. (2012). Genetic Correction of Huntington's Disease Phenotypes in Induced Pluripotent Stem Cells. *Cell Stem Cell*.
- Awano, T., Katz, M. L., O'Brien, D. P., Sohar, I., Lobel, P., Coates, J. R., Khan, S., Johnson, G. C., Giger, U. and Johnson, G. S. (2006). A frame shift mutation in canine TPP1 (the ortholog of human CLN2) in a juvenile Dachshund with neuronal ceroid lipofuscinosis. *Mol Genet Metab* **89**(3): 254-260.
- Baloyannis, S. J., Costa, V. and Michmizos, D. (2004). Mitochondrial alterations in Alzheimer's disease. *Am J Alzheimers Dis Other Demen* **19**(2): 89-93.
- Bernardini, F. and Warburton, M. J. (2001). The substrate range of tripeptidyl-peptidase I. *Eur J Paediatr Neurol* **5 Suppl A**: 69-72.
- Bras, J., Verloes, A., Schneider, S. A., Mole, S. E. and Guerreiro, R. J. (2012). Mutation of the parkinsonism gene ATP13A2 causes neuronal ceroid-lipofuscinosis. *Hum Mol Genet* **21**(12): 2646-2650.
- Brook, F. A. and Gardner, R. L. (1997). The origin and efficient derivation of embryonic stem cells in the mouse. *Proc Natl Acad Sci U S A* **94**(11): 5709-5712.
- Brown, M. E., Rondon, E., Rajesh, D., Mack, A., Lewis, R., Feng, X., Zitur, L. J., Learish, R. D. and Nuwaysir, E. F. (2010). Derivation of induced pluripotent stem cells from human peripheral blood T lymphocytes. *PLoS One* **5**(6): e11373.
- Cao, Y., Espinola, J. A., Fossale, E., Massey, A. C., Cuervo, A. M., MacDonald, M. E. and Cotman, S. L. (2006). Autophagy is disrupted in a knock-in mouse model of juvenile neuronal ceroid lipofuscinosis. *J Biol Chem* **281**(29): 20483-20493.
- Cao, Y., Staropoli, J. F., Biswas, S., Espinola, J. A., MacDonald, M. E., Lee, J. M. and Cotman, S. L. (2011). Distinct early molecular responses to mutations causing vLINCL and JNCL presage ATP synthase subunit C accumulation in cerebellar cells. *PLoS One* **6**(2): e17118.
- Chambers, S. M., Fasano, C. A., Papapetrou, E. P., Tomishima, M., Sadelain, M. and Studer, L. (2009). Highly efficient neural conversion of human ES and iPS cells by dual inhibition of SMAD signaling. *Nat Biotechnol* **27**(3): 275-280.
- Chambers, S. M., Mica, Y., Studer, L. and Tomishima, M. J. (2011). Converting human pluripotent stem cells to neural tissue and neurons to model neurodegeneration. *Methods Mol Biol* **793**: 87-97.

- Chang, J. W., Choi, H., Cotman, S. L. and Jung, Y. K. (2011).** Lithium rescues the impaired autophagy process in CbCln3(Deltaex7/8/Deltaex7/8) cerebellar cells and reduces neuronal vulnerability to cell death via IMPase inhibition. *J Neurochem* **116**(4): 659-668.
- Chang, M., Cooper, J. D., Sleat, D. E., Cheng, S. H., Dodge, J. C., Passini, M. A., Lobel, P. and Davidson, B. L. (2008).** Intraventricular enzyme replacement improves disease phenotypes in a mouse model of late infantile neuronal ceroid lipofuscinosis. *Mol Ther* **16**(4): 649-656.
- Chen, R., Fearnley, I. M., Palmer, D. N. and Walker, J. E. (2004).** Lysine 43 is trimethylated in subunit C from bovine mitochondrial ATP synthase and in storage bodies associated with batten disease. *J Biol Chem* **279**(21): 21883-21887.
- Cho, Y. M., Kwon, S., Pak, Y. K., Seol, H. W., Choi, Y. M., Park do, J., Park, K. S. and Lee, H. K. (2006).** Dynamic changes in mitochondrial biogenesis and antioxidant enzymes during the spontaneous differentiation of human embryonic stem cells. *Biochem Biophys Res Commun* **348**(4): 1472-1478.
- Codlin, S. and Mole, S. E. (2009).** S. pombe btn1, the orthologue of the Batten disease gene CLN3, is required for vacuole protein sorting of Cpy1p and Golgi exit of Vps10p. *J Cell Sci* **122**(Pt 8): 1163-1173.
- Cooper, O., Hargus, G., Deleidi, M., Blak, A., Osborn, T., Marlow, E., Lee, K., Levy, A., Perez-Torres, E., Yow, A. and Isacson, O. (2010).** Differentiation of human ES and Parkinson's disease iPS cells into ventral midbrain dopaminergic neurons requires a high activity form of SHH, FGF8a and specific regionalization by retinoic acid. *Mol Cell Neurosci* **45**(3): 258-266.
- Correia, S. C., Santos, R. X., Perry, G., Zhu, X., Moreira, P. I. and Smith, M. A. (2012).** Mitochondrial importance in Alzheimer's, Huntington's and Parkinson's diseases. *Adv Exp Med Biol* **724**: 205-221.
- Cotman, S. L. and Staropoli, J. F. (2012).** The juvenile Batten disease protein, CLN3, and its role in regulating anterograde and retrograde post-Golgi trafficking. *Clin Lipidol* **7**(1): 79-91.
- Cotman, S. L., Vrbanac, V., Lebel, L. A., Lee, R. L., Johnson, K. A., Donahue, L. R., Teed, A. M., Antonellis, K., Bronson, R. T., Lerner, T. J. and MacDonald, M. E. (2002).** Cln3(Deltaex7/8) knock-in mice with the common JNCL mutation exhibit progressive neurologic disease that begins before birth. *Hum Mol Genet* **11**(22): 2709-2721.
- Dimos, J. T., Rodolfa, K. T., Niakan, K. K., Weisenthal, L. M., Mitsumoto, H., Chung, W., Croft, G. F., Saphier, G., Leibel, R., Golland, R., Wichterle, H., Henderson, C. E. and Eggan, K. (2008).** Induced pluripotent stem cells generated from patients with ALS can be differentiated into motor neurons. *Science* **321**(5893): 1218-1221.
- Ding, S. L., Tecedor, L., Stein, C. S. and Davidson, B. L. (2011).** A knock-in reporter mouse model for Batten disease reveals predominant expression of Cln3 in visual, limbic and subcortical motor structures. *Neurobiol Dis* **41**(2): 237-248.

---

**Ebert, A. D., Yu, J., Rose, F. F., Jr., Mattis, V. B., Lorson, C. L., Thomson, J. A. and Svendsen, C. N. (2009).** Induced pluripotent stem cells from a spinal muscular atrophy patient. *Nature* **457**(7227): 277-280.

**Eiberg, H., Gardiner, R. M. and Mohr, J. (1989).** Batten disease (Spielmeyer-Sjogren disease) and haptoglobins (HP): indication of linkage and assignment to chr. 16. *Clin Genet* **36**(4): 217-218.

**Eiselleova, L., Peterkova, I., Neradil, J., Slaninova, I., Hampl, A. and Dvorak, P. (2008).** Comparative study of mouse and human feeder cells for human embryonic stem cells. *Int J Dev Biol* **52**(4): 353-363.

**Elkabetz, Y., Panagiotakos, G., Al Shamy, G., Socci, N. D., Tabar, V. and Studer, L. (2008a).** Human ES cell-derived neural rosettes reveal a functionally distinct early neural stem cell stage. *Genes Dev* **22**(2): 152-165.

**Elkabetz, Y. and Studer, L. (2008b).** Human ESC-derived neural rosettes and neural stem cell progression. *Cold Spring Harb Symp Quant Biol* **73**: 377-387.

**Engin, F. and Hotamisligil, G. S. (2010).** Restoring endoplasmic reticulum function by chemical chaperones: an emerging therapeutic approach for metabolic diseases. *Diabetes Obes Metab* **12 Suppl 2**: 108-115.

**Eskelinen, E. L., Tanaka, Y. and Saftig, P. (2003).** At the acidic edge: emerging functions for lysosomal membrane proteins. *Trends Cell Biol* **13**(3): 137-145.

**Ezaki, J., Takeda-Ezaki, M., Oda, K. and Kominami, E. (2000).** Characterization of endopeptidase activity of tripeptidyl peptidase-I/CLN2 protein which is deficient in classical late infantile neuronal ceroid lipofuscinosis. *Biochem Biophys Res Commun* **268**(3): 904-908.

**Ezaki, J., Tanida, I., Kanehagi, N. and Kominami, E. (1999).** A lysosomal proteinase, the late infantile neuronal ceroid lipofuscinosis gene (CLN2) product, is essential for degradation of a hydrophobic protein, the subunit c of ATP synthase. *J Neurochem* **72**(6): 2573-2582.

**Facucho-Oliveira, J. M., Alderson, J., Spikings, E. C., Egginton, S. and St John, J. C. (2007).** Mitochondrial DNA replication during differentiation of murine embryonic stem cells. *J Cell Sci* **120**(Pt 22): 4025-4034.

**Falk, A., Koch, P., Kesavan, J., Takashima, Y., Ladewig, J., Alexander, M., Wiskow, O., Tailor, J., Trotter, M., Pollard, S., Smith, A. and Brustle, O. (2012).** Capture of neuroepithelial-like stem cells from pluripotent stem cells provides a versatile system for in vitro production of human neurons. *PLoS One* **7**(1): e29597.

**Fan, J., Hu, Z., Zeng, L., Lu, W., Tang, X., Zhang, J. and Li, T. (2008).** Golgi apparatus and neurodegenerative diseases. *Int J Dev Neurosci* **26**(6): 523-534.

**Fossale, E., Wolf, P., Espinola, J. A., Lubicz-Nawrocka, T., Teed, A. M., Gao, H., Rigamonti, D., Cattaneo, E., MacDonald, M. E. and Cotman, S. L. (2004).** Membrane trafficking and mitochondrial abnormalities precede subunit c deposition in a cerebellar cell model of juvenile neuronal ceroid lipofuscinosis. *BMC Neurosci* **5**: 57.

- Fujimoto, Y., Abematsu, M., Falk, A., Tsujimura, K., Sanosaka, T., Juliandi, B., Semi, K., Namihira, M., Komiya, S., Smith, A. and Nakashima, K. (2012).** Treatment of a mouse model of spinal cord injury by transplantation of human induced pluripotent stem cell-derived long-term self-renewing neuroepithelial-like stem cells. *Stem Cells* **30**(6): 1163-1173.
- Fujita, Y., Ohama, E., Takatama, M., Al-Sarraj, S. and Okamoto, K. (2006).** Fragmentation of Golgi apparatus of nigral neurons with alpha-synuclein-positive inclusions in patients with Parkinson's disease. *Acta Neuropathol* **112**(3): 261-265.
- Fujita, Y., Okamoto, K., Sakurai, A., Gonatas, N. K. and Hirano, A. (2000).** Fragmentation of the Golgi apparatus of the anterior horn cells in patients with familial amyotrophic lateral sclerosis with SOD1 mutations and posterior column involvement. *J Neurol Sci* **174**(2): 137-140.
- Galizzi, G., Russo, D., Deidda, I., Cascio, C., Passantino, R., Guarneri, R., Bigini, P., Mennini, T., Drago, G. and Guarneri, P. (2011).** Different early ER-stress responses in the CLN8(mnd) mouse model of neuronal ceroid lipofuscinosis. *Neurosci Lett* **488**(3): 258-262.
- Galli, R., Gritti, A., Bonfanti, L. and Vescovi, A. L. (2003).** Neural stem cells: an overview. *Circ Res* **92**(6): 598-608.
- Gaspard, N. and Vanderhaeghen, P. (2010).** Mechanisms of neural specification from embryonic stem cells. *Curr Opin Neurobiol* **20**(1): 37-43.
- Gavrieli, Y., Sherman, Y. and Ben-Sasson, S. A. (1992).** Identification of programmed cell death in situ via specific labeling of nuclear DNA fragmentation. *J Cell Biol* **119**(3): 493-501.
- Getty, A. L. and Pearce, D. A. (2011).** Interactions of the proteins of neuronal ceroid lipofuscinosis: clues to function. *Cell Mol Life Sci* **68**(3): 453-474.
- Golabek, A. A. and Kida, E. (2006).** Tripeptidyl-peptidase I in health and disease. *Biol Chem* **387**(8): 1091-1099.
- Gomi, M., Takagi, Y., Morizane, A., Doi, D., Nishimura, M., Miyamoto, S. and Takahashi, J. (2012).** Functional recovery of the murine brain ischemia model using human induced pluripotent stem cell-derived telencephalic progenitors. *Brain Res* **1459**: 52-60.
- Gorczyca, W., Gong, J. and Darzynkiewicz, Z. (1993).** Detection of DNA strand breaks in individual apoptotic cells by the in situ terminal deoxynucleotidyl transferase and nick translation assays. *Cancer Res* **53**(8): 1945-1951.
- Greene, N. D., Bernard, D. L., Taschner, P. E., Lake, B. D., de Vos, N., Breuning, M. H., Gardiner, R. M., Mole, S. E., Nussbaum, R. L. and Mitchison, H. M. (1999).** A murine model for juvenile NCL: gene targeting of mouse Cln3. *Mol Genet Metab* **66**(4): 309-313.
- Gritti, A., Vescovi, A. L. and Galli, R. (2002).** Adult neural stem cells: plasticity and developmental potential. *J Physiol Paris* **96**(1-2): 81-90.



---

**Haddad, S. E., Khoury, M., Daoud, M., Kantar, R., Ghanem, S., Mousallem, T., Alzate, O., Meyer, B. and Boustany, R. M. (2012).** CLN9, CLN5, CLN8 proteins and ceramide synthases. *13th International Conference on Neuronal Ceroid Lipofuscinoses*.

**Haltia, M. (2003).** The neuronal ceroid-lipofuscinoses. *J Neuropathol Exp Neurol* **62**(1): 1-13.

**Hargus, G., Cooper, O., Deleidi, M., Levy, A., Lee, K., Marlow, E., Yow, A., Soldner, F., Hockemeyer, D., Hallett, P. J., Osborn, T., Jaenisch, R. and Isacson, O. (2010).** Differentiated Parkinson patient-derived induced pluripotent stem cells grow in the adult rodent brain and reduce motor asymmetry in Parkinsonian rats. *Proc Natl Acad Sci U S A* **107**(36): 15921-15926.

**Hotta, A. and Ellis, J. (2008).** Retroviral vector silencing during iPS cell induction: an epigenetic beacon that signals distinct pluripotent states. *J Cell Biochem* **105**(4): 940-948.

**Howden, S. E., Gore, A., Li, Z., Fung, H. L., Nisler, B. S., Nie, J., Chen, G., McIntosh, B. E., Gulbranson, D. R., Diol, N. R., Taapken, S. M., Vereide, D. T., Montgomery, K. D., Zhang, K., Gamm, D. M. and Thomson, J. A. (2011).** Genetic correction and analysis of induced pluripotent stem cells from a patient with gyrate atrophy. *Proc Natl Acad Sci U S A* **108**(16): 6537-6542.

**Jalanko, A. and Braulke, T. (2009).** Neuronal ceroid lipofuscinoses. *Biochim Biophys Acta* **1793**(4): 697-709.

**Jin, Z. B., Okamoto, S., Osakada, F., Homma, K., Assawachananont, J., Hirami, Y., Iwata, T. and Takahashi, M. (2011).** Modeling retinal degeneration using patient-specific induced pluripotent stem cells. *PLoS One* **6**(2): e17084.

**Ju, W., Wronska, A., Moroziewicz, D. N., Zhong, R., Wisniewski, N., Jurkiewicz, A., Fiory, M., Wisniewski, K. E., Johnston, L., Brown, W. T. and Zhong, N. (2006).** Genotype-phenotype analyses of classic neuronal ceroid lipofuscinosis (NCLs): genetic predictions from clinical and pathological findings. *Beijing Da Xue Xue Bao* **38**(1): 41-48.

**Kama, R., Kanneganti, V., Ungermann, C. and Gerst, J. E. (2011).** The yeast Batten disease orthologue Btn1 controls endosome-Golgi retrograde transport via SNARE assembly. *J Cell Biol* **195**(2): 203-215.

**Karumbayaram, S., Novitch, B. G., Patterson, M., Umbach, J. A., Richter, L., Lindgren, A., Conway, A. E., Clark, A. T., Goldman, S. A., Plath, K., Wiedau-Pazos, M., Kornblum, H. I. and Lowry, W. E. (2009).** Directed differentiation of human-induced pluripotent stem cells generates active motor neurons. *Stem Cells* **27**(4): 806-811.

**Katz, M. L., Johnson, G. S., Tullis, G. E. and Lei, B. (2008).** Phenotypic characterization of a mouse model of juvenile neuronal ceroid lipofuscinosis. *Neurobiol Dis* **29**(2): 242-253.

**Kazuki, Y., Hiratsuka, M., Takiguchi, M., Osaki, M., Kajitani, N., Hoshiya, H., Hiramatsu, K., Yoshino, T., Kazuki, K., Ishihara, C., Takehara, S., Higaki, K., Nakagawa, M., Takahashi, K., Yamanaka, S. and Oshimura, M. (2010).** Complete genetic correction of ips cells from Duchenne muscular dystrophy. *Mol Ther* **18**(2): 386-393.

- 
- Kim, D., Kim, C. H., Moon, J. I., Chung, Y. G., Chang, M. Y., Han, B. S., Ko, S., Yang, E., Cha, K. Y., Lanza, R. and Kim, K. S. (2009).** Generation of human induced pluripotent stem cells by direct delivery of reprogramming proteins. *Cell Stem Cell* **4**(6): 472-476.
- Kim, J. B., Greber, B., Arauzo-Bravo, M. J., Meyer, J., Park, K. I., Zaehres, H. and Scholer, H. R. (2009).** Direct reprogramming of human neural stem cells by OCT4. *Nature* **461**(7264): 649-643.
- Kim, S. J., Zhang, Z., Hitomi, E., Lee, Y. C. and Mukherjee, A. B. (2006).** Endoplasmic reticulum stress-induced caspase-4 activation mediates apoptosis and neurodegeneration in INCL. *Hum Mol Genet* **15**(11): 1826-1834.
- Kitzmuller, C., Haines, R. L., Codlin, S., Cutler, D. F. and Mole, S. E. (2008).** A function retained by the common mutant CLN3 protein is responsible for the late onset of juvenile neuronal ceroid lipofuscinosis. *Hum Mol Genet* **17**(2): 303-312.
- Koike, M., Shibata, M., Waguri, S., Yoshimura, K., Tanida, I., Kominami, E., Gotow, T., Peters, C., von Figura, K., Mizushima, N., Saftig, P. and Uchiyama, Y. (2005).** Participation of autophagy in storage of lysosomes in neurons from mouse models of neuronal ceroid-lipofuscinoses (Batten disease). *Am J Pathol* **167**(6): 1713-1728.
- Kousi, M., Lehesjoki, A. E. and Mole, S. E. (2012).** Update of the mutation spectrum and clinical correlations of over 360 mutations in eight genes that underlie the neuronal ceroid lipofuscinoses. *Hum Mutat* **33**(1): 42-63.
- Kremmidiotis, G., Lensink, I. L., Bilton, R. L., Woollatt, E., Chataway, T. K., Sutherland, G. R. and Callen, D. F. (1999).** The Batten disease gene product (CLN3p) is a Golgi integral membrane protein. *Hum Mol Genet* **8**(3): 523-531.
- Lemonnier, T., Blanchard, S., Toli, D., Roy, E., Bigou, S., Froissart, R., Rouvet, I., Vitry, S., Heard, J. M. and Bohl, D. (2011).** Modeling neuronal defects associated with a lysosomal disorder using patient-derived induced pluripotent stem cells. *Hum Mol Genet* **20**(18): 3653-3666.
- Lie, K. H., Chung, H. C. and Sidhu, K. S. (2012).** Derivation, propagation, and characterization of neuroprogenitors from pluripotent stem cells (hESCs and hiPSCs). *Methods Mol Biol* **873**: 237-246.
- Lin, L., Sohar, I., Lackland, H. and Lobel, P. (2001).** The human CLN2 protein/tripeptidyl-peptidase I is a serine protease that autoactivates at acidic pH. *J Biol Chem* **276**(3): 2249-2255.
- Liu, C. G., Sleat, D. E., Donnelly, R. J. and Lobel, P. (1998).** Structural organization and sequence of CLN2, the defective gene in classical late infantile neuronal ceroid lipofuscinosis. *Genomics* **50**(2): 206-212.
- Lojewski, X. (2009).** Entwicklung und Charakterisierung einer nischenfreien Kultur adulter humaner neuraler Stammzellen. *Diploma thesis*.

- 
- Lukacs, Z., Santavuori, P., Keil, A., Steinfeld, R. and Kohlschutter, A. (2003).** Rapid and simple assay for the determination of tripeptidyl peptidase and palmitoyl protein thioesterase activities in dried blood spots. *Clin Chem* **49**(3): 509-511.
- Macauley, S. L., Pekny, M. and Sands, M. S. (2011).** The role of attenuated astrocyte activation in infantile neuronal ceroid lipofuscinosis. *J Neurosci* **31**(43): 15575-15585.
- Maherali, N., Sridharan, R., Xie, W., Utikal, J., Eminli, S., Arnold, K., Stadtfeld, M., Yachechko, R., Tchieu, J., Jaenisch, R., Plath, K. and Hochedlinger, K. (2007).** Directly reprogrammed fibroblasts show global epigenetic remodeling and widespread tissue contribution. *Cell Stem Cell* **1**(1): 55-70.
- Mao, Q., Foster, B. J., Xia, H. and Davidson, B. L. (2003).** Membrane topology of CLN3, the protein underlying Batten disease. *FEBS Lett* **541**(1-3): 40-46.
- March, P. A., Wurzelmann, S. and Walkley, S. U. (1995).** Morphological alterations in neocortical and cerebellar GABAergic neurons in a canine model of juvenile Batten disease. *Am J Med Genet* **57**(2): 204-212.
- Marchetto, M. C., Carromeu, C., Acab, A., Yu, D., Yeo, G. W., Mu, Y., Chen, G., Gage, F. H. and Muotri, A. R. (2010).** A model for neural development and treatment of Rett syndrome using human induced pluripotent stem cells. *Cell* **143**(4): 527-539.
- Martin, L. J. (2012).** Biology of mitochondria in neurodegenerative diseases. *Prog Mol Biol Transl Sci* **107**: 355-415.
- Mazzulli, J. R., Xu, Y. H., Sun, Y., Knight, A. L., McLean, P. J., Caldwell, G. A., Sidransky, E., Grabowski, G. A. and Krainc, D. (2011).** Gaucher disease glucocerebrosidase and alpha-synuclein form a bidirectional pathogenic loop in synucleinopathies. *Cell* **146**(1): 37-52.
- Nugent, T., Mole, S. E. and Jones, D. T. (2008).** The transmembrane topology of Batten disease protein CLN3 determined by consensus computational prediction constrained by experimental data. *FEBS Lett* **582**(7): 1019-1024.
- O'Connor, M. D., Kardel, M. D., Iosifina, I., Youssef, D., Lu, M., Li, M. M., Vercauteren, S., Nagy, A. and Eaves, C. J. (2008).** Alkaline phosphatase-positive colony formation is a sensitive, specific, and quantitative indicator of undifferentiated human embryonic stem cells. *Stem Cells* **26**(5): 1109-1116.
- Okita, K., Nakagawa, M., Hyenjong, H., Ichisaka, T. and Yamanaka, S. (2008).** Generation of mouse induced pluripotent stem cells without viral vectors. *Science* **322**(5903): 949-953.
- Oswald, M. J., Palmer, D. N., Kay, G. W., Shemilt, S. J., Rezaie, P. and Cooper, J. D. (2005).** Glial activation spreads from specific cerebral foci and precedes neurodegeneration in presymptomatic ovine neuronal ceroid lipofuscinosis (CLN6). *Neurobiol Dis* **20**(1): 49-63.

- 
- Padilla-Lopez, S., Langager, D., Chan, C. H. and Pearce, D. A. (2012).** BTN1, the *Saccharomyces cerevisiae* homolog to the human Batten disease gene, is involved in phospholipid distribution. *Dis Model Mech* **5**(2): 191-199.
- Page, A. E., Fuller, K., Chambers, T. J. and Warburton, M. J. (1993).** Purification and characterization of a tripeptidyl peptidase I from human osteoclastomas: evidence for its role in bone resorption. *Arch Biochem Biophys* **306**(2): 354-359.
- Palmer, D. N., Fearnley, I. M., Walker, J. E., Hall, N. A., Lake, B. D., Wolfe, L. S., Haltia, M., Martinus, R. D. and Jolly, R. D. (1992).** Mitochondrial ATP synthase subunit c storage in the ceroid-lipofuscinoses (Batten disease). *Am J Med Genet* **42**(4): 561-567.
- Park, I. H., Arora, N., Huo, H., Maherali, N., Ahfeldt, T., Shimamura, A., Lensch, M. W., Cowan, C., Hochedlinger, K. and Daley, G. Q. (2008).** Disease-specific induced pluripotent stem cells. *Cell* **134**(5): 877-886.
- Pearce, D. A., Ferea, T., Nosel, S. A., Das, B. and Sherman, F. (1999).** Action of BTN1, the yeast orthologue of the gene mutated in Batten disease. *Nat Genet* **22**(1): 55-58.
- Pezzini, F., Gismondi, F., Tessa, A., Tonin, P., Carrozzo, R., Mole, S. E., Santorelli, F. M. and Simonati, A. (2011).** Involvement of the mitochondrial compartment in human NCL fibroblasts. *Biochem Biophys Res Commun* **416**(1-2): 159-164.
- Pontikis, C. C., Cotman, S. L., MacDonald, M. E. and Cooper, J. D. (2005).** Thalamocortical neuron loss and localized astrocytosis in the *Cln3Deltaex7/8* knock-in mouse model of Batten disease. *Neurobiol Dis* **20**(3): 823-836.
- Prigione, A. and Adjaye, J. (2010a).** Modulation of mitochondrial biogenesis and bioenergetic metabolism upon in vitro and in vivo differentiation of human ES and iPS cells. *Int J Dev Biol* **54**(11-12): 1729-1741.
- Prigione, A., Fauler, B., Lurz, R., Lehrach, H. and Adjaye, J. (2010b).** The senescence-related mitochondrial/oxidative stress pathway is repressed in human induced pluripotent stem cells. *Stem Cells* **28**(4): 721-733.
- Rapola, J. (1993).** Neuronal ceroid-lipofuscinoses in childhood. *Perspect Pediatr Pathol* **17**: 7-44.
- Raya, A., Rodriguez-Piza, I., Guenechea, G., Vassena, R., Navarro, S., Barrero, M. J., Consiglio, A., Castella, M., Rio, P., Sleep, E., Gonzalez, F., Tiscornia, G., Garreta, E., Aasen, T., Veiga, A., Verma, I. M., Surralles, J., Bueren, J. and Izpisua Belmonte, J. C. (2009).** Disease-corrected haematopoietic progenitors from Fanconi anaemia induced pluripotent stem cells. *Nature* **460**(7251): 53-59.
- Sanders, D. N., Farias, F. H., Johnson, G. S., Chiang, V., Cook, J. R., O'Brien, D. P., Hofmann, S. L., Lu, J. Y. and Katz, M. L. (2010).** A mutation in canine PPT1 causes early onset neuronal ceroid lipofuscinosis in a Dachshund. *Mol Genet Metab* **100**(4): 349-356.
- Santavuori, P. (1988).** Neuronal ceroid-lipofuscinoses in childhood. *Brain Dev* **10**(2): 80-83.

- Sasaki, S. (2010).** Endoplasmic reticulum stress in motor neurons of the spinal cord in sporadic amyotrophic lateral sclerosis. *J Neuropathol Exp Neurol* **69**(4): 346-355.
- Schneider, H. C., Berthold, J., Bauer, M. F., Dietmeier, K., Guiard, B., Brunner, M. and Neupert, W. (1994).** Mitochondrial Hsp70/MIM44 complex facilitates protein import. *Nature* **371**(6500): 768-774.
- Schroder, M. (2008).** Endoplasmic reticulum stress responses. *Cell Mol Life Sci* **65**(6): 862-894.
- Schulz, A., Dhar, S., Rylova, S., Dbaiibo, G., Alroy, J., Hagel, C., Artacho, I., Kohlschutter, A., Lin, S. and Boustany, R. M. (2004).** Impaired cell adhesion and apoptosis in a novel CLN9 Batten disease variant. *Ann Neurol* **56**(3): 342-350.
- Sharp, J. D., Wheeler, R. B., Lake, B. D., Savukoski, M., Jarvela, I. E., Peltonen, L., Gardiner, R. M. and Williams, R. E. (1997).** Loci for classical and a variant late infantile neuronal ceroid lipofuscinosis map to chromosomes 11p15 and 15q21-23. *Hum Mol Genet* **6**(4): 591-595.
- Sheridan, S. D., Surampudi, V. and Rao, R. R. (2012).** Analysis of embryoid bodies derived from human induced pluripotent stem cells as a means to assess pluripotency. *Stem Cells Int* **2012**: 738910.
- Sheridan, S. D., Theriault, K. M., Reis, S. A., Zhou, F., Madison, J. M., Daheron, L., Loring, J. F. and Haggarty, S. J. (2011).** Epigenetic characterization of the FMR1 gene and aberrant neurodevelopment in human induced pluripotent stem cell models of fragile X syndrome. *PLoS One* **6**(10): e26203.
- Sibigtroth, C. M., Coates, J. R., Katz, M. L., Castaner, L., Flournoy, C. A., O'Brien, D. P., Vuilleminot, B. R., Kennedy, D., Reed, R., Adams, E. and O'Neill, C. A. (2012).** Treatment with recombinant human tripeptidyl peptidase-1 (rhTPP1) delays onset of neurologic signs in a canine model of late infantile neuronal ceroid lipofuscinosis (LINCL). *13th International Conference on Neuronal Ceroid Lipofuscinoses*.
- Sleat, D. E., El-Banna, M., Sohar, I., Kim, K. H., Dobrenis, K., Walkley, S. U. and Lobel, P. (2008).** Residual levels of tripeptidyl-peptidase I activity dramatically ameliorate disease in late-infantile neuronal ceroid lipofuscinosis. *Mol Genet Metab* **94**(2): 222-233.
- Sleat, D. E., Wiseman, J. A., El-Banna, M., Kim, K. H., Mao, Q., Price, S., Macauley, S. L., Sidman, R. L., Shen, M. M., Zhao, Q., Passini, M. A., Davidson, B. L., Stewart, G. R. and Lobel, P. (2004).** A mouse model of classical late-infantile neuronal ceroid lipofuscinosis based on targeted disruption of the CLN2 gene results in a loss of tripeptidyl-peptidase I activity and progressive neurodegeneration. *J Neurosci* **24**(41): 9117-9126.
- Smith, K. R., Dahl, H. H., Canafoglia, L., Andermann, E., Damiano, J., Franceschetti, S., Cossette, P., Saftig, P., Schwake, M., Morbin, M., Ferguson, R., Aguglia, U., Zini, A., Meletti, S., Mullen, S., Andermann, F., Simonati, A., Staropoli, J. F., Sims, K. B., Mole, S. E., Chapman, H. A., Carpenter, S., Berkovic, S. F. and Bahlo, M. (2012a).** Mutations in the gene encoding cathepsin F are cause of type B Kufs disease. *13th International Conference on Neuronal Ceroid Lipofuscinoses*.

---

**Smith, K. R., Damiano, J., Franceschetti, S., Carpenter, S., Canafoglia, L., Morbin, M., Rossi, G., Pareyson, D., Mole, S. E., Staropoli, J. F., Sims, K. B., Lewis, J., Lin, W. L., Dickson, D. W., Dahl, H. H., Bahlo, M. and Berkovic, S. F. (2012b).** Strikingly different clinicopathological phenotypes determined by progranulin-mutation dosage. *Am J Hum Genet* **90**(6): 1102-1107.

**Sohar, I., Lin, L. and Lobel, P. (2000).** Enzyme-based diagnosis of classical late infantile neuronal ceroid lipofuscinosis: comparison of tripeptidyl peptidase I and pepstatin-insensitive protease assays. *Clin Chem* **46**(7): 1005-1008.

**Sohar, I., Sleat, D. E., Jadot, M. and Lobel, P. (1999).** Biochemical characterization of a lysosomal protease deficient in classical late infantile neuronal ceroid lipofuscinosis (LINCL) and development of an enzyme-based assay for diagnosis and exclusion of LINCL in human specimens and animal models. *J Neurochem* **73**(2): 700-711.

**Sommer, C. A., Sommer, A. G., Longmire, T. A., Christodoulou, C., Thomas, D. D., Gostissa, M., Alt, F. W., Murphy, G. J., Kotton, D. N. and Mostoslavsky, G. (2010).** Excision of reprogramming transgenes improves the differentiation potential of iPS cells generated with a single excisable vector. *Stem Cells* **28**(1): 64-74.

**Staropoli, J. F., Karaa, A., Lim, E. T., Kirby, A., Elbalalesy, N., Romansky, S. G., Leydiker, K. B., Coppel, S. H., Barone, R., Xin, W., Macdonald, M. E., Abdenur, J. E., Daly, M. J., Sims, K. B. and Cotman, S. L. (2012).** A Homozygous Mutation in KCTD7 Links Neuronal Ceroid Lipofuscinosis to the Ubiquitin-Proteasome System. *Am J Hum Genet*.

**Steinfeld, R., Heim, P., von Gregory, H., Meyer, K., Ullrich, K., Goebel, H. H. and Kohlschutter, A. (2002).** Late infantile neuronal ceroid lipofuscinosis: quantitative description of the clinical course in patients with CLN2 mutations. *Am J Med Genet* **112**(4): 347-354.

**Takahashi, K., Tanabe, K., Ohnuki, M., Narita, M., Ichisaka, T., Tomoda, K. and Yamanaka, S. (2007).** Induction of pluripotent stem cells from adult human fibroblasts by defined factors. *Cell* **131**(5): 861-872.

**Takahashi, K. and Yamanaka, S. (2006).** Induction of pluripotent stem cells from mouse embryonic and adult fibroblast cultures by defined factors. *Cell* **126**(4): 663-676.

**Taschner, P. E., de Vos, N. and Breuning, M. H. (1997).** Cross-species homology of the CLN3 gene. *Neuropediatrics* **28**(1): 18-20.

**Tecedor, L., Wininger, F. A., Coates, J. R., Flournoy, C. A., Nice, K., Kordower, J. H., Katz, M. L. and Davidson, B. L. (2012).** AAV-TPP1 transduction of brain ependyma in TPP1-null dogs results in widespread CNS distribution of TPP1 enzyme and improves NCL disease phenotypes. *13th International Conference on Neuronal Ceroid Lipofuscinoses*.

**Thelen, M., Damumue, M., Schweizer, M., Hagel, C., Wong, A. M., Cooper, J. D., Braulke, T. and Galliciotti, G. (2012).** Disruption of the autophagy-lysosome pathway is involved in neuropathology of the nclf mouse model of neuronal ceroid lipofuscinosis. *PLoS One* **7**(4): e35493.

- 
- Tolar, J., Park, I. H., Xia, L., Lees, C. J., Peacock, B., Webber, B., McElmurry, R. T., Eide, C. R., Orchard, P. J., Kyba, M., Osborn, M. J., Lund, T. C., Wagner, J. E., Daley, G. Q. and Blazar, B. R. (2011).** Hematopoietic differentiation of induced pluripotent stem cells from patients with mucopolysaccharidosis type I (Hurler syndrome). *Blood* **117**(3): 839-847.
- Tucker, B. A., Park, I. H., Qi, S. D., Klassen, H. J., Jiang, C., Yao, J., Redenti, S., Daley, G. Q. and Young, M. J. (2011).** Transplantation of adult mouse iPS cell-derived photoreceptor precursors restores retinal structure and function in degenerative mice. *PLoS One* **6**(4): e18992.
- Tuxworth, R. I., Chen, H., Vivancos, V., Carvajal, N., Huang, X. and Tear, G. (2011).** The Batten disease gene CLN3 is required for the response to oxidative stress. *Hum Mol Genet* **20**(10): 2037-2047.
- Usenovic, M. and Krainc, D. (2012).** Lysosomal dysfunction in neurodegeneration: The role of ATP13A2/PARK9. *Autophagy* **8**(6).
- Uvebrant, P. and Hagberg, B. (1997).** Neuronal ceroid lipofuscinoses in Scandinavia. Epidemiology and clinical pictures. *Neuropediatrics* **28**(1): 6-8.
- Vines, D. and Warburton, M. J. (1998).** Purification and characterisation of a tripeptidyl aminopeptidase I from rat spleen. *Biochim Biophys Acta* **1384**(2): 233-242.
- Vuillemenot, B. R., Katz, M. L., Coates, J. R., Kennedy, D., Tiger, P., Kanazono, S., Lobel, P., Sohar, I., Xu, S., Cahayag, R., Keve, S., Koren, E., Bunting, S., Tsuruda, L. S. and O'Neill, C. A. (2011).** Intrathecal tripeptidyl-peptidase 1 reduces lysosomal storage in a canine model of late infantile neuronal ceroid lipofuscinosis. *Mol Genet Metab* **104**(3): 325-337.
- Walker, A., Ward, C., Sheldrake, T. A., Dransfield, I., Rossi, A. G., Pryde, J. G. and Haslett, C. (2004).** Golgi fragmentation during Fas-mediated apoptosis is associated with the rapid loss of GM130. *Biochem Biophys Res Commun* **316**(1): 6-11.
- Wang, Y., Zheng, C. G., Jiang, Y., Zhang, J., Chen, J., Yao, C., Zhao, Q., Liu, S., Chen, K., Du, J., Yang, Z. and Gao, S. (2012).** Genetic correction of beta-thalassemia patient-specific iPS cells and its use in improving hemoglobin production in irradiated SCID mice. *Cell Res* **22**(4): 637-648.
- Warren, L., Manos, P. D., Ahfeldt, T., Loh, Y. H., Li, H., Lau, F., Ebina, W., Mandal, P. K., Smith, Z. D., Meissner, A., Daley, G. Q., Brack, A. S., Collins, J. J., Cowan, C., Schlaeger, T. M. and Rossi, D. J. (2010).** Highly efficient reprogramming to pluripotency and directed differentiation of human cells with synthetic modified mRNA. *Cell Stem Cell* **7**(5): 618-630.
- Watanabe, K., Kamiya, D., Nishiyama, A., Katayama, T., Nozaki, S., Kawasaki, H., Watanabe, Y., Mizuseki, K. and Sasai, Y. (2005).** Directed differentiation of telencephalic precursors from embryonic stem cells. *Nat Neurosci* **8**(3): 288-296.

- 
- Wei, H., Kim, S. J., Zhang, Z., Tsai, P. C., Wisniewski, K. E. and Mukherjee, A. B. (2008).** ER and oxidative stresses are common mediators of apoptosis in both neurodegenerative and non-neurodegenerative lysosomal storage disorders and are alleviated by chemical chaperones. *Hum Mol Genet* **17**(4): 469-477.
- Wernig, M., Zhao, J. P., Pruszak, J., Hedlund, E., Fu, D., Soldner, F., Broccoli, V., Constantine-Paton, M., Isacson, O. and Jaenisch, R. (2008).** Neurons derived from reprogrammed fibroblasts functionally integrate into the fetal brain and improve symptoms of rats with Parkinson's disease. *Proc Natl Acad Sci U S A* **105**(15): 5856-5861.
- Wisniewski, K. E., Zhong, N. and Philippart, M. (2001).** Pheno/genotypic correlations of neuronal ceroid lipofuscinoses. *Neurology* **57**(4): 576-581.
- Woltjen, K., Michael, I. P., Mohseni, P., Desai, R., Mileikovsky, M., Hamalainen, R., Cowling, R., Wang, W., Liu, P., Gertsenstein, M., Kaji, K., Sung, H. K. and Nagy, A. (2009).** piggyBac transposition reprograms fibroblasts to induced pluripotent stem cells. *Nature* **458**(7239): 766-770.
- Yagi, T., Ito, D., Okada, Y., Akamatsu, W., Nihei, Y., Yoshizaki, T., Yamanaka, S., Okano, H. and Suzuki, N. (2011).** Modeling familial Alzheimer's disease with induced pluripotent stem cells. *Hum Mol Genet* **20**(23): 4530-4539.
- Yahata, N., Asai, M., Kitaoka, S., Takahashi, K., Asaka, I., Hioki, H., Kaneko, T., Maruyama, K., Saïdo, T. C., Nakahata, T., Asada, T., Yamanaka, S., Iwata, N. and Inoue, H. (2011).** Anti-Abeta drug screening platform using human iPS cell-derived neurons for the treatment of Alzheimer's disease. *PLoS One* **6**(9): e25788.
- Yan, X., Qin, H., Qu, C., Tuan, R. S., Shi, S. and Huang, G. T. (2010).** iPS cells reprogrammed from human mesenchymal-like stem/progenitor cells of dental tissue origin. *Stem Cells Dev* **19**(4): 469-480.
- Zaehres, H., Kim, J. B. and Scholer, H. R. (2010).** Induced pluripotent stem cells. *Methods Enzymol* **476**: 309-325.
- Zeng, H., Guo, M., Martins-Taylor, K., Wang, X., Zhang, Z., Park, J. W., Zhan, S., Kronenberg, M. S., Lichtler, A., Liu, H. X., Chen, F. P., Yue, L., Li, X. J. and Xu, R. H. (2010).** Specification of region-specific neurons including forebrain glutamatergic neurons from human induced pluripotent stem cells. *PLoS One* **5**(7): e11853.
- Zhou, H., Wu, S., Joo, J. Y., Zhu, S., Han, D. W., Lin, T., Trauger, S., Bien, G., Yao, S., Zhu, Y., Siuzdak, G., Scholer, H. R., Duan, L. and Ding, S. (2009).** Generation of induced pluripotent stem cells using recombinant proteins. *Cell Stem Cell* **4**(5): 381-384.
- Zick, M., Rabl, R. and Reichert, A. S. (2009).** Cristae formation-linking ultrastructure and function of mitochondria. *Biochim Biophys Acta* **1793**(1): 5-19.



## 7 Acknowledgments

I would like to express my gratitude to my supervisor, Prof. Storch, for having provided me with this very interesting topic and for giving me the opportunity to work on this project in various laboratories.

Very special thanks to Prof. van Pée and his group for their interest in my work and for helpful discussions and advices.

Furthermore, I would like to thank Prof. Schöler and Dr. Cotman for their expertise and advices during the work in their laboratories. I especially would like to thank Dr. Cotman for all the discussions and ideas that helped moving forward with this project.

I want to express special thanks to all the families and patients who participated in this study. Furthermore, I want to acknowledge the NCL Stiftung for having funded this project.

I would like to acknowledge Dr. Staropoli and Dr. Hermann for the positive review of this thesis and for their great ideas which considerably contributed to this thesis. Furthermore, I would like to thank Dr. Staropoli for his help with assays and EM imaging.

I especially want to thank Peter Reinhardt, who provided me with countless advices and with his expertise in iPSC culture.

I want to thank Peter, Rhea, Susanne, Michael and Jan for having made my stay in Münster so enjoyable.

I need to thank Uma, John, Larissa, Anton, Amel, Cassie and Sadie for their help and support during my stay in Boston.

I would like to thank the Storch group, especially Katja, Lena, Lisa, Meri and Nicole for their support during my stay in the USA. I especially would like to thank Christin for her relentless support and countless hours of discussions which considerably contributed to this work.

I would like to thank all my friends for their tireless help and support during my studies.

Zum Abschluss möchte ich mich ganz besonders bei meinem Papa bedanken, der mir stets mit Rat und Tat zur Seite stand und ohne dessen Hilfe ich vieles nicht erreicht hätte.

## 8 Versicherung und Erklärung

Hiermit versichere ich, dass ich die vorliegende Arbeit ohne unzulässige Hilfe Dritter und ohne Benutzung anderer als der angegebenen Hilfsmittel angefertigt habe; die aus fremden Quellen direkt oder indirekt übernommenen Gedanken sind als solche kenntlich gemacht. Die Arbeit wurde bisher weder im Inland noch im Ausland in gleicher oder ähnlicher Form einer anderen Prüfungsbehörde vorgelegt.

Die vorliegende Arbeit wurde am Institut für Neurologie, Universitätsklinikum Carl Gustav Carus, unter der wissenschaftlichen Betreuung von Herrn Prof. Dr. med. habil. Alexander Storch angefertigt.

Hiermit erkenne ich die Promotionsordnung der Fakultät Mathematik und Naturwissenschaften an der Technischen Universität Dresden vom 23.02.2011 an.

Dresden, d. 23.11.2012

\_\_\_\_\_  
Ort, Datum

\_\_\_\_\_  
Unterschrift